St Petersburg State University

Kamenskii Mikhail Aleksandrovich

Electrochemical properties of cathode materials based on manganese oxides for aqueous zinc-ion batteries

Scientific specialty 1.4.6. Electrochemistry

Dissertation
submitted for the degree of Candidate of Chemical Sciences

Translation from Russian

Scientific supervisors:
Doctor of Chemical Sciences Kondratiev V.V.
Candidate of Chemical Sciences Eliseeva S.N.

Saint Petersburg 2024

Content

Introduction

Relevance of the topic

Over the last twenty years, lithium-ion batteries have been the most widely used power source in various applications (from portable electronics to electric vehicles), due to their high energy and power density. Along with them, lead-acid batteries are used in many countries for stationary energy storage and accumulation (backup or emergency power supply systems) due to their low production and maintenance costs. However, both of these battery types have a number of disadvantages. The disadvantages of lithium-ion systems are the high toxicity and explosion hazard of cyclic ester-based electrolytes, cobalt-based cathode materials, difficulty of manufacture and recycling, and limited resources and high cost of components, especially lithium salts. The drawbacks of lead-acid batteries are the toxicity of lead and its compounds, the limited operating thermal stability range, the low practical energy density (about 30 $W \cdot h \cdot kg^{-1}$ against a theoretical one of 167 $W \cdot h \cdot kg^{-1}$) and the relatively short lifespan (up to 1000 recharge cycles). Therefore, with the rapid growth in demand for batteries and the expansion of the scope and scale of their use in electric vehicles, stationary energy storage and other applications, the requirements for their safety, cost, availability and environmental friendliness, while maintaining competitive functional performance, are increasing. As a consequence, alternative electrochemical systems, in particular post-lithium metal-ion batteries, are attracting increasing research attention, especially for stationary energy storage and energy storage applications. Sodium-ion and potassium-ion batteries, for which the availability of sodium and potassium compounds is an obvious advantage, are primarily considered, but the disadvantages inherent in lithium-ion systems, namely the toxicity and explosion hazard of the cell components, are even more pronounced for these two types of batteries due to the faster kinetics of side reactions between metals and trace amounts of water.

In the last decade, metal-ion batteries have been developed using non-aggressive aqueous electrolyte solutions with a pH in the range 4 - 8. Despite the loss of energy density, the use of such electrolytes increases the safety of the batteries, which is valuable to the consumer, and reduces the cost of production and subsequent recycling of the batteries. In addition, metal-ion systems with aqueous electrolytes have high energy density values ($100 - 250$ $W \cdot h \cdot kg^{-1}$ and even higher 300 $W \cdot h \cdot kg^{-1}$) compared to lead-acid or metal-ion batteries with alkaline electrolytes (approximately 150 $W \cdot h \cdot kg^{-1}$) [1–4]. The zinc anode, which is widely used in alkaline cells, has a moderate redox transition potential (−0.762 V vs. H_2/H^+) and a high theoretical gravimetric (820 $mAh \cdot g^{-1}$) and volumetric (5855 $mAh \cdot cm^{-3}$) capacity, and reacts extremely slowly with water, allowing the use of a zinc metal anode, unlike other metals considered for use as an anode for single metal-ion systems.

Aqueous zinc-ion batteries (AZIBs) are one of the most intensively developed areas in the field, as evidenced by the dramatic increase in the number of publications on the subject, currently around 1000

per year (particularly in the last 3 years) [5]. Laboratory aqueous zinc-ion cells with aqueous electrolytes how high specific capacities (250 $mAh \cdot g^{-1}$ and higher at low current densities) and high cyclic stability during hundreds and thousands of cycles (up to ≈ 80% capacity retention at a current density of 1.0 $A \cdot g^{-1}$) [6] as well as safer operation compared to acid and alkaline batteries [7]. Despite the fact that this field has been developed relatively recently (since 2012 [8]), while alkaline batteries with metallic zinc have been known for more than 50 years, aqueous zinc-ion systems show better performance at the laboratory level, making them promising candidates for practical applications [4].

Battery capacity is determined by the balance between the achievable capacity values for the cathode and anode materials. In the case of aqueous zinc-ion systems, metallic zinc is usually used as the anode, the theoretical capacity value of which is higher than the practically observed specific capacity values for any cathode material. For this reason, the main research in the field of AZIBs has focused on the development of various cathode materials compatible with aqueous neutral or weakly acidic electrolytes. Among different cathode materials applied in AZIBs, manganese oxides are attractive due to high redox transition potential (1.3 – 1.5 V vs. Zn/Zn^{2+}) which determines the high capacity of the cathode material, wide availability, moderately high theoretical capacity (308 $mAh \cdot g^{-1}$), ease of synthesis and great variability of materials with different crystal structures. In particular, manganese dioxide MnO_2 is capable to form various crystal polymorphs: tunnel-type (α–, β–, γ–MnO_2), spinel-type (ε–, λ–, R–MnO_2, $MeMn_2O_4$), layered-type (δ–MnO_2) [9,10]. Among the MnO_2 polymorphs, birnessite (or δ–MnO_2) is the most suitable for intercalation of Zn^{2+} cations due to the large interlayer distance (≈ 7 Å), which facilitates the transport of zinc ions into the oxide crystal lattice [11–13].

As an alternative to zinc-ion cells, zinc-hybrid batteries are being researched, in which instead of one charge carrier (e.g. Zn^{2+} as assumed for AZIBs), two charge carriers participate in separate electrochemical reactions. In aqueous zinc-hybrid batteries, Zn^{2+} ions are involved in the anode reaction while the second cation (Li^+, Na^+, etc.) takes part in the cathode reaction [14]. Manganese oxides, in particular the lithium-manganese spinel $LiMn_2O_4$ have been intensively studied as cathode materials for zinc-hybrid batteries because of a number of advantages: high redox transition potential (1.8 – 1.9 V vs. Zn/Zn^{2+}), fast kinetics of intercalation of Li^+ ions into the $LiMn_2O_4$ structure in aqueous solutions.

Nowadays, the key problem that limits the development of both cathode materials and aqueous zinc-ion batteries in general, including hindering the targeted search for new compositions of MnO_2-based composite cathode materials, is the ambiguity and discussion of the mechanism of electrochemical reaction in an aqueous electrolyte solution. First of all, it is related to the complex composition of the used aqueous solutions and, consequently, to a number of ongoing reactions involving ions and molecules in hydrated and dehydrated forms (Zn^{2+}, $[Zn(H_2O)_6]^{2+}$, Mn^{2+},

$[Mn(H_2O)_6]^{2+}$, H^+, H_2O). In addition, the formation of insoluble surface compounds during the discharge process should be considered. Authors of numerous papers claim that during the charge/discharge processes a number of structural changes of the material occur with the participation of the listed ions [15]. However, the combined data obtained by physicochemical methods (both X-ray diffraction and electron microscopy techniques) are not always consistent due to various factors and therefore do not fully allow a correct analysis of the phases formed and destroyed during charge/discharge.

Thus, the relevance of this work is caused by the importance of solving both the practical problem of developing novel cathode materials based on manganese oxides for aqueous zinc-ion batteries and the fundamental problem of studying charge transport in the Zn//MnO_2 electrochemical system. Understanding the mechanism of electrochemical processes is a key issue for the improvement of functional properties, the design of novel cathode materials for the creation of full-size zinc-ion batteries, their further development and scaling, and their introduction into production.

Research topic development level

Manganese oxide-based cathodes, one of the most intensively studied for AZIBs, have several drawbacks, the most important of which is the spontaneous cathode dissolution (both for MnO_2 and $LiMn_2O_4$) during charge/discharge processes due to the disproportionation reaction of the Mn^{3+} cation formed during reduction into the Mn^{2+} and Mn^{4+} ions. To eliminate or mask these processes, a number of strategies aimed at modifying the properties of the electroactive component or the electrode material as a whole are used: synthesis of MnO_2 nanoparticles with a given morphology including the synthetic introduction of foreign metal ions into the cathode structure (so-called pre-intercalation), development of MnO_2-based composite materials with highly conductive additives such as carbon-based materials or conducting polymers, and the variation of the electrolyte composition. Several approaches are being actively used in parallel.

One of the approaches used is to modify the electrolyte solution. To increase the number of charge/discharge cycles and the cyclic stability of Zn//MnO_2 systems, a small amount of manganese (II) salt ($0.1 – 0.5\ mol \cdot L^{-1}$) is added to the electrolyte solution [16–18]. In the mixed electrolyte solution containing zinc and manganese salts, the stability of the capacity values of the cathode increases significantly, and in some cases, there is an increase in the specific capacity during cycling, caused by the deposition of additional electroactive phase MnO_x (ε-MnO_2) from the solution on the surface of the cathode material, which is particularly pronounced for cathodes with low mass loading [18,19]. It was found that Mn^{2+} ions present in the solution ($MnSO_4$) not only inhibit the dissolution of the initial oxide by creating an excess concentration of the reduced form in the near-electrode layer. During the oxidation process (E = 1.7 V), Mn^{2+} cations that are converted to MnO_2 increase the concentration of free H^+ ions in the near-electrode layer. During discharge, H^+ ions interact with the

cathode material, resulting in the reverse transition $Mn^{IV} \rightarrow Mn^{III}$, and some of the Mn^{3+} ions are converted to Mn^{2+} ions, resulting in local alkalinization and the formation of the basic zinc salt [19,20]. This is also confirmed by a number of works in which the properties of cathode materials have been studied in electrolytes without manganese additives and in which the cathode material has practically no electroactivity [21–23].

To improve the properties of MnO_2-based cathode materials, modification of the material with conducting polymers could be one of the options. A number of works focus on the study of manganese oxide based composites with polyaniline [24–26], polypyrrole [27–29] or ternary composites with conducting polymers and carbon-based materials [30–33]. Despite the excellent electrochemical performance in terms of specific capacity or cyclic stability, the synthetic routes for such composites are not universal for all MnO_2 polymorphs, most commonly the resulting product of oxide preparation in the presence of aniline or pyrrole is a tunnel-type structure. There are fewer studies in which MnO_2 was modified with poly(3,4-ethylenedioxythiophene) (PEDOT) compared to other works [34–36]. Poly(3,4-ethylenedioxythiophene) is one of the conducting polymers that has a wide range of electroactivity as well as improved chemical and electrochemical stability compared to other conducting polymers. Its availability as a polyelectrolyte complex with polystyrene sulfonate (PEDOT:PSS), available as an aqueous dispersion, greatly facilitates the development of composite materials.

An important issue in the study of the Zn//MnO_2 system is the complexity of the electrochemical reaction mechanism in which several ions are involved: Zn^{2+}, Mn^{2+}, H^+ as well as solvent molecules could be involved. The obligatory presence of several types of ions in the electrolyte solution indicates their participation in the electrochemical process, which complicates the interpretation of the reaction mechanism. It is important to note that the full disclosure of the mechanism of the electrochemical reaction is a task that, despite the efforts of many scientific groups in the world, remains unsolved and controversial. The main variants of the mechanism currently considered in the literature are as follows [37]:

1. Reversible intercalation of Zn^{2+} ions;
2. Reversible co-intercalation of Zn^{2+} and H^+ ions;
3. Conversion reaction $MnO_2 \rightarrow MnOOH$ with H^+ ions participating;
4. MnO_2 electrolytic dissolution/deposition.

Meanwhile, the complex composition of the aqueous electrolyte, the wide variety of MnO_2 forms and the precipitate of the basic zinc salt $Zn_4(OH)_6SO_4 \cdot nH_2O$, which is constantly formed on the cathode surface during discharge, make it difficult to interpret both the phases present in the cathode and the chemical states of the elements. Questions remain about the role of the addition of manganese salt to the electrolyte in the functioning of the cell, the ratio of intercalation and phase transformation

processes, as well as the role of surface precipitates. The approaches to cathode structure analysis proposed in the literature, both *ex situ* and *post mortem*, do not provide a clear answer to this question. Since contradictory conclusions can be drawn depending on the analysis of the cathode structure by different methods, the question of the mechanism remains debatable. controversial. The problem of the possible involvement of H^+ cations in intercalation processes in aqueous batteries is not only valid for Zn//MnO_2 systems, but also for cathode materials for zinc-hybrid batteries, in particular, Zn//$LiMn_2O_4$. Since the H^+ and Li^+ cations are small in size and carry a single positive charge, it is expected that they can both intercalate into the $LiMn_2O_4$ structure. This process is almost completely undescribed in the literature.

Thus, this research is aimed to establish the mechanism of the electrochemical reactions occurring by varying the electrolyte composition and controlling the acidity of the solution, including the use of comprehensive electrochemical analysis and *in operando* electrode mass studies using the electrochemical quartz crystal microbalance method to provide experimental evidence of the charge transport mechanism consistent with a large number of literature data. The practical aspect of the study is the development of a new simple and versatile method to modify MnO_2-based electrode materials with layered structure with the conducting polymer poly(3,4-ethylenedioxythiophene) in order to improve the functional properties of the cathodes, in particular the stability of the capacitive response during cycling.

The main **objectives** of the work can be divided into practical and fundamental ones. The practical objective is to develop novel types of cathode materials based on manganese oxides for aqueous zinc-ion batteries, modified with the conducting polymer poly(3,4-ethylenedioxythiophene) to enhance their electrochemical performance (high-rate specific capacity, cyclic stability). The fundamental objective of the study is to identify the overall mechanisms of intercalation processes in aqueous Zn//MnO_2 zinc-ion systems, including the elucidation of the electrochemical reaction mechanism during the first and subsequent charge/discharge cycles, as well as the role of the electrolyte and the influence of its composition on the electrochemical properties of the Zn//MnO_2 system.

To achieve the aims, the following **tasks** should be resolved:

1. Investigation of electrochemical properties of $LiMn_2O_4$-based cathode materials in different zinc-containing electrolyte solutions, including consideration of the possibility of electrochemical conversion of $LiMn_2O_4$ to λ-MnO_2 or $Zn_xMn_2O_4$ in the electrolyte solution containing no Li^+ ions.
2. Chemical synthesis of manganese oxide with layered-type structure (δ-MnO_2) at different conditions and carrying out complex structural, morphological analysis and electrochemical tests.

3. Development of novel types of δ-MnO_2-based cathode materials modified with the conducting polymer PEDOT by different methods: introduction of chemically synthesized polymer into the electrode material composition, formation of a coating from aqueous dispersion of PEDOT:PSS or electrochemical coating of the as-prepared cathode with a layer of PEDOT.
4. Determination of correlations between electrochemical performance (specific capacities at different current densities, capacity stability during cycling, structural and chemical stability) and composition, morphology and method of preparation of composite materials.
5. Investigation of charge/discharge processes in conducting polymer-modified cathode materials and structural transformations of electrodes during cycling.
6. Study of the influence of electrolyte composition on the electrochemical properties of MnO_2 as a function of electrolyte formulation and acidity, in order to test existing hypotheses on the electrochemical reaction mechanism.
7. Analysis of the mass transfer processes *in operando* by electrochemical quartz crystal microbalance in different solutions of electrolytes based on zinc salts, determination of the dominant process in the first and subsequent cycles.
8. Analysis of the results presented in the literature and their comparison with the obtained experimental data with the conclusion about the mechanism of charge/discharge processes in the studied systems.

The scientific novelty of the work

For the first time, the dependence of the electrochemical properties of $LiMn_2O_4$-based cathode materials on the composition of the zinc-containing electrolyte was demonstrated. It was found that only Li^+ ions are involved in the intercalation processes in the cathode material structure. Zn^{2+} ions are almost irreversibly incorporated into the spinel structure, blocking of the cathode surface occurs, as a result of which the reaction of electrochemical conversion of $LiMn_2O_4$ into λ-MnO_2 does not occur and degradation of the electrochemical properties of the cathode material is observed. Thus, the presence of lithium salt in the electrolyte composition is essential for $LiMn_2O_4$ cathodes. The addition of manganese salt allows to increase the initial values of the specific capacity of $LiMn_2O_4$, but does not allow to achieve a significant improvement of the stability during prolonged cycling due to the competing processes of oxidation of Mn^{2+} ions and water with the release of oxygen.

The comparative analysis of the electrochemical performance of cathode materials with the same crystal structure (δ-MnO_2) obtained hydrothermally in different ways: by reaction of interaction between potassium permanganate and manganese sulfate (method I) and by decomposition of potassium permanganate aqueous solution (method II) was carried out. Increasing the synthesis temperature and the reaction time allows us to obtain the material with low agglomeration, i.e. higher

crystallinity which has higher initial specific capacity. However, during galvanostatic charge/discharge tests, the cyclic stability was less than 50% for 100 cycles which is due to the destruction of the bonds between the particles of the electroactive material. This results in a significant deterioration of the contact between the electroactive material particles and an increase in the charge transfer resistance within the cathode material. A more amorphous material is less susceptible to structural disordering processes during cycling and thus better maintains its electrochemical properties.

The practical novelty of the work consists in the preparation and comprehensive electrochemical analysis of new composite cathode materials based on manganese dioxide with layered structure (δ-MnO_2) with conducting polymer poly(3,4-ethylenedioxythiophene) (PEDOT) using different modification methods: addition of the polymer to the composite electrode, fabrication of a PEDOT:PSS-based coating by dispersing MnO_2 grains in an aqueous dispersion with subsequent drying or electrodeposition of the polymer on the as-prepared electrode. It has been shown that the mechanical coating on the synthesized MnO_2, obtained by dispersing the oxide in PEDOT:PSS aqueous dispersion, plays a dual role: improving the electronic and ionic contact between the oxide particles due to the conductivity of the PEDOT:PSS polymer and limiting the direct contact of MnO_2 with the electrolyte solution, which reduces the dissolution of the cathode material. This modification method is quite simple and reproducible and can be applied to manganese oxides of any composition and crystal structure.

Analysis of the dependence of the electrochemical properties of MnO_2 on the electrolyte composition, carried out in aqueous solutions based on zinc and manganese sulfates, showed that both cations (Zn^{2+} and Mn^{2+}) should be present in the sulfate-based solution (pH ≈ 4.5). *In operando* measurements of the electrode mass, carried out with an electrochemical quartz crystal microbalance in solutions with the addition of alkali metal salts (Li^+, Na^+) to the sulfate electrolyte showed that the intercalation of the monovalent ion occurs during the discharge processes. Along with changes in the pH value of the electrolyte solution, this confirms the intercalation of H^+ ions in 2 M $ZnSO_4$ / 0.1 M $MnSO_4$ solution. H^+ ions could intercalate reversibly into the manganese oxide only in a mixed electrolyte. Zn^{2+} ions present in the form of $[Zn(H_2O)_6]^{2+}$ participate in several processes: desolvation of the complex cation and its subsequent incorporation into the cathode structure, dissociation of the hydrate shell, and formation of the basic salt $Zn_4(OH)_6SO_4 \cdot nH_2O$ on the MnO_2 surface. The participation of H^+ ions in the course of MnO_2 discharge and the subsequent formation of the surface salt $Zn_4(OH)_6SO_4 \cdot nH_2O$ regulate the pH value of the aqueous electrolyte.

Practical significance of the work

In this research the influence of various factors – morphology of manganese oxide particles, presence of conducting polymer-based modifier, electrolyte composition – on the functional properties

of manganese oxide-based cathode materials for aqueous zinc-ion and zinc-hybrid batteries was considered.

The effect of the electrolyte composition on the properties of $LiMn_2O_4$-based cathode materials for aqueous zinc-hybrid batteries was studied. In particular, the influence of Mn^{2+} ions added to the electrolyte solution to suppress the dissolution of the cathode material during the cycling process was studied. The increased initial specific capacity values were obtained at low current densities.

Among all studied MnO_2-based electrode materials with birnessite-type structure the best one for practical application is the material with low crystallinity, whose surface is modified by the conducting polymer poly(3,4-ethylenedioxythiophene):polystyrene sulfonate. During 100 cycles at a current density of 0.3 $A \cdot g^{-1}$, the capacity retention was 99% (278 $mAh \cdot g^{-1}$), and the highest specific capacity values were observed at high current densities (133 $mAh \cdot g^{-1}$ at current density 2.0 $A \cdot g^{-1}$).

Theoretical significance of the work

A systematic analysis of the electrochemical behavior of the $Zn//MnO_2$ system as a function of the electrolyte composition was carried out in order to establish the reaction mechanism. In particular, the experiments carried out in zinc sulfate and manganese sulfate solutions showed the necessity of the presence of both types of cations (Zn^{2+} and Mn^{2+}) to obtain a stable and reproducible electrochemical response of the system. In the solutions based on 2 M $ZnSO_4$ / 0.1 M $MnSO_4$ with the addition of alkali metal ions (Li^+, Na^+), the participation of the latter in the intercalation processes was established by the electrochemical quartz crystal microbalance, which indirectly proves the participation of monovalent cations (H^+ or H_3O^+) in the overall reaction. Adjusting the pH of the electrolyte solution based on zinc and manganese acetates allowed us to verify the participation of H^+ cations in the overall reaction, including the processes of electrolytic precipitation/dissolution of MnO_2. Injection of Zn^{2+} ions in the crystal lattice was confirmed by structural and elemental analysis of cathode materials after electrochemical tests.

The existing hypotheses on the mechanism of the electrochemical reaction in MnO_2 in zinc-containing electrolytes have been analyzed in combination with the results obtained experimentally in this work, and the main concepts for describing the mechanism of charge transport have been summarized. A new hypothesis is proposed to explain the mechanism of electrochemical processes occurring in the $Zn//MnO_2$ system in solutions based on zinc and manganese sulfates. During the cathodic process, two parallel reactions occur: co-intercalation of Zn^{2+} and H^+ ions and dissociation of a water molecule within the hydrate shell of the $[Zn(H_2O)_6]^{2+}$ cation. This leads to the appearance of additional free H^+ ions capable of intercalating into the MnO_2 structure, as well as to the formation of $[Zn(H_2O)_5OH]^+$ ions acting as a precursor for the synthesis of the basic salt $Zn_4(OH)_6SO_4 \cdot nH_2O$ on the surface of MnO_2 particles in the composite cathode.

Studies in pH-controlled solutions (based on zinc and manganese acetates) have shown that in the case of stronger binding of Zn^{2+} cations to acetate ions and formation of a buffer solution, the reaction mechanism can change: at high and constant concentration of H^+ ions, the overall reaction can be described as electrolytic precipitation/dissolution of MnO_2.

Degree of reliability and approbation of scientific results

The reliability and validity of the presented results are determined by the use of modern methods and measuring instruments, the consistency of the data obtained in the work with the data presented in the literature, as well as the consistency and coherence of the results of the applied methods. Based on the results of this work, 4 scientific articles, including one review article, were published in international peer-reviewed journals, referenced in the databases of Scopus, Web of Science and RSCI.

1. M.A. Kamenskii, S.N. Eliseeva, A.I. Volkov, V.V. Kondratiev, Electrochemical Performance of $LiMn_2O_4$ Cathodes in Zn-Containing Aqueous Electrolytes, *J. Electrochem. Sci. Technol.,* vol. 13 (2022), pp. 177–185. DOI 10.33961/jecst.2021.00689.
2. M.A. Kamenskii, F.S. Volkov, S.N. Eliseeva, R. Holze, V.V. Kondratiev, Comparative Study of PEDOT- and PEDOT:PSS Modified δ-MnO_2 Cathodes for Aqueous Zinc Batteries with Enhanced Properties, *J. Electrochem. Soc.,* vol 170 (2023), p. 010505. DOI 10.1149/1945-7111/acabec.
3. M.A. Kamenskii, F.S. Volkov, S.N. Eliseeva, E.G. Tolstopyatova, V.V. Kondratiev, Enhancement of Electrochemical Performance of Aqueous Zinc Ion Batteries by Structural and Interfacial Design of MnO_2 Cathodes: The Metal Ion Doping and Introduction of Conducting Polymers, *Energies*, vol. 16 (2023), p. 3221. DOI 10.3390/en16073221.
4. M.A. Kamenskii, A.Yu. Popov, S.N. Eliseeva, V.V. Kondratiev, The Effect of the Synthesis Method of the Layered Manganese Dioxide on the Properties of Cathode Materials for Aqueous Zinc-Ion Batteries, *Russ. J. Electrochem.*, vol. 59 (2023), p.1092–1101. DOI 10.1134/S1023193523120066

Obtained results were presented as oral and poster reports at the Russian and international conferences:

1. M.A. Kamenskii, S.N. Eliseeva, V.V. Kondratiev, The Electrochemical Performance of δ-MnO_2 Cathode Material for Aqueous Zinc-Ion Batteries: The Role of Current Collector (August 22 – 25, 2021) – *22nd International conference "Advanced Batteries, Accumulators and Fuel Cells" (ABAF)*, Brno, Czech Republic.
2. M.A. Kamenskii, S.N. Eliseeva, V.V. Kondratiev, Enhancement of the Electrochemical Performance of δ-MnO_2 Electrodes by Introducing Conducting Polymer (November 9 – 11, 2021) – *International Student Conference "Science and Progress"*, St Petersburg, Russia.

3. M.A. Kamenskii, S.N. Eliseeva, V.V. Kondratiev, Synthesis and electrochemical performance of δ-MnO_2 as cathode material for aqueous zinc-ion batteries (September 20 – 24, 2021) – *XVI International conference "Current Problems of Energy Conversion in Lithium Electrochemical Systems",* Ufa, Russia.
4. M.A. Kamenskii, S.N. Eliseeva, V.V. Kondratiev, Electrochemical properties of δ–MnO_2 coated by conducting polymer as cathodes for zinc-ion batteries (14 – 22 November, 2022) – *XVII conference "Current Problems of Energy Conversion in Lithium Electrochemical Systems*", Moscow, Russia (in Russian).
5. M.A. Kamenskii, Studies of electrochemical reactions occurring during charge/discharge in aqueous Zn//MnO_2 batteries (April 10 – 21, 2023) – *International scientific conference of students and young scientists "Lomonosov-2023"*, Moscow, Russia (in Russian).
6. M.A. Kamenskii, A.Yu. Popov, S.N. Eliseeva, V.V. Kondratiev, Electrochemical properties of cathode materials for aqueous zinc-ion batteries based on manganese dioxide (July 3 – 7, 2023) – *XIV Plyos international scientific conference "Modern issues of theoretical and applied electrochemistry: electrochemistry now and in future"*, Plyos, Russia (in Russian).
7. M.A. Kamenskii, Influence of electrolyte cation composition on electrochemical reaction properties in Zn//MnO_2 batteries (April 12 – 26, 2024) – *XXXI International scientific conference of students and young scientists "Lomonosov"*, Moscow, Russia (in Russian).

The personal contribution of the author was the definition of the tasks and objectives of the work, the planning of the experiment together with the two supervisors. The main experimental results obtained by electrochemical techniques, their interpretation and analysis, as well as the preparation of the results for publication in scientific journals and presentation at conferences were performed by the applicant personally.

Investigations of structure, morphology and composition of the obtained samples were carried out jointly with the staff of the Interdisciplinary Resource Center for Nanotechnology, the Center for X-ray Diffraction Studies, the Center for Physical Methods of Surface Investigation and Chemical Analysis, and the Materials Research Center of the Research Park of Saint Petersburg State University. Detailed analysis and generalization of the obtained structural-chemical data were carried out by the applicant personally.

Main scientific results:

1. It has been found that the functional properties of cathode materials based on manganese oxide with a layered structure (δ-MnO_2): specific capacity and cyclic stability during long-term cycling, increase significantly as a result of preparing the composite materials with conducting polymer poly(3,4-ethylenedioxythiophene) by two methods: by adding 5 wt% of chemically synthesized polymer or as a mechanical coating of polystyrene sulphonate

on the surface of MnO_2 particles. The PEDOT:PSS coating on the MnO_2 surface allows obtaining the maximum specific capacity during long-term cycling due to improved electron-ion contact and a "protective layer" that suppresses cathode material dissolution. The capacity of the composite electrode was 276 $mAh \cdot g^{-1}$ at $I = 0.3$ $A \cdot g^{-1}$, twice that of the MnO_2-based cathode (134 $mAh \cdot g^{-1}$). The results described are presented in section 3.3 of the thesis and published in [38].

2. A new mechanism of co-intercalation of Zn^{2+} and H^+ ions during the electrochemical reaction occurring in rechargeable Zn//MnO_2 electrochemical systems has been proposed. It involves the co-insertion of H^+ and Zn^{2+} ions present in the electrolyte solution and the splitting of H+ ions from water molecules in the coordination sphere of $[Zn(H_2O)_6]^{2+}$ ions with the formation of free H^+ ions and the $[Zn(H_2O)_5OH]^+$ cations, which further react with excess sulphate anions to form the basic salt $Zn_4(OH)_6SO_4 \cdot nH_2O$. The results described are presented in Chapter 5 of the thesis.
3. The necessity of simultaneous presence of Zn^{2+} and Mn^{2+} ions in the electrolyte composition for Zn//MnO_2 rechargeable systems has been confirmed, because in the absence of one of the cations a deterioration of the properties occurs. *In operando* measurements of the electrode mass change by electrochemical quartz microgravimetry with registration of cyclic voltammetry in solutions containing excess in concentration of alkali metal ions (Li^+, Na^+) their participation in the intercalation process in the region of potentials $E \approx 1.4$ V vs Zn/Zn^{2+} was established. The results described are summarized in chapter 4 of the thesis.
4. It was shown that varying the solution composition and the temperature of the hydrothermal synthesis, the same crystalline phase of MnO_2 with a layered structure but different morphology and degree of crystallinity can be obtained. An increase in the degree of crystallinity of the initial oxide leads to an almost twofold increase in the initial specific capacity of the manganese dioxide cathode (222 $mAh \cdot g^{-1}$, for more amorphous material – 103 $mAh \cdot g^{-1}$). The higher degree of amorphous oxide allows to increase the cyclic stability of the electrode materials up to 90% at a current density of 0.3 $A \cdot g^{-1}$. The results are described in section 3.2 of the study and published in [39].
5. A systematic and detailed analysis of the influence of the nature of the conducting polymer and the pre-intercalated cation on the electrochemical performance of cathode materials based on manganese oxide MnO_2 has been carried out on the basis of literature data. The main hypotheses of the electrochemical reaction mechanism in Zn//MnO_2 electrochemical systems proposed by the scientific community are critically reviewed. The analyses carried

out are presented in chapters 1 and 5 of the study and also published in the form of a review article [40].

6. For $LiMn_2O_4$-based cathode materials the obligatory presence of Li^+ ions in the electrolyte solution are shown to achieve reproducible functional characteristics. Electrochemical conversion of $LiMn_2O_4$ to $ZnMn_2O_4$ by replacing the electrolyte solution does not occur due to the blocking of the cathode surface by Zn^{2+} ions as a result of their injection. These results are described in section 3.1 of the study and published in [41].

Provisions being defended:

1. The reversible intercalation of Li^+ ions and irreversible introduction of Zn^{2+} ions into the structure of cathode materials based on $LiMn_2O_4$ have been experimentally proved by changing the cationic composition of the electrolyte.
2. Depending on the conditions of hydrothermal synthesis of MnO_2 (reagents, temperature and time), materials with the same crystalline structure of birnessite (δ-MnO_2) and with different degrees of crystallinity are obtained, which affects their electrochemical properties: materials with amorphous structure show lower initial specific capacity, but are more stable during long-term cycling.
3. MnO_2-based composite materials with the conducting polymer poly(3,4-ethylenedioxythiophene) show improved electrochemical performance (291 $mAh \cdot g^{-1}$ at $I = 0.1$ $A \cdot g^{-1}$) in the mixed 2 M $ZnSO_4$ / 0.1 M $MnSO_4$ electrolyte.
4. The formation of a polymer coating based on PEDOT:PSS on the surface of MnO_2 allows to obtain the maximum specific capacity during long-term cycling (276 $mAh \cdot g^{-1}$ at $I = 0.3$ $A \cdot g^{-1}$) due to the improved electron-ion contact and a “protective layer” that inhibits the dissolution of the cathode material.
5. The participation of the monovalent ion (H^+) in the electrochemical reaction was indirectly confirmed by the addition of an excess by concentration of the monovalent alkali metal ion in solutions of electrolytes based on zinc and manganese sulfates, whose introduction into the MnO_2 nanolayers during cycling was evaluated by in situ registration of the cathode mass changes by electrochemical quartz crystal microbalance.
6. Depending on the pH of the zinc acetate electrolyte solution, it was found that at pH = 4.5 the processes of electrolytic precipitation and incomplete dissolution of MnO_2 are observed, while at pH ≈ 6.0 a different picture is observed due to the low concentration of H^+ ions. In acetate electrolytes, the mechanism of electrolytic precipitation/dissolution of manganese oxide dominates. During the discharge process in the zinc sulfate-based solutions, first the intercalation of H^+ cations occurs with the parallel transition Mn^{IV} – Mn^{III} (E = 1.4 V),

further H^+ intercalation and simultaneous injection of Zn^{2+} ions led to the formation of basic zinc sulfate $Zn_4(OH)_6SO_4 \cdot nH_2O$ (E = 1.2 V).

7. During MnO_2 oxidation (at charge process), dissolution of basic zinc salt occurs with simultaneous deintercalation of Zn^{2+} and H^+ ions, which starts the process of deposition of additional MnO_2 layer by oxidation of Mn^{2+} ions.
8. The overall mechanism of the electrochemical process for the Zn//MnO_2 electrochemical system can be described as the co-intercalation of Zn^{2+} and H^+ cations, conjugated with the electrolytic precipitation and dissolution of MnO_2, proceeding with the participation of Mn^{2+} cations and the precipitation/dissolution of the ZHS basic salt precipitate.

Chapter 1. Literature review

1.1. Batteries as chemical power sources

Batteries are secondary chemical power sources, i.e. electrochemical devices that can be recharged when connected to an external circuit. The first battery developed in 1859 was the lead-acid battery. This battery consists of two lead plates immersed in a sulfuric acid solution, one of which is coated with lead dioxide PbO_2. This technology is still widely used both in stationary devices such as backup or emergency power systems and in in car starter batteries, despite its obvious drawbacks: toxicity of lead and its compounds, poor thermal stability (from −10 to +45 °C), low practical energy density (about 30 $W{\cdot}h{\cdot}kg^{-1}$ with a theoretical one of 167 $W{\cdot}h{\cdot}kg^{-1}$) as well as its significant weight.

On the second stage of batteries development nickel-based electrochemical systems were invented, particularly, nickel-cadmium batteries (1899) and nickel-metal hydride alkali batteries (1967) which have found their application in different types of electro vehicles, high-power devices as well as in the equipment operated at sub-zero temperatures. However, nowadays their usage is limited because of low environmental friendliness. Among other disadvantages nickel-based batteries it could be named low cycle lifetime (about 300 charge/discharge cycles) and high self-discharge rate.

In 1991, a new lithium-ion battery technology emerged in the battery industry, which now dominates portable electronics (laptops, smartphones, other "smart" devices) and is being introduced in electric vehicles (e.g., Tesla electric cars). The advantages of lithium-ion systems include high specific energy density (100 – 260 $W{\cdot}h{\cdot}kg^{-1}$), low self-discharge, high charge current density, and long life. However, lithium-ion batteries have several disadvantages, such as high flammability due to the use of ester-based organic electrolytes and cobalt-based cathode materials ($LiCoO_2$, $LiCo_xNi_yMn_zO_2$), high toxicity, low content and high cost of lithium and cobalt compounds.

The concept of the metal-ion battery, proposed in 1976 for lithium-ion systems, is based on the movement of metal cations contained in the electrolyte between the cathode and the anode with their subsequent reversible intercalation into the crystal lattice of the electrode materials. Based on this mechanism of electrochemical device operation, post-lithium metal-ion batteries are being developed [42–44] in which lithium ions are replaced by other monovalent (Na^+, K^+) [45–47] or multivalent cations (Mg^{2+}, Ca^{2+}, Zn^{2+}, Al^{3+}) [48–50]. The specific energy values of sodium-ion and potassium-ion batteries are lower than those of lithium-ion batteries: about 100 – 150 $W{\cdot}h{\cdot}kg^{-1}$ for sodium-ion and ≈ 150 – 180 $W{\cdot}h{\cdot}kg^{-1}$ for potassium-ion cells (Figure 1) [46]. In addition, it is worth noting that due to the large size of the dehydrated of Na^+ and K^+ ions, the selection of intercalation-type cathode materials is complicated by the need to create large channels for ion introduction. Comparative analysis shows that potassium-ion batteries have some advantages over sodium-ion ones: a more negative redox potential (−2.71 V for Na/Na^+ and −2.93 V for K/K^+), larger ionic radius, as a result of

K^+ ions are weaker Lewis acids which leads to less solvation effects, and higher specific capacity of graphite anode (273 mAh·g^{-1} for K^+ and 35 mAh·g^{-1} for Na^+), however, this technology is not mature enough to challenge the leadership of lithium-ion batteries [51].

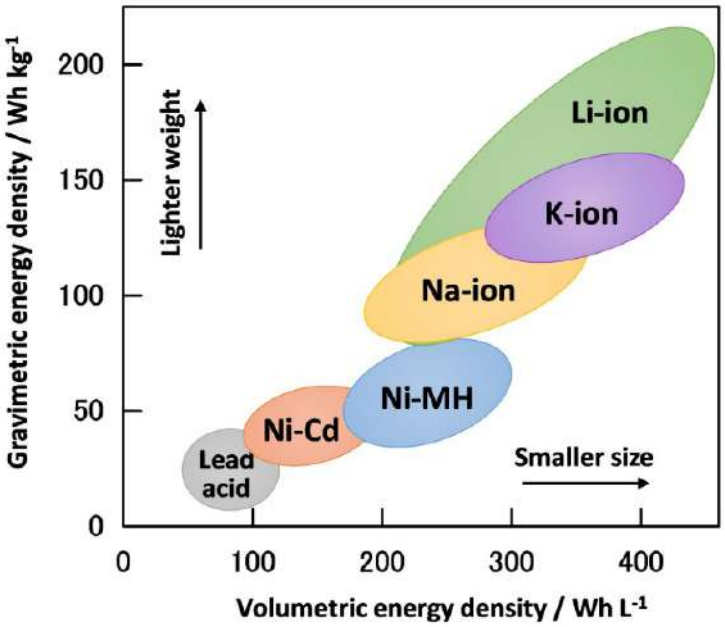

Figure 1. Energy density for different types of batteries [46].

The main advantage of multivalent metal-ion batteries over monovalent systems is their good compatibility with aqueous electrolytes, which increases the operational safety and environmental friendliness of this type of system. In addition, since these elements (Mg, Ca, Zn, Al) are widely distributed in the Earth's crust, the cost of producing batteries based on them will be lower compared to lithium-ion systems. To date, aqueous batteries with zinc anodes have been the most intensively researched [50]. However, one of the most challenging aspects of the study of multivalent metal-ion systems is the fundamental question of the mechanism of charge storage in these systems, which is complicated by stronger electrostatic interactions due to the larger charge of the cation, as well as the involvement of different cation species [49].

1.2. Aqueous zinc-ion batteries: operating principles

Among metal-ion batteries, aqueous zinc-ion batteries (AZIBs), in which metallic zinc is widely used as the anode, could be mentioned separately; they can also be called zinc-metal batteries. These electrochemical systems have attracted attention due to several factors: high abundance and consequently low cost of zinc, moderate negative potential (−0.76 V vs. $H_2/2H^+$) and high gravimetric (820 mAh·g^{-1}) and volumetric (5855 mAh·cm^{-3}) theoretical capacity of zinc-metal anode [52–56].

The operating principle of AZIBs is based on the electrochemical reaction associated with the migration of Zn^{2+} cations in the electrolyte solution between the cathode and the anode [57]. Contrary to the more common description of the mechanism of functioning lithium-ion batteries, in which the reversible intercalation of Li^{+} ions into the material structure is unambiguously realized (the so-called "rocking chair" mechanism [58]), the reversible intercalation of zinc ions into the cathode material structure is not unambiguously realized; therefore, possible electrochemical reaction pathways or multiple reactions occurring in such a system are intensively studied. Nevertheless, it is believed that during cell discharge, zinc ions enter the near-electrode space or cathode structure, participate in various electrochemical processes, and leave the cathode/electrolyte interface during charging. At the anode, there is a reversible process of zinc dissolution from the anode surface during discharge and its deposition during charging ($Zn^{0} \rightleftharpoons Zn^{2+} + 2\ e^{-}$). The scheme of this cell is shown in Figure 2.

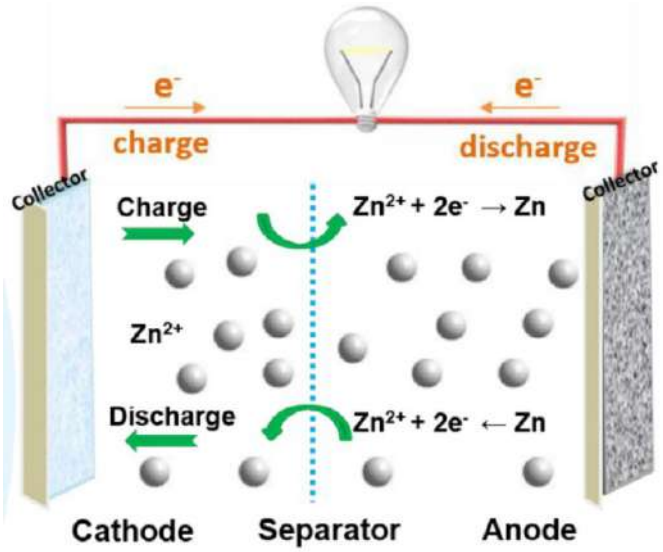

Figure 2. Scheme of aqueous zinc-ion battery [52].

Historically, electrochemical systems with a metal zinc anode have been known since 1865, when the salt galvanic cell or Leclanché cell was constructed. In this cell, in addition to zinc, a paste electrode based on MnO_2 was used, and the electrolyte was ammonium chloride solution, which is alkaline due to hydrolysis. Despite the researches published at the end of the XX century on the study of Zn//MnO_2 electrochemical system in solutions based on zinc sulfate with neutral or near neutral medium [59], the beginning of the research of MnO_2-based cathode materials with aqueous mildly acidic electrolyte for the rechargeable AZIBs is 2009, when the possibility of reversible intercalation of zinc ions into the MnO_2 structure with formation of $ZnMn_2O_4$ was found [60], and two years later the same research group proposed the concept of "zinc-ion batteries" [8]. The advantages of these cells include high capacity, charge/discharge rate, safety and environmental friendliness [54,61,62].

The practical importance of such batteries is due to several factors: the high abundance and consequently low cost of zinc, the availability and environmental friendliness of cathode materials (in the case of MnO_2 cathodes) [63], the compatibility of zinc with aqueous electrolytes, which allows the development of completely safe and non-flammable electrochemical systems. It is estimated that the energy cost of zinc-ion systems will be in the order of $65/kW·h, while the energy cost of lithium-ion battery is at least $300/kW·h [64]. Since 2022, there is a startup that aims to develop a full production cycle of zinc-ion battery: Salient Energy, Canada (company website https://salientenergyinc.com).

However, despite the development prospects, zinc-ion battery technology has not yet been widely adopted and industrialized. It is associated with the drawbacks inherent to cathode materials, metal zinc anodes and electrolyte solutions. In the case of cathode materials, the main problems are their dissolution during cycling, poor or low intrinsic electronic conductivity, slow diffusion of zinc ions due to strong electrostatic interactions with the cathode, and formation of by-products during discharge [56,64]. The electrochemical reaction mechanism is also complicated by interactions between cathode materials and Zn^{2+} cations in the electrolyte solution with water molecules or their autoprotholysis (H^+ or OH^- ions) [56].

Major problems with zinc anodes include zinc anode corrosion, which can promote a number of side processes: cathode product formation [65], zinc dendrite formation and hydrogen evolution reaction on the zinc surface, and zinc self-passivation during cycling [66]. To minimize surface side reactions, various porous organic (conducting polymers) and inorganic (oxide and salt films) coatings are applied to the anodes, and the electrolyte composition is varied to increase the reversibility of the anodic zinc deposition/dissolution reaction [52,67,68].

An important component of AZIBs is the electrolyte, which not only enables the transfer of zinc cations from the cathode to the anode, but can also influence the cathodic and/or anodic reaction mechanism. The main electrolytes are aqueous solutions of $ZnSO_4$ or $Zn(CF_3SO_3)_2$ with different concentrations [69,70] and pH value ≈ 4 – 5, which have the disadvantages of narrow electrochemical stability range, low Coulombic efficiency of zinc deposition/dissolution. Other salts ($ZnCl_2$, $Zn(NO_3)_2$, $Zn(ClO_4)_2$, $Zn(CH_3COO)_2$, $Zn[(CF_3SO_2)_2N]_2$) can also be used, non-aqueous electrolytes based on organic solvents are used much less frequently which is related to lower specific capacity values for cathode materials in these solutions [71]. Electrolyte improvement strategies are primarily aimed at improving interfacial contacts with the electrode surface, extending the range of electrochemical stability and operating temperatures, and improving zinc deposition efficiency.

Despite all the problems mentioned above, the properties of the battery are primarily determined by the properties of the cathode material. Many different variations of cathode materials have been proposed for AZIBs, which can be divided into several groups: transition metal oxides, of which manganese (MnO_2) or vanadium (V_2O_5) oxides are the most intensively studied [72],

hexacyanoferrates ($Zn_3[Fe(CN)_6]_2 \cdot H_2O$) and transition metal dichalcogenides (MoS_2), and organic cathodes based on quinone or polyaniline derivatives [10,63,73,74]. Based on the data comparing the energy and power of different cathode materials, it can be seen that manganese and vanadium-based materials are the most promising for commercial applications (Figure 3).

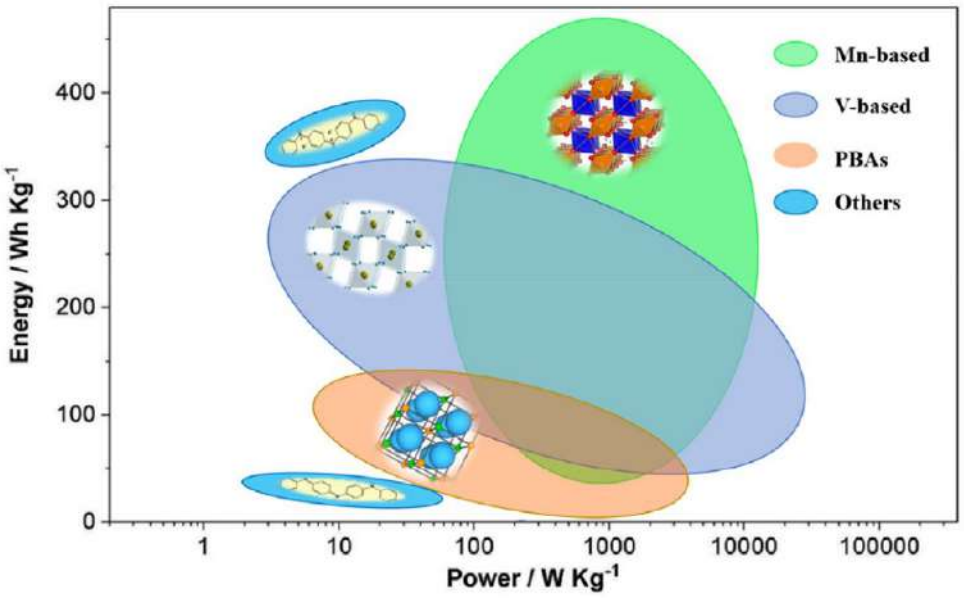

Figure 3. Ragone plot for different cathode materials for AZIBs [74].

1.3. Manganese oxide as cathode for aqueous zinc-ion batteries

Manganese dioxide MnO_2 is one of the first materials to be proposed as a cathode for aqueous zinc-ion batteries [6,60], and is still being intensively researched. Manganese oxide is composed of MnO_6 octahedrons which, depending on the coordination method, can form different structures of tunnel, layered or spinel type (Figure 4). The most abundant and intensively studied MnO_2 polymorphs are α-MnO_2 (2x2 tunnels, hollandite), β-MnO_2 (1x1 tunnels, pyrolusite), T-MnO_2 (3x3 tunnels, todorokite) γ-MnO_2 (2x1 tunnels, nsutite), ε-MnO_2 (dense structure, akhtenskite), δ-MnO_2 (1x∞ tunnels or layered structure, birnessite) and λ-MnO_2 or $ZnMn_2O_4$ (spinel structure) [10,75].

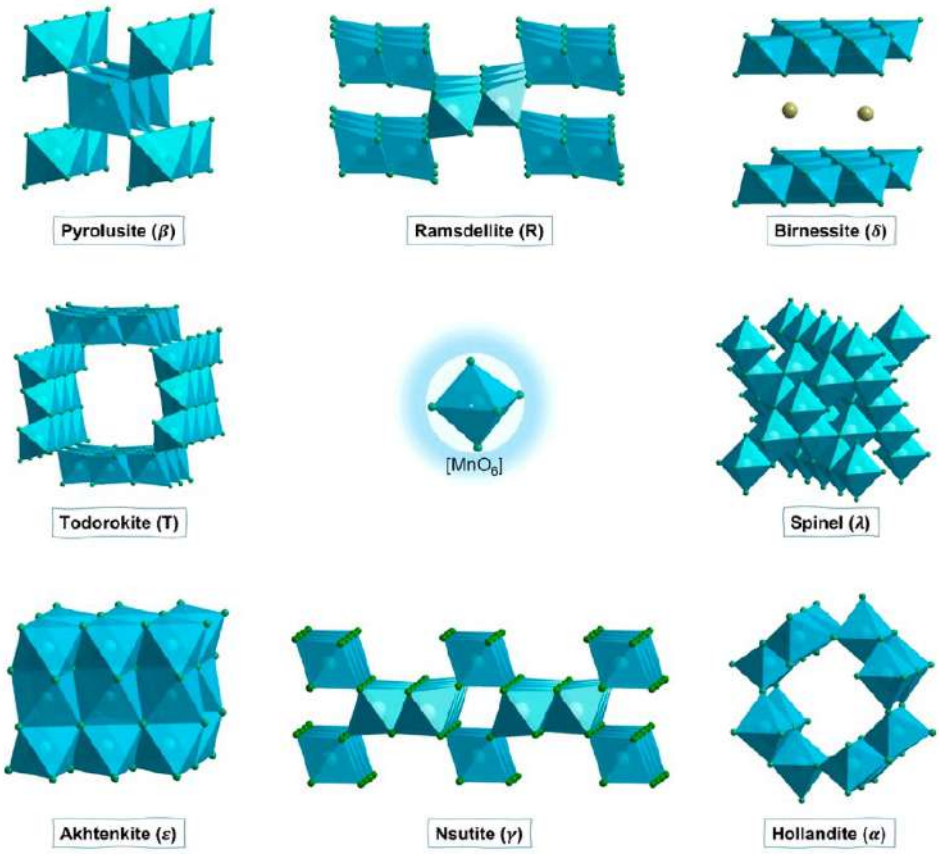

Figure 4. Crystal structures of various MnO_2 polymorphs [10].

Despite the different crystal lattice coordination types, the specific capacity of cathode materials is slightly dependent on the initial oxide structure due to the same redox process, in particular, Mn^{IV} – Mn^{III} or Mn^{IV} – Mn^{II} transitions [76,77]. However, different crystal structures influence the thermodynamics and kinetics of cation intercalation and deintercalation processes, affecting parameters such as initial material capacity, cyclic stability, and charge transfer parameters [77,78]. In particular, the spinel structures regardless of the characteristics described in the literature [79–81] are not the most suitable for the intercalation of Zn^{2+} ions due to the strong electrostatic repulsion of zinc, located in the tetrahedral position, from the MnO_6 octahedrons [82]. On the other hand, the layered materials held by weak interactions are attractive only because of the large interlayer distances (for example, in the structure of δ-MnO_2, also called birnessite, this parameter is 0.7 nm).

As mentioned above, high energy density values could be obtained for manganese oxide-based cathode materials. This could be related to several reasons: the high value of the redox transition potential (≈ 1.5 V vs. Zn/Zn^{2+}), moderate theoretical specific capacity (308 $mAh \cdot g^{-1}$ for Mn^{IV} – Mn^{III} transition or 616 $mAh \cdot g^{-1}$ for Mn^{IV} – Mn^{II} reaction) [83]. In addition, manganese oxide has a number of other advantages: low cost, environmental friendliness, ease of synthesis, and the ability to control the crystal lattice and morphology of the material by modifying certain synthetic procedures, i.e., to synthesize a material with the desired properties.

However, two major problems characterize MnO_2-based cathode materials: the low value of the intrinsic electronic conductivity ($\approx 5 \cdot 10^{-6}$ S·cm^{-1}) and the capacity loss during cycling process [17]. This is related to the reduction of Mn^{4+} to Mn^{3+} cation, which is unstable due to the distorted geometry of the structure (Jahn-Teller effect), leading to the disproportionation of Mn^{3+} to Mn^{4+} ions and soluble Mn^{2+} ions.

The main way to solve the problem of cathode dissolution is to add a salt containing Mn^{2+} cations to the electrolyte solution to suppress the dissolution of the oxide by excess concentration of Mn^{2+} ions [17,18,84,85]. Indeed, this approach has become extremely widespread, and currently a mixed electrolyte containing zinc and manganese salts is used in almost all studies of the properties of these cathode materials.

The following strategies can be considered as approaches to improve the properties of MnO_2-based cathode materials [6]:

1) MnO_2 crystal lattice control (synthesis of MnO_2 particles with given morphology);
2) Directed creation of defects in the MnO_2 crystal lattice;
3) Doping with foreign particles, including pre-intercalation with metal cations;
4) Development of MnO_2-based composite materials (addition of carbonaceous materials, conducting polymers).

All of the above approaches lead to a significant change in a number of properties at once: structure, morphology, conductivity, resulting in a change in the functional properties of cathode materials. They can also be used together for mutual reinforcement and greater improvement of cathode properties.

Another important issue is the question of the complex mechanism of electrochemical reactions in aqueous Zn//MnO_2 batteries. This complexity arises from the involvement of three types of cations (Zn^{2+}, Mn^{2+}, and H^+) and water molecules. The main difficulty is to reliably demonstrate the reversible movement of Zn^{2+} ions into the crystal lattice of MnO_2 due to strong electrostatic repulsion.

1.4. Approaches to enhance the properties of δ-MnO_2 based cathodes

Among the various strategies for modifying MnO_2-based cathodes, controlling the crystal phase is less common because most MnO_2 polymorphs are electroactive in aqueous mildly acidic zinc- and manganese-sulfate-based electrolytes. Nevertheless, layered manganese dioxide has a higher initial specific capacity compared to β-MnO_2 (126 mAh·g^{-1} and 100 mAh·g^{-1}, respectively, at the same current density value) due to more effective intercalation of H^+ ions in the oxide structure, i.e. lower charge transfer resistance due to greater interlayer distance [86]. Therefore, the use of layered manganese oxide is of greater interest because various metal cations, including Zn^{2+} cations, can be incorporated into the layered structure [11–13].

However, the layered structure is unstable during long-term cycling due to changes in the initial crystal lattice. To improve the cycling stability, different synthetic approaches could be used to obtain materials with different morphology. For example, manganese oxide nanoflakes obtained by thermal decomposition of $KMnO_4$ solution show poor cyclic stability (capacity retention ≈ 50% during 100 cycles) in the manganese-free electrolyte solution [87]. δ-MnO_2 nanosheets tested in the mixed 1 M $ZnSO_4$ / 0.1 M $MnSO_4$ electrolyte retain 66.5% of the maximum capacity at a current density of 0.1 $A \cdot g^{-1}$, which the authors attribute to the two-dimensional material structure with more surface contact with the electrolyte [88]. Manganese oxide with nanoflower morphology synthesized on the carbon paper surface showed an initial capacity value of 323 $mAh \cdot g^{-1}$ at current a density of 0.3 $A \cdot g^{-1}$ and during cycling at I = 5.0 $A \cdot g^{-1}$ almost 70% capacity increase up from 100 $mAh \cdot g^{-1}$ was observed over 5000 cycles [89]. The capacity increase effect could be related to additional manganese oxide deposition from the electrolyte solution on the cathode surface with low mass loading of electroactive material as well as the capacity response of the carbon current collector [88].

Another effective way to control the morphology of cathode materials is the development of nanostructured materials. For example, a 3D intertwined nano-network consisting of 1D δ-MnO_2 nanowires has been synthesized by hydrothermal method [90]. During the preparation of this material, carbon black, used as a conductive additive, penetrates inside the network, which leads to an increase in the overall electron-ion conductivity of the cathode and causes high values of specific capacities (342 $mAh \cdot g^{-1}$ at I = 0.162 $A \cdot g^{-1}$ and 150 $mAh \cdot g^{-1}$ at I = 6.5 $A \cdot g^{-1}$) as well as 75% of capacity retention over 400 cycles at I = 1.623 $A \cdot g^{-1}$. An alternative to such three-dimensional structures are hollow materials in which a void is created inside the grain of the active component. δ-MnO_2 hollow nanospheres were obtained on the surface of SiO_2 particles which were used as a template and further etched by alkaline solution (Figure 5, a) [91]. Materials with a hollow structure are preferable for the intercalation of ions because the diffusion of intercalated cations should be easier, which the authors confirm by measuring the impedance spectra at open circuit potential before and after the first charge/discharge cycle. The decrease of the charge transfer resistance after the first discharge is due to the facilitation of the intercalation processes of Zn^{2+} cations into the cathode structure. As a consequence, during 100 charge/discharge cycles at a current of 1 C for hollow materials, a gradual increase in the specific capacity is observed (Figure 5, b).

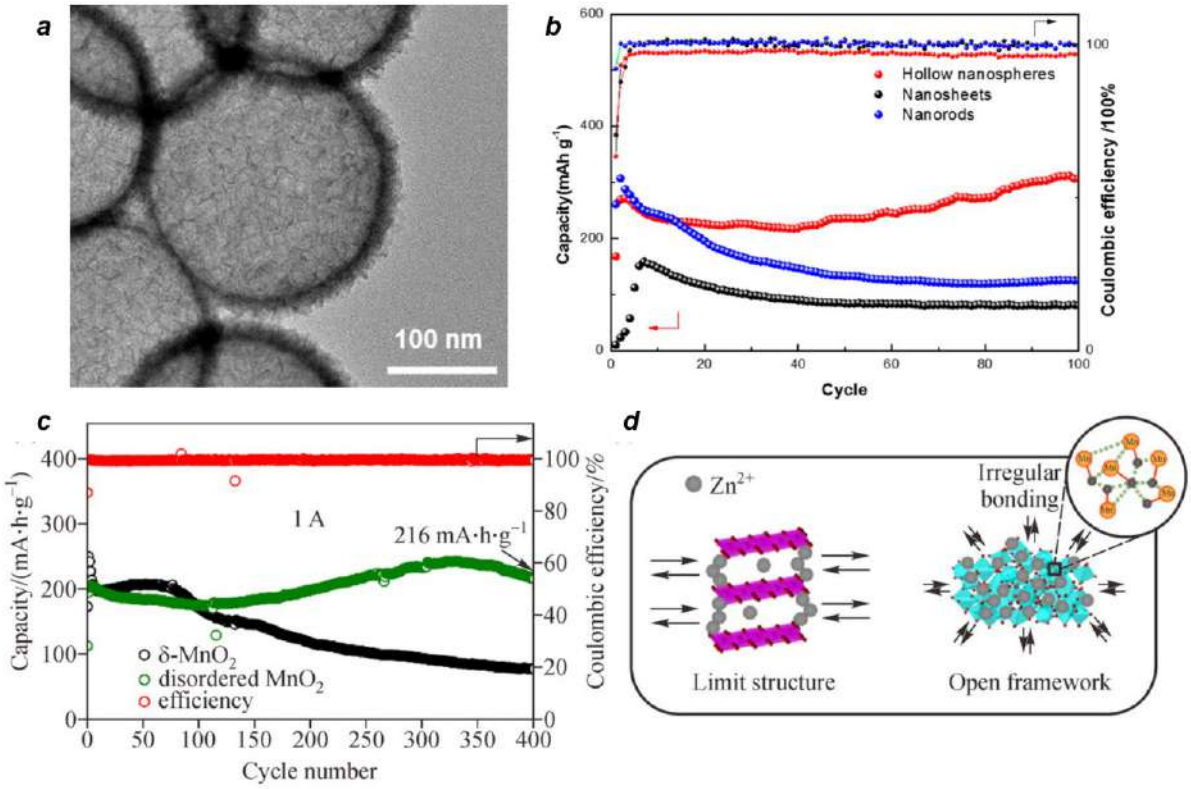

Figure 5. a) High-resolution TEM-image of MnO_2 hollow nanospheres; b) cyclic stability of MnO_2-based cathodes with different morphology [91]*; c) cyclic stability of MnO_2-cathodes with different crystallinity; d) ion diffusion pathways in crystalline and disordered materials* [92].

In most cases, to ensure high ion diffusion rates in the lattice of a material, researchers try to design materials with a high crystallinity, which is justified in the case of materials in which Li^+ or Na^+ cations are intercalated. Hydrated Zn^{2+} ions have a larger effective radius compared to Li^+ or Na^+, in addition, the higher charge leads to stronger electrostatic interactions with the crystal lattice of the material, resulting in the appearance of lattice defects and its "amorphization". Thus, the targeted development of disordered manganese oxides is also of interest to obtain improved functional properties [92,93]. In amorphous metal oxides, a high concentration of crystal lattice defects is observed, which reduces the number of interfaces and, consequently, the charge transfer resistance in the prepared electrode materials. In addition, the wettability of disordered materials is higher than that of crystalline materials [92]. During cycling, an artificial capacity growth was observed for such materials due to the deposition of additional electroactive ε-MnO_2 layer, and higher efficiency at higher discharge current density: ≈ 170 $mAh \cdot g^{-1}$ at a current density of 5.0 $A \cdot g^{-1}$ which is caused by an increase in the active vacancy quantity, which led to easier ion diffusion in the disordered material structure (Figure 5, c, d).

The design of MnO_2-based composite materials with different carbon-based substances is a traditional way to firstly improve the electronic contact between active material grains and specific surface area. In particular, the use of graphite as a matrix to form δ-MnO_2 nanoflowers led to at least a

twofold increase in the specific capacity of the material (up to 300 $mAh \cdot g^{-1}$ at a current density of 0.2 $A \cdot g^{-1}$) but did not affect the cyclic stability: the capacity fading was almost 50% of the maximum value after 100 cycles at a current density of 0.4 $A \cdot g^{-1}$ [94]. The preparation of the cathode material by electrodeposition of MnO_2 on the carbon nanotubes used by the authors [95] showed that despite the outstanding capacity values (≈ 200 $mAh \cdot g^{-1}$ at current density 2.0 $A \cdot g^{-1}$) the achieved effects of reducing the interfacial resistance and facilitating the ionic transport did not solve the problem of low cyclic stability. The addition of a layer of carbon nanotubes on the surface of carbon paper allowed the synthesis of a binder-free δ-MnO_2 cathode with high volumetric capacity (1.9 $mAh \cdot cm^{-2}$) and satisfactory cyclic stability (capacity retention was 76.7% of the initial value after 400 cycles at I = 0.2 $mA \cdot cm^{-2}$) [96]. The formation of carbon coatings of organic matter (lignin or dopamine) on the surface of the electroactive material grains improved the stability of the materials by reducing the direct contact between the cathode material and the electrolyte, which, according to the authors, reduced its dissolution [97,98].

Besides carbon-based materials, the approach of modifying cathode materials with conducting polymers is widely used and efficient due to their high electronic and ionic conductivity, chemical and electrochemical stability in aqueous electrolytes and low solubility in aqueous media [99,100]. The most commonly used conducting polymers are polyaniline (PANI), polypyrrole (PPy) and poly(3,4-ethylenedioxythiophene) (PEDOT) because of the wide range of easily controllable synthetic routes and conditions of the polymers themselves or composite materials incorporating them. It should be noted that conducting polymers could be used as coatings for electroactive grains or to intercalate polymer fragments into the manganese dioxide lattice, as will be shown later. Furthermore, it has been found that coating the zinc anode with conducting polymers (e.g. PPy) also improves the stability of the Zn//MnO_2 cell [101].

One way to obtain polymer-modified materials is the interaction at the interface between aqueous and organic phases or at the gas-liquid interface, which has been tested for MnO_2/PANI composites (Figure 6, a) [24,25]. As a result of the reaction, a manganese oxide with a birnessite structure is formed layer-by-layer, with polymer layers between the oxide layers, i.e. a partial introduction of polymer fragments into the MnO_2 structure takes place, which was indirectly demonstrated by an increase in the interlayer distances in the composite to ≈ 1.0 nm based on selected area electron diffraction data. In addition, the specific surface area is also improved by polymer incorporation. The specific capacity of the cathode material was 250 – 300 $mAh \cdot g^{-1}$ at a current density of 0.2 $A \cdot g^{-1}$, as well as high (> 90%) cyclability and coulombic efficiency at different current densities (Figure 6, b). Another method of aniline polymerization is to use the MnO_2 matrix as an oxidizing agent, so that during monomer oxidation there is a controllable decrease in the oxidation state of manganese in the resulting composite. Nevertheless, the main valence state of manganese is Mn^{4+} based on XPS

data [26]. As in the case of the polymer-intercalated material, the cyclic stability at different current densities is significantly improved (in particular, at I = 2.0 A·g^{-1} the capacity fading was 18% after 2000 cycles). This improvement is due both to the formation of a physical barrier to the uncontrolled dissolution of MnO_2 and to the facilitation of ion diffusion.

The strategy of developing ternary composites based on manganese oxides, carbon materials and conducting polymers has also proved successful in the field of electrode materials for metal-ion batteries. A polyaniline-coated composite material with reduced graphene oxide (rGO), was prepared by a two-step process of mechanical mixing of MnO_2 and rGO and hydrothermal treatment, followed by synthesis of PANI the presence of ammonium persulfate on the surface of the material [32]. The presence of the polymer increased the specific surface area of the composite and improved the electronic contact between the composite particles, and PANI also acted as a protective barrier, suppressing the dissolution processes of the cathode material. Together, this resulted in a 20 – 30% increase in specific capacity over a wide current range, as well as an improvement in cyclic stability (capacity retention was 83% over 600 cycles at 1.0 A·g^{-1}). Similar characteristics were achieved when MnO_2 itself was used as an oxidizing agent [33]. In addition to the capacity improvement, analysis of the material properties by cyclic voltammetry showed that for any value of the scan rate, the pseudocapacitive contribution to the total capacity of the material increases in the presence of the polymer. The use of the aniline derivative 4,4'-bis-oxybenzylamine for the deposition of the polymer on the carbon paper surface followed by the electrodeposition of MnO_2 nanospheres, allowed to obtain a cathode material without the use of conductive additives and binders, with high capacity and cyclability (150 mAh·g^{-1} at I = 2.0 A·g^{-1} and capacity retention of 89.3% over 2000 cycles) [102]. Using density functional theory method, it was shown that Mn–O–C bonds between the oxide lattice and the carbon matrix, as well as Mn–N bonds between MnO_2 and PANI, stabilize the cathode structure and thus improve the electronic and ionic contact in the material.

Compared to polyaniline, polypyrrole has a higher thermal and chemical stability due to its heterocyclic structure, which also determines its application in cathode materials for AZIBs [103]. Both MnO_2//PPy composites [27,28] and ternary composites with carbon-based materials [30,31,104] have been studied. The incorporation of conducting polymer allows to increase the cyclic stability of cathode materials and to promote more intense artificial capacity growth at low current density due to the formation of Mn–N bonds [27]. In turn, the co-synthesis of MnO_2 in the presence of pyrrole allows the preparation of microspheres composed of β-MnO_2 nanorods and PPy nanowires. This composite material showed the specific capacity value of 105 mAh·g^{-1} at I = 1.0 A·g^{-1} and high cyclic stability at low current density value [28]. The use of carbon nanotubes resulted in the increase of the initial specific capacity up to 160 mAh·g^{-1} at a current density of 1.0 A·g^{-1} due to the sharp decrease of the charge transfer resistance, as well as the facilitation of the ionic diffusion in the three-dimensional

highly porous structure with uniform distribution of all components [30]. The authors [31] deposited MnO_2 on graphene oxide followed by polypyrrole coating. The material consisted of continuous yarns in which oxide nanowires were coated with the polymer, which allowed achieving the specific capacity of 190 $mAh \cdot g^{-1}$ at I = 1.0 $A \cdot g^{-1}$. Thus, the main contribution to the improvement of the electrochemical properties of cathode materials is made by the carbon additive, and the conducting polymer additionally enhances its effect.

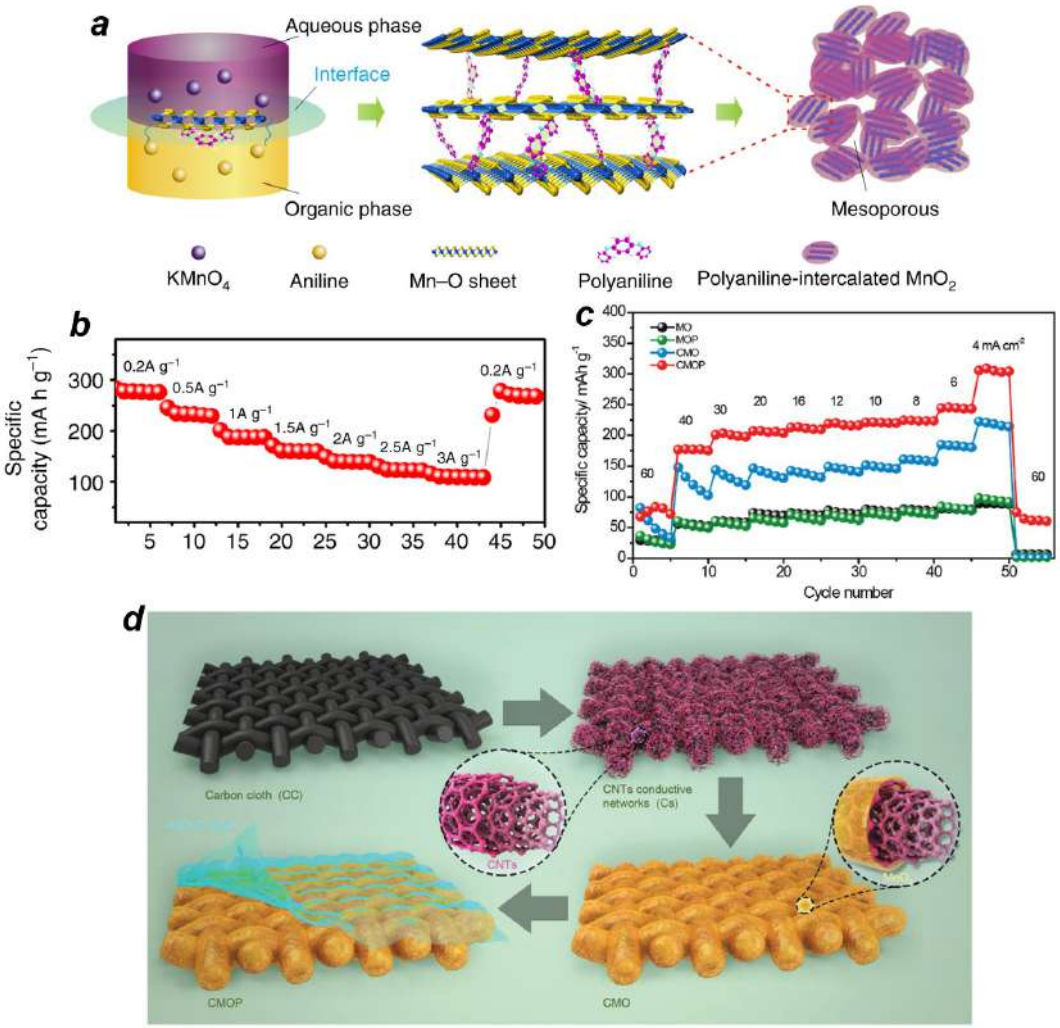

Figure 6. a) Schematic illustration of expanded intercalated structure of polyaniline (PANI)-intercalated MnO_2 nanolayers [25]*; C-rate capabilities for PANI-intercalated oxide (b)* [25] *and for PEDOT-modified cathode (c)* [105]*; d) schematic diagram illustrating the 3D structure of CNTs conductive networks and PEDOT-modified MnO_2-based ternary composite* [105].

One of the most widely considered conducting polymers at present is poly(3,4-ethylenedioxythiophene) (PEDOT) due to its high chemical, thermal and electrochemical stability as well as low solubility in almost any type of solvent and excellent conductivity for this class of compounds and the various available preparation methods [106]. In particular, chemical precipitation of PEDOT using potassium permanganate as oxidant and MnO_2 precursor is possible, but this method

is rather long. During *in situ* polymerization and $KMnO_4$ reduction, the polymer-coated δ-MnO_2 nanowires were obtained with the length of hundreds of nanometers, with additional voids formed between them [107]. This composite showed the specific capacity of 133 $mAh \cdot g^{-1}$ at a current density of 2.0 $A \cdot g^{-1}$, due to the increased pseudocapacitive contribution to the total capacity of the material due to the presence of the polymer coating. Cyclic stability was also improved, with capacity retention of 85% over 1000 cycles at 2.0 $A \cdot g^{-1}$ over 1000 cycles. The specific energy of this material amounted ≈ 406 $W \cdot h \cdot kg^{-1}$ at the power of 0.5 $kW \cdot kg^{-1}$. The oxidation reaction of a solution containing EDOT monomer and manganese sulfate with potassium permanganate solution yielded manganese oxide with a layered structure with oligomeric fragments between the oxide layers [108]. Although the authors claim an increase in the interlayer spacing, which they confirm by X-ray diffraction and transmission electron microscopy, this increase is insignificant (d ≈ 0.7 nm), which is standard for birnessite. The polymer content in the composite was about 6.5%, which resulted in an increase in the porosity of the material, leading to improved contact with the electrolyte, and a non-significant increase in the interlayer spacing to facilitate ionic transport. Another way to form a polymer coating on the surface of a material, using manganese oxide as an oxidizing matrix, was used to deposit a PEDOT coating on the surface of MnO_2 microspheres [34]. During the synthesis, ε-MnO_2 particles of ≈ 1.5 μm in size were obtained, the thickness of the polymer coating was up to 4 nm, and the polymer content was up to 8.8%. The values of the specific capacity are comparable to the previously discussed composite [108] (135 $mAh \cdot g^{-1}$ at I = 2.0 $A \cdot g^{-1}$), and the increase in the pseudocapacitive contribution was also shown, i.e., the polymer coating plays the role of a physical barrier and contributes to the specific capacity through the accumulation of double-layer capacity by the nonfaradaic mechanism, regardless of the initial oxide structure.

Preparation of ternary composites based on MnO_2, PEDOT and carbon additives also improved both functional properties and kinetic parameters of charge transfer. The most unusual example is the preparation of conventional electrode material from the mixture of manganese dioxides (α-MnO_2 and δ-MnO_2) on the carbon paper with subsequent electrodeposition of PEDOT on the electrode surface [35]. According to transmission electron microscopy data, the particles of δ-MnO_2 were homogeneously distributed and interconnected by α-MnO_2 nanowires, and a polymer layer was deposited on the surface for greater stability. This route resulted in superior specific capacity values (360.5 $mAh \cdot g^{-1}$ at 0.1 C and 94 $mAh \cdot g^{-1}$ at 5 C) and also significantly increased the rate of ion diffusion into the material structure. An alternative approach of deposition of MnO_2 on the surface of carbon material followed by application of PEDOT:PSS dispersion was used to obtain a graphene matrix composite [36]. This three-layer structure resulted in a highly porous material as well as a three-dimensional network for electrolyte distribution within it. This allowed to achieve a specific capacity of 148 $mAh \cdot g^{-1}$ at I = 6.0 $A \cdot g^{-1}$ and a capacity retention of 68% after 1000 cycles at I = 5.0 $A \cdot g^{-1}$.

Sequential electrodeposition on the surface of carbon nanotube-modified carbon cloth first with MnO_2 and then with PEDOT, yielded a coaxial cable structure based on interconnected nanotubes coated with MnO_2 and a rough thick layer of PEDOT uniformly distributed on the surface [105]. This material exhibited a capacity of 176 mAh·g^{-1} at I = 10.8 A·g^{-1}, which is one of the highest achieved at high material loading (about 3 mg·cm^{-2}) (Figure 6, c, d).

Another frequently used strategy to improve the properties of cathode materials for AZIBs is the introduction of heteroatoms into the MnO_2 structure. [109]. The introduction of foreign metals allows to achieve several positive effects: increase of interlayer distances in the crystal lattice of the material, formation of a larger number of defects in the structure and lattice stabilization due to the formation of new chemical bonds between MnO_6 octahedrons and metal cations. To date, a large number of papers have been published on the synthesis of pre-intercalated manganese oxides and their study in various fields, including aqueous zinc-ion systems. Very different ions can be considered as dopant cations: M^+ (Li^+, Na^+, K^+, NH_4^+), M^{2+} (Ca^{2+}, Zn^{2+}, Co^{2+}, Cu^{2+}), M^{3+} (Al^{3+}, Bi^{3+}, Fe^{3+}, Co^{3+}, La^{3+}, Ce^{3+}) and others (Sn^{4+}, V^{5+}, Mo^{4+} – Mo^{6+}). The manipulation of lattice parameters in the case of layered manganese oxide is of particular interest due to the stabilization of the structure and prevention of dissolution of the material during cycling.

Comparative analysis of cathode materials based on MnO_2 doped with different ions of the same chemical nature has been performed for alkali metal ions [110] and VIII group transition metal ions [111]. In the case of doping by M^+ ions, K^+-doped materials were found to have the best functional performance (270 mAh·g^{-1} at I = 0.1 A·g^{-1} and 95 mAh·g^{-1} at I = 3.0 A·g^{-1}), for which larger interlayer spacing values (0.65 nm) were obtained by high-resolution transmission electron microscopy and X-ray diffraction compared to Li^+ (0.52 nm) or Na^+ (0.55 nm) doped materials (Figure 7, a, b). The slight decrease relative to the standard interlayer spacing in the birnessite structure in all doped materials is caused by the absence of intercalated water molecules [110]. In this context, potassium ions, whose presence in the structure is most often due to the use of $KMnO_4$ as a precursor, give the greatest positive effect on the properties of cathode materials, which is confirmed by a number of studies [112–116]. For the transition metal ions (Fe, Co, Ni) the comparative analysis showed that the Fe_xMnO_2 material is more stable during long cycling than the Co- and Ni-doped ones [111]. Nevertheless, Co^{2+} ions are often used to improve manganese oxide-based cathodes [117–119], since cobalt cations are able to suppress the Jahn-Teller effect and also have a positive effect on the electronic and ionic conductivity of the cathode material. An interesting effect in the presence of cobalt ions is the facilitation of MnO_x deposition on the cathode surface due to the intrinsic electrochemical transition of $Co^{2+} \leftrightarrow Co^{3+}$, which led to the constant capacity growth at low current densities (Figure 7, c) [117]. Electrodeposition of Co-doped MnO_2 on the carbon cloth from solution containing Zn^{2+}, Mn^{2+} and Co^{2+} ions allows obtaining the material doped by Zn^{2+} and Co^{3+} ions which resulted in a

significant increase in the cyclic efficiency at high current rates: in particular, the values of the specific capacity of 280 mAh·g^{-1} at I = 1.2 A·g^{-1} and 205 mAh·g^{-1} at I = 3.0 A·g^{-1} were obtained while the unmodified material exhibited 170 and 70 mAh·g^{-1} at the same current densities [118].

The pre-intercalation of Zn^{2+} into the MnO_2 crystal lattice is an attractive way to improve the electrochemical performance due to their intended reversible insertion/extraction into the MnO_2 host during the cycling process in Zn-containing electrolytes [120–123]. The introduction of zinc ions into the layered structure of manganese oxide led to an increase in the strength of the crystal structure of the oxide and also significantly increased the specific surface area of the particles. In manganese-containing electrolyte solution Zn-doped materials demonstrated extremely high cyclic stability, the capacity fading in different modes (1 and 3 A·g^{-1} over 500 and 2000 cycles, respectively) was too low (about 10% over 2000 cycles Such high stability could be related to the increase of the specific surface area and the deposition of MnO_2 from the electrolyte solution [120]. Enhancement of the positive effects of doping with metal ions can be achieved by additional modification with carbon materials. In particular, the synthesis of a complex composite material based on Zn-doped MnO_2 with graphene quantum dots (GQDs) allowed to obtain nanoflowers up to 200 nm in size, uniformly covered with quantum dots (Figure 7, d). This synergistic effect reduced the polarization in the cell by 50 – 100 mV and also significantly reduced the charge transfer resistance between the particles, which is due to the improved electronic contact (Figure 7, f, g). The specific capacity value at a current density of 1.0 A·g^{-1} was about 370 mAh·g^{-1}, the capacity retention was 88% of the initial value over 500 cycles [123].

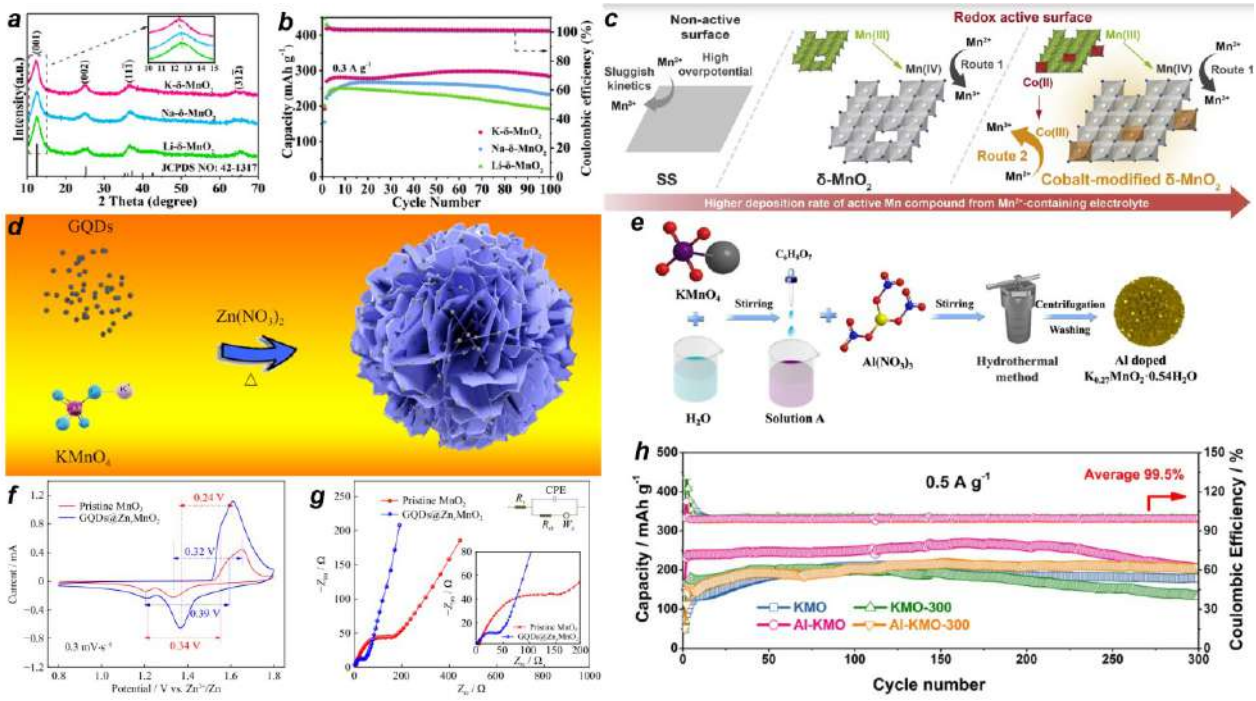

Figure 7. X-ray diffraction patterns (a) and cyclic stability at a current density of 0.3 A·g^{-1} (b) for M-δ-MnO$_2$ cathodes (M = Li, Na, K) [110]*; illustration of the mechanism of the catalysis effect via Mn self-catalysis (Route 1) and via cobalt-induced catalysis (Route 2) (c)* [117]*; synthesis of Zn-MnO$_2$ composite with graphene quantum dots (d)* [123] *and Al-doped K$_{0.27}$MnO$_2$ (e)* [124]*; CV curves (f) and impedance spectra (g) for GQDs@Zn$_x$MnO$_2$ composite material* [123]*; h) cyclic stability of MnO$_2$-cathode doped by K$^+$ and Al^{3+} ions* [124].

Strong bonds between trivalent metal ions and the oxygen sublattice of manganese oxide significantly improve the structural stability of doped materials. M^{3+} metal ions, i.e. Al^{3+}, La^{3+}, Bi^{3+}, can be used as dopants [124–128]. Large heterovalent particles (La^{3+}, Bi^{3+}) increase the size of diffusion channels, which facilitates the processes of ion transport into the lattice of the cathode material. However, due to the large radius of the dopant ions, the intrinsic electron transfer in the cathode structure is disturbed, leading to a decrease in the functional properties, as has been shown for Bi-doped δ-MnO_2-based cathodes [128]. Thus, a balance between the charge of the cation and its size is required to ensure stability of the crystal structure and high ionic conductivity.

An interesting approach is the simultaneous introduction of two ions of similar or different chemical nature. For example, the introduction of two alkali metal ions (Na^+ and K^+) into the layered structure of δ-MnO_2 led to an increase in the interlayer distances in the material structure, which facilitated the diffusion of ions in the material and increased the cyclic stability up to 95% at a current density of 0.5 A·g^{-1} [129]. The simultaneous use of monovalent (K^+) and trivalent (Al^{3+}) ions in the hydrothermal synthesis of bi-doped δ-MnO_2 structure (Figure 7, d) [124] allowed the authors to obtain the material with a smaller crystallite size (the grain size for bi-doped Al-KMO was 6.7 nm, and for KMO it was 8.4 nm), i.e. the presence of Al^{3+} ions facilitated the nucleation of the material particles. This technique increased both the specific capacity of the material (314 mAh·g^{-1} at 0.2 A·g^{-1}) and the

stability during cycling (capacity retention was 85% over 300 cycles at 0.5 $A \cdot g^{-1}$). In addition, the authors declare that doping with Al^{3+} cations stabilize the layered oxide structure, which allows achieving a high degree of cyclability of the material (Figure 7, h).

The electrochemical properties of metal ion-doped oxides can also be improved by the addition of carbon-based materials. For example, the directed electrodeposition of Na-doped manganese oxide on the surface of a graphene-like carbon substrate made it possible to produce an oxide uniformly distributed on the surface of the carbon material, which was further used as an electrode without the preparation of conventional electrode material [130]. The outstanding electrochemical performance of this cathode material (382 $mAh \cdot g^{-1}$ at 0.1 $A \cdot g^{-1}$ and 75% of capacity retention over 1000 cycles at 1.0 $A \cdot g^{-1}$) is related to the highly porous 3D structure of the composite material and the stronger electrostatic interaction between Zn^{2+} ions and the MnO_2 crystal lattice, which was confirmed by theoretical calculations. Chemical synthesis of manganese oxide doped with potassium cations on the surface of SiO_2 spheres as a template, followed by its removal, led to the preparation of hollow porous spheres of hydrated K-doped MnO_2 coated with a carbon shell [131]. This material was able to operate efficiently at high charge/discharge rates due to its large porosity and many voids, and it also provided a cyclic stability of over 80% during 2000 or even 6000 cycles. Due to the synergistic effect of the intercalation of K^+ ions, a large number of oxygen vacancies and mesoporous hollow carbon nanospheres in the structure, improved charge transport and reduced material volume change during cycling are achieved, resulting in brilliant charge transfer kinetics, as shown by impedance spectroscopy: a threefold decrease in charge transfer resistance after 30 charge/discharge cycles was observed, as well as a decrease in the Warburg constant, indicating the facilitation of diffusion processes.

Cathode materials based on doped manganese oxides modified with conducting polymers are also intensively studied nowadays, since the application of a conducting polymer coating allows stabilizing the material and minimizing the dissolution process, and doping, by partially changing the crystal lattice and increasing the interlayer distance, facilitates the transport of charge and ions in the material lattice. For example, Fe^{3+}-doped α-MnO_2 was coated by PPy [29] during chemical polymerization, where MnO_2 itself was used as an oxidant, while Fe^{3+} ions did not participate in the oxidation reaction. An alternative way to obtain the polymer coating is electrochemical polymerization, which was applied to PEDOT/Co-MnO_2 composite [132]. In both cases, an improved performance in terms of discharge capacity and cyclic stability of the cathode materials was achieved due to the above-mentioned factors, which was confirmed both by the reduction of the charge transfer resistance and by various methods of diffusion parameter estimation.

Thus, there are several ways to control and improve the properties of MnO_2-based cathode materials, but the most interesting are those that are readily available and reproducible, as well as

advantageous in terms of the characteristics obtained. Obviously, a combination of different approaches is more effective than any single approach, but these are, in most cases, difficult to scale up processes where it is difficult to achieve 100% reproducibility of both structural-morphological and electrochemical properties of cathode materials.

1.5. Electrochemical reaction mechanism of Zn//MnO_2 batteries

One of the most important issues in aqueous zinc-ion batteries has been the mechanism of the electrochemical reaction in the mildly acidic aqueous electrolyte. The presence of water molecules and Mn^{2+} ions along with the presence of Zn^{2+} in the electrolyte solutions competing with each other complicates a better understanding of the reactions that occur.

Nowadays, several main opinions about the electrochemical reaction mechanism in Zn//MnO_2 cell have been proposed [37,133,134]:

1) Reversible intercalation of only Zn^{2+} ions;
2) Absence of zinc intercalation and participation only of H^+/H_3O^+ ions;
3) Co-intercalation of Zn^{2+} and H^+ ions mechanism;
4) Electrolytic deposition/dissolution of MnO_2.

In addition, some difficulties are caused by the formation of the salt $Zn_4(OH)_6SO_4 \cdot nH_2O$ (zinc hydroxide sulfate, ZHS) during discharge, which occurs due to the local due to the local change in the pH of the electrode layer and the increase in the concentration of $[Zn(H_2O)_6]^{2+}$ complex ions [135]. The role of this basic salt is not limited to the formation of a physical barrier to further ion intercalation and/or a barrier to the dissolution of MnO_2 from the cathode surface. On the contrary, since its reversible dissolution occurs during cycling, this surface process affects the content of Zn^{2+} and H^+ ions in the near-electrode layer, thus forming a dynamic equilibrium near the cathode surface [136].

In accordance with the more common monovalent metal-ion systems (lithium-ion, sodium-ion batteries), a mechanism of reversible intercalation of zinc ions into the crystal lattice of the cathode material and, in the case of layered oxides, into the interlayer space has been proposed [17,29,113,125,137]. It should be noted that in recent reports this mechanism is discussed only for pre-intercalated manganese oxides, which could be related to the influence of the doping ion on the crystal lattice and, as a consequence, the suppression of some of the possible reactions (Figure 9, a). This mechanism can be considered historically as the first one proposed [8,60], but numerous studies by other authors have shown that this approach was not quite correct, since it did not take into account a number of parameters important for the functioning of the cell.

Another variant of the mechanism mentioned in the literature, which generally does not take into account the participation of zinc in the cathodic reaction, is the reversible intercalation of H^+/H_3O^+

ions, which causes the transformation of the original MnO_2 lattice [20,22,138–140]. In this mechanism, the change in proton concentration due to their intercalation leads to local changes in pH, which explains the fact that the functional properties depend on the acidity of the solution. A detailed study of the pH changes during cycling [22,138] showed that the local pH value changed from 4.3 to 5.2 because further pH increase up to 5.6 led to the oxygen evolution reaction, which can be a competitive process at high cell voltages. This mechanism explains the formation of the surface layer of ZHS salt as a product of local alkalinization of the near-electrode area during which Zn^{2+} ions are not intercalated into the cathode structure but react with the formed OH^- anions, resulting in the formation of the basic salt precipitate on the electrode surface (Figure 9, b). *In operando* pH measurements in different electrolytes performed in [22] showed that for pristine $ZnSO_4$ solution pH value reached 5 and practically unchanged during cycling, while in $MnSO_4$ solution and mixed electrolyte pH fluctuations are observed: decrease in the potential region $E \approx 1.7$ V and increase at $E \approx 1.3$ V, which correlate with the precipitation processes of MnO_2 and ZHS, respectively (Figure 8).

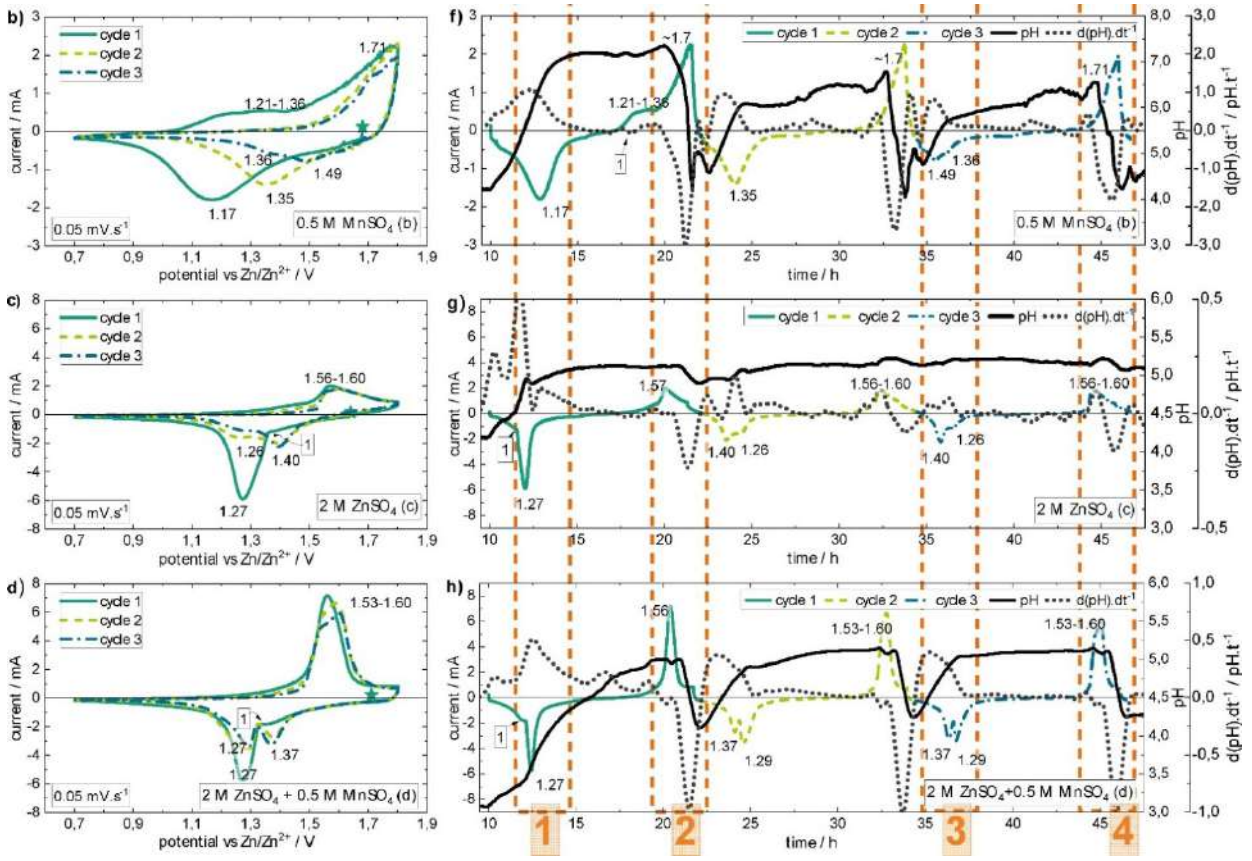

Figure 8. CV curves for Zn//MnO_2 cell depending on the electrolyte composition (left) and CV curves as I – t dependencies combined with pH measurements in operando (right) [22]

Similar observations have been made with other additives that buffer the system, i.e. after the addition of 0.1 M KH_2PO_4 solution [141]. The authors observed that in the presence of potassium

dihydrophosphate in solution, the pH of the electrolyte did not exceed 2.8, they also observed the improved functional performance at high current densities (61% capacity retention after 9000 cycles at 5 $A \cdot g^{-1}$). Nevertheless, the purely proton mechanism does not explain in any way the shape of the CVs or charge/discharge curves, nor does it account for the formation of the observed zinc-containing phases on the cathode's surface.

The most common version of the description of the electrochemical reaction mechanism is the double intercalation or co-intercalation of Zn^{2+} and H^+ ions. One of the versions of such mechanism is shown in the scheme below: during the first cycle Zn^{2+} ions intercalate, then H^+ ion becomes the main participant of the reaction, and as a result of the process Zn_xMnO_2 and MnOOH phases are formed (Figure 9, d) [11]. These discharge products can be related to the joint introduction of protons and Zn^{2+} ions into the lattice with partial reduction of MnO_2 and local pH increase near the electrode surface. The *ex situ* XPS data showed that the valence state of manganese in the fully discharged state is close to Mn^{3+} and also confirmed the presence of Zn^{2+} ions, leaving the cathode structure in parallel with the ongoing process of manganese oxidation $Mn^{3+} \rightarrow Mn^{4+}$ [142].

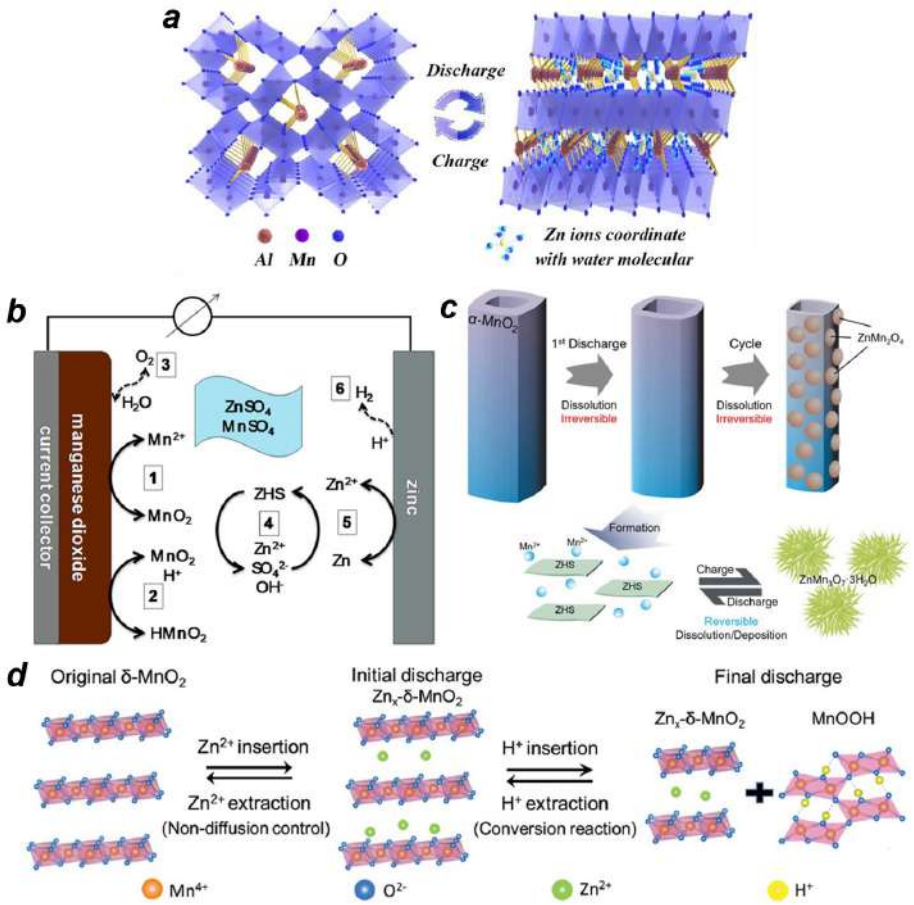

Figure 9. a) Scheme of phase transitions in Al-doped MnO_2 material with reversible intercalation of Zn^{2+} ions [125]*; b) Summary of the chemical processes in the AZIB with a Zn/$ZnSO_4$+$MnSO_4$/MnO_2 cell in the absence of Zn^{2+} intercalation* [22]*; c) Schematic illustration of the reaction mechanism of α-MnO_2 in AZIBs with the dissolution/deposition mechanism* [143]*; d) Joint non-diffusion controlled Zn^{2+} intercalation and H^+ conversion reaction mechanism in δ-MnO_2* [11].

This process also explains well the formation of electrochemically inactive phases such as $ZnMn_3O_7$ by the reaction between the ZHS surface salt and Mn^{2+} ions from the electrolyte solution, while MnOOH is converted to MnO_2 during the charging process. This indicates that all three types of ions (H^+, Zn^{2+} and Mn^{2+}) are involved in the reaction, and many forms of zinc-containing manganese oxides and ZHS coexist in the discharged state after prolonged cycling, and all phases except ZHS are formed irreversibly [136]. In addition, according to this version of the mechanism, the intercalation of different ions occurs at different stages of the discharge: in the region of potentials $E \approx 1.4$ V the intercalation of H^+ is usually assumed, and in the region of potentials $E \approx 1.2$ V – the participation of Zn^{2+} ions [25,28,88,90,97].

Nevertheless, in several reports, no or weak reversible intercalation of Zn^{2+} occurred, while irreversible insertion of Zn^{2+} with structural transformations of MnO_2 cathodes was observed [20,139]. This leads to the following interpretation of the mechanism, which has been actively discussed in the last 2-3 years, according to which the main process of charge storage in the cell is the electrolytic deposition and dissolution of manganese oxide during cycling (Figure 9, c) [140,143–145]. One of the most obvious factors supporting this version of the mechanism is the decrease in the electroactivity of the system in solutions without Mn^{2+} ions [21]. In addition, the maintenance of the reversible cathode capacity under conditions of suppressed Zn^{2+} ion transport can also serve as evidence for this reaction pathway. For example, the use of chelating agents, such as sodium trimetaphosphate, allowed to reduce the zinc fraction in the overall electrochemical reaction due to the formation of strong complexes with Zn^{2+} ions, and to suppress the formation of the basic zinc salt on the cathode surface, while the electroactivity of the system was retained [139]. This mechanism is based on the process of formation and dissolution of the “active phase” of MnO_2 on the surface of the cathode (or current collector), however, despite a number of experimental evidences [145], it does not explain the participation of Zn^{2+} ions, repeatedly stated by other authors.

Studies of non-aqueous Zn//MnO_2 systems are worth considering separately, since the use of aprotic solvents primarily excludes the possibility of H^+ ion transport, so the main process should be the reversible intercalation of Zn^{2+} ions. In particular, the Zn//MnO_2 cell was tested in a solution of $Zn[N(CF_3SO_2)_2]_2$ dissolved in acetonitrile [146]. In non-aqueous solvent and in the absence of manganese ion additives in the electrolyte, the reversible capacity of the cell was 123 $mAh \cdot g^{-1}$ at a current density of 0.04 C. Moreover, the shape of the charge/discharge profiles is drastically different from those observed in aqueous electrolytes: a plateau is observed at $E = 1.37$ V, and the general shape of the curve resembles a pseudo-capacitive curve with a quasi-linear potential drop (Figure 10). The capacity value correlates with the intercalation of 0.2 mol of Zn^{2+} per one structural unit of MnO_2, while a reversible transition between the layered structure and spinel structure occurs, which is

confirmed by XRD data. Thus, in non-aqueous electrolytes, the main charge storage process is indeed the intercalation of Zn^{2+} ions, which causes a structural transformation of the material, resulting in a slow capacity decrease. These processes have also been observed in lithiated manganese oxides [71].

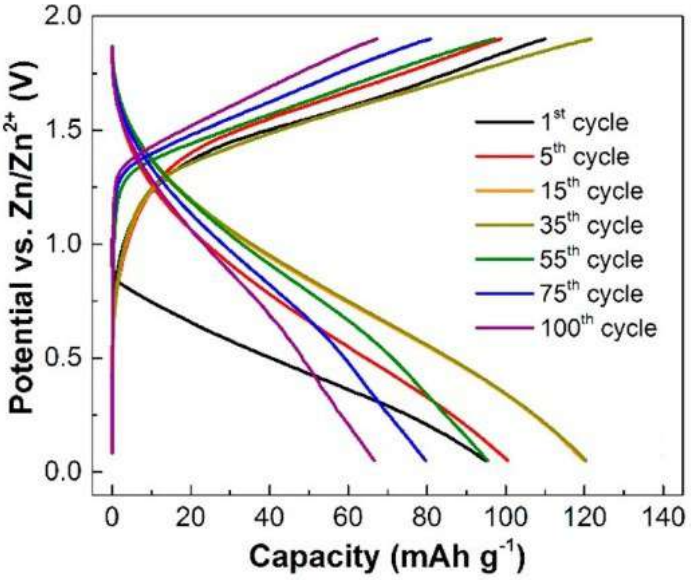

Figure 10. Charge/discharge curves for Zn//MnO_2 cell in the 0.5 M Zn[$N(CF_3SO_2)_2$]$_2$ electrolyte dissolved in acetonitrile at current density 0.04 C [146]

In summary, the most commonly encountered version of the mechanism of electrochemical reaction is the joint intercalation of H^+ and Zn^{2+} ions, while the H^+ concentration-dependent electrolytic dissolution/deposition mechanism of MnO_2 cathode is not contradictory but complementary. Many reports have confirmed that the trapping of Zn^{2+} and the formation of electrochemically inactive Zn-containing manganese oxide led to capacity degradation, while the formation of $Zn_4(OH)_6SO_4 \cdot nH_2O$ complex salt during discharge is the pH-controlled process that has a significant effect on the reversibility and properties of Zn//MnO_2 rechargeable cells.

1.6. Hybrid zinc-ion batteries

In addition to zinc-ion batteries, in which electrochemical reactions involving Zn^{2+} ions are realized in the anodic and cathodic processes, hybrid systems in which there are two types of charge carriers: M^{n+} (Li^+, Na^+, K^+, Mg^{2+}, Al^{3+}) cations and Zn^{2+} ions – are actively studied [1,147]. In these cells, anodic processes involving Zn^{2+} cations and cathodic processes involving the second cation are realized. These hybrid batteries based on zinc and alkali metal cations (Li^+, Na^+, K^+) are attractive due to the two separate reactions, thanks to which it is possible to achieve high electrochemical performance (Figure 11).

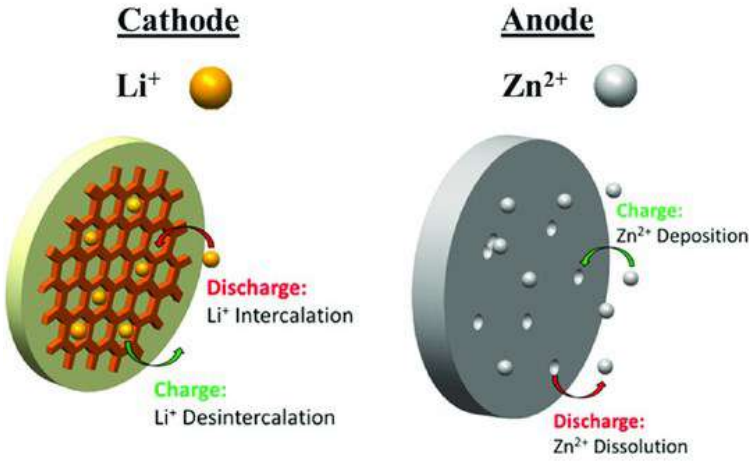

Figure 11. Operating mechanism of aqueous zinc-lithium hybrid battery [14].

One of the first versions of zinc-lithium hybrid batteries was a Zn//$LiMn_2O_4$ system with a 3 M LiCl / 4 M $ZnCl_2$ aqueous electrolyte proposed in 2012 [148]. The electrochemical reaction in this cell is written as follows:

$$Zn^0 - 2e^- \leftrightarrow Zn^{2+} \text{ (anode)} \quad (1)$$

$$LiMn_2O_4 \leftrightarrow Li_{1-x}Mn_2O_4 + xLi^+ + xe^- \text{ (cathode)} \quad (2)$$

Currently, other cathode materials used in lithium-ion batteries besides $LiMn_2O_4$ could be used in these hybrid cells: $LiFePO_4$ [14,149,150], $LiNi_{0.33}Mn_{0.33}Co_{0.33}O_2$ [151], $Li_3V_2(PO_4)_3$ [152,153]. Due to the disadvantages of these materials, such as the high tendency of electrochemical degradation of cobalt and vanadium oxide-based cathodes and the low redox transition potential of $LiFePO_4$-based cathodes, LMO-based cathodes are among the most attractive cathodes to be investigated. The perspective of this system can be explained by the following factors: high average cell voltage (≈ 1.9 V), good compatibility of manganese-based materials with aqueous electrolytes, ability for fast recharging (current densities up to 10 C), ease of synthesis and modification of LMO cathodes, and low cost of battery energy density ($50 per 1 kW·h) [154]. In contrast, $LiMn_2O_4$-based cathode materials have a tendency to dissolve due to the disproportionation reaction of the Mn^{3+} cation formed during discharge, and also have low electronic conductivity (≈ 10^{-6} S·cm^{-1}). In addition, due to the high Mn^{3+} – Mn^{4+} transition potential, the competing process on the cathode is the water oxidation reaction with release of oxygen, and on the zinc anode – the hydrogen evolution reaction, which occurs at lower potentials (Figure 12).

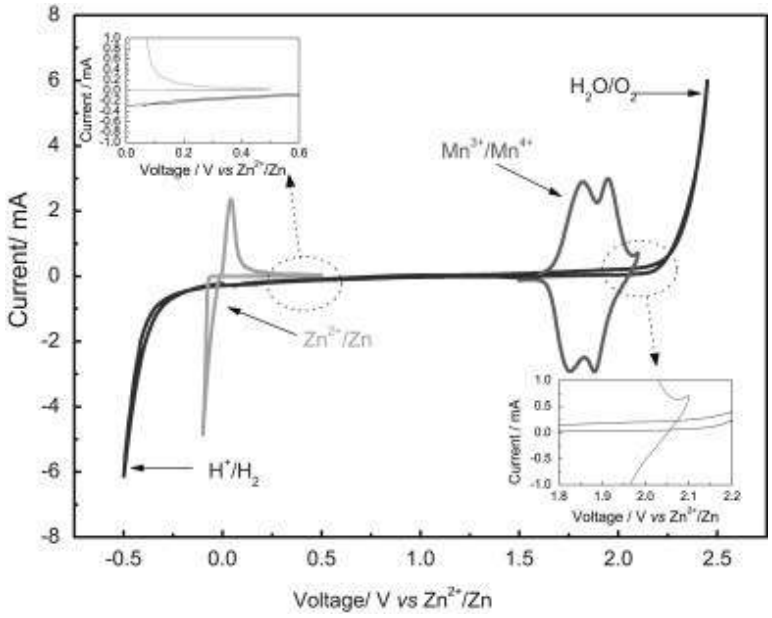

Figure 12. CV for the components of Zn//LMO cell in aqueous electrolyte solution 3 M LiCl / 4 M $ZnCl_2$ at the scan rate υ = 0.5 $mV \cdot s^{-1}$ [148].

Since the physicochemical and electrochemical properties of LMO-based cathodes in aqueous and non-aqueous electrolytes are similar, as found for thin film cathodes [155], the ways to improve cathode materials will be similar to those for Li-ion batteries and can be divided into the following main groups:

- Synthesis of nanoscale $LiMn_2O_4$ particles with given morphology;
- Development of LMO-based composites with carbon-based materials;
- Design of electrolyte compositions.

Depending on the method or conditions used to synthesize the cathode material, samples with different morphologies can be obtained. In particular, to obtain LMO nanoparticles with a particle size of 100 – 300 nm, MnO_2 was first obtained by calcining potassium permanganate solution, which was further treated with alcoholic LiOH solution and calcined [156]. The specific capacities of the nanoscale LMO-based cathode materials in aqueous 0.5 CH_3COOLi / 0.5 $Zn(CH_3COO)_2$ electrolyte solution were 129 $mAh \cdot g^{-1}$ at 0.2 C and 66.3 $mAh \cdot g^{-1}$ at 10 C (1 C = 148 $mA \cdot g^{-1}$) which are 12% and 35% higher than for larger LMO particles. This effect is caused by an increase in the effective surface area of the cathode due to a decrease in particle size and a larger electrode/electrolyte interface. Mechanical grinding of LMO particles on a ball mill allowed to obtain homogeneous particles with sizes from 300 to 900 nm regardless of the grinding time [157]. This resulted in a nearly 5-fold increase in the diffusion coefficient for the ground material ($D_{Li} = 1.542 \cdot 10^{-14}$ $cm^2 \cdot s^{-1}$) which significantly improved the cyclic stability of the cathode material in both the CR2032 cells and the full-size 5 A·h battery packs (Figure 13, a, b).

One of the widely used approaches to improve the properties of electrode materials is modification with carbon-based materials. In particular, carbon nanotubes are a frequently used carbon material for LMO cathodes [158,159]. The combination of acetylene black and carbon nanotubes produced a 3D composite material in which LMO grains were embedded in a carbon mesh (Figure 13, d) which significantly increased the electronic and ionic conductivity of the electrode material and had a significant effect on the value of specific capacities in the current range 1 C – 10 C (1 C = 120 $mA \cdot g^{-1}$) (Figure 13, e) but did not achieve a high percentage of capacity retention during cycling [158]. The same effects were achieved when LMO particles were placed in a matrix based on graphene and carbon nanotubes [159]. Carbon-based materials can also be used as coatings for LMO grains to increase the electronic conductivity and active surface area of the material. In particular, a graphene-based coating was applied as an artificial surface ionic layer for an LMO cathode tested in a mixed solution of zinc and lithium sulfates [160], which increased the specific capacity and cyclic stability over a wide range of currents. The reasons for this increase are the intrinsic storage capacity of the graphene coating, as well as the decrease in the direct contact between the LMO and the electrolyte solution, which suppresses the disproportionation and dissolution of the cathode material.

In addition to improving the properties of the cathode material itself, modification of the electrolyte also affects the properties of the materials in the battery layout. For example, the application of the ternary electrolyte based on the Leclanché cell electrolyte – containing ammonium chloride with the composition of 0.5 M $ZnCl_2$ / 2.34 M NH_4Cl / 2 M LiCl – allowed the authors to significantly improve the ionic conductivity compared to the 3 M LiCl / 4 M $ZnCl_2$ electrolyte solution (235 $mS \cdot cm^{-1}$ for the ternary electrolyte and 107.5 $mS \cdot cm^{-1}$ for the binary one) [14]. The specific capacities of LMO cathodes at low current densities were weakly dependent on the electrolyte composition; however, when the current was increased to 3 C (1 C = 130 $mA \cdot g^{-1}$) in the ternary electrolyte the specific capacity was 80 $mAh \cdot g^{-1}$, which was 80% higher than that of the binary solution. The cyclic stability of the cathodes over 80 cycles at I = 0.2 C was also significantly higher in the electrolyte with the addition of NH_4Cl: up to 75% of the capacity is retained compared to 18% in the case of unmodified solution (Figure 13, c). The reason for these effects is the stronger interaction of NH_4Cl with the active material of the cathode due to the tetrahedral geometry of the NH_4^+ cation, which alters the charge transfer processes in the electrode material. Another advantage of the ammonium ion is that it acts as an inhibitor of the hydrogen evolution reaction as it concentrates along the interface between the anode and the electrolyte, reducing the contact area between the metal zinc and the aqueous solution.

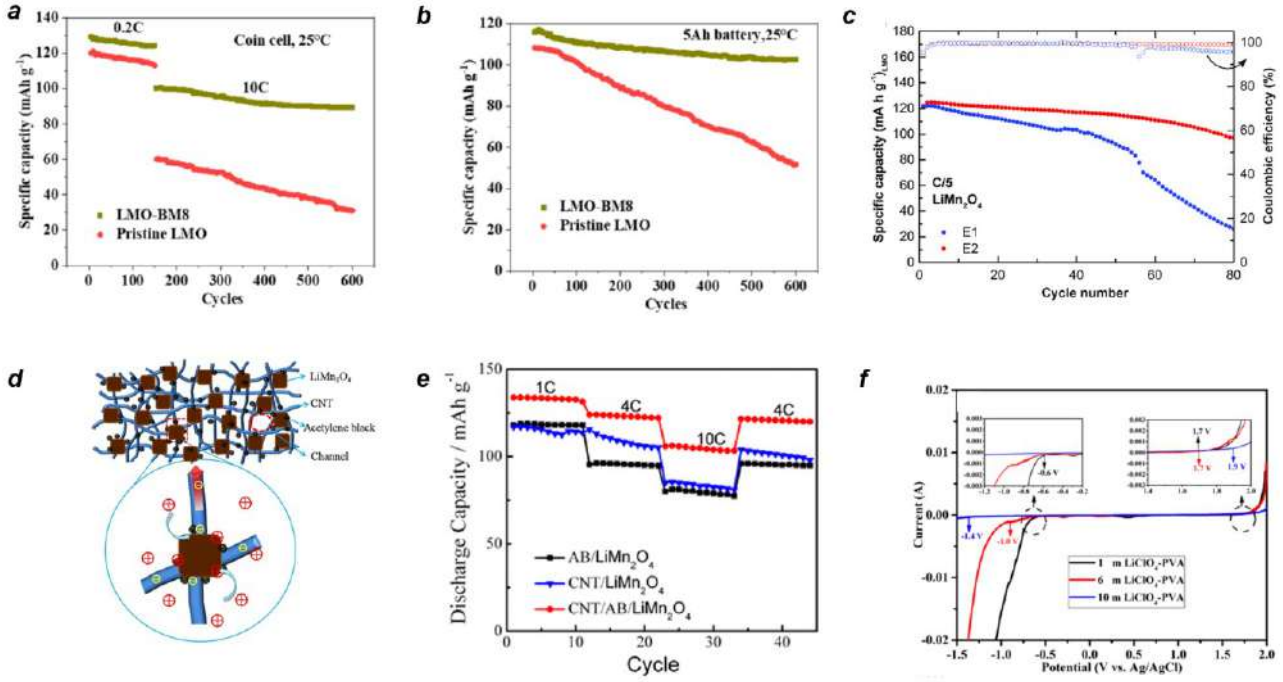

Figure 13. Cyclic stability of LMO-cathodes before and after ball-milling in CR2032 coin cells at 10 C (a) and for 5 Ah industrial-level configuration (b) [157]; *cyclic stability for LMO-cathodes in the E1 (3 M LiCl / 4 M $ZnCl_2$) and E2 (0.5 M $ZnCl_2$ / 2.34 M NH_4Cl / 2 M LiCl) electrolyte solutions (c)* [14]; *Schematic illustration for preparing hierarchical CNT/AB/ $LiMn_2O_4$ electrode (d) and C-rate capability of LMO-cathodes with different composition (e)* [158]*; electrochemical stability range for gel electrolyte in dependence on lithium perchlorate concentration (f)* [161].

The use of highly concentrated electrolytes (so-called “water-in-salt” electrolytes) [149,162] or gel polymer electrolytes [161,163,164] can also improve the cyclic stability of Zn//$LiMn_2O_4$ cells. In particular, in water-in-salt electrolytes, free water is practically absent due to the large number of strong bonds with ions. The electrolyte composition proposed in 2018, 1 m $Zn[N(CF_3SO_2)_2]_2$ + 20 m $Li[N(CF_3SO_2)_2]$ first stabilized the anode reaction, which improved the overall cyclic stability of the Zn//LMO cell at current densities of 0.2 C (88.4% of the initial capacity after 500 cycles) and 4 C (85% of the initial capacity after 4000 cycles), but the achieved capacities were too low (70 and 30 $mAh \cdot g^{-1}$, respectively) [162]. Replacing the large organic cation with the much smaller acetate anion resulted in a significant increase in the ionic conductivity of the electrolyte solution of the same concentration [165]. When tested in a mixed solution of 30 m CH_3COOK / 3 m CH_3COOLi / 3 m $Zn(CH_3COO)_2$, whose conductivity was 6.5 $mS \cdot cm^{-1}$ due to the extremely high content of acetate ions, which is comparable to the ionic conductivity of 2 M $ZnSO_4$ electrolyte (9.7 $mS \cdot cm^{-1}$), a specific capacity of 122 $mAh \cdot g^{-1}$ was observed for LMO cathodes at a current density of 0.05 C (1 C = 148 $mA \cdot g^{-1}$) [149]. During 300 cycles at a current density of 2 C, the capacity loss of the cathode material was ≈ 50% due to the cathode dissolution process during cycling.

The use of gel or gel-polymer electrolytes reduces dendrite formation on the zinc anode, which increases the reversibility of the anode process and the overall cycling stability of the cell. The use of

the 2 M $ZnSO_4$ / 1 M Li_2SO_4 electrolyte with polyethylene glycol (3 wt.%) and fumed silica (2 wt.%) allows the suppression of parasitic anodic reactions, which improves the cyclic stability to 39% during 1000 cycles [163]. Gel electrolytes based on highly concentrated salt solutions also regulate the solvate shell of the Zn^{2+} cation, which allows stabilizing the anodic reaction as well as extending the cycling range up to 2.7 V due to the suppression of hydrogen and oxygen generation processes (Figure 13, e) [161].

The development of hybrid batteries is currently under active investigation, not least due to the availability of cathodes, potential scaling and commercialization of these electrochemical systems. It is worth noting that all the examples discussed above consider the case where the electrolyte solution necessarily contains Li^+ ions, which provide the cathode reaction. Meanwhile, according to equation (2), in the case of complete deintercalation of lithium ions from the electrolyte solution, the MnO_2 with spinel structure (λ-MnO_2) is formed on the cathode surface [166]. The formed spinel phase is capable of reversibly transforming into $ZnMn_2O_4$, as demonstrated by *in situ* X-ray diffraction [80]. However, the possibility of electrochemical conversion of $LiMn_2O_4$ to $ZnMn_2O_4$ has not been considered previously.

1.7. Summary

The trend of developing aqueous rechargeable power sources with zinc metal anode is certainly promising both in the field of stationary energy storage and in some areas of portable electronics, primarily related to medicine. Manganese dioxide-based cathode materials, which are used in both non-rechargeable power cells and lithium-ion batteries, are well positioned for further development and commercialization due to the above advantages. The existing strategies to improve MnO_2 cathode have sufficient efficiency, but some of them are still far from practical use due to various factors: difficult availability of some reagents, complicated synthesis procedures, low probability of scalability. Difficulties in interpreting the mechanism of the electrochemical reaction in Zn//MnO_2 cells inhibit the practical development of AZIBs, but still provide a large scope for research aimed at the final establishment and verification of the electrochemical and chemical reactions occurring in the system. The possibility of electrochemical substitution of lithium cations for zinc cations in the structure of lithium manganese spinel can contribute to effective ways of obtaining novel cathode materials based on commercially available $LiMn_2O_4$.

Based on the above stated points, the objectives of this work were (i) to consider the possibility of electrochemical transformation of lithium-manganese spinel into zinc-containing phase in an appropriate electrolyte solution, (ii) to develop and study the functional properties of new types of manganese oxide-based cathode materials, and (iii) to fundamentally investigate the electrochemical reaction mechanism occurring in Zn//MnO_2 cells.

Proving the intercalation of zinc ions into the $LiMn_2O_4$ structure is an interesting task aimed both at solving the problem of design an efficient high-voltage cathode material for zinc-ion batteries by varying the electrolyte composition, and at confirming an alternative hybrid electrochemical reaction mechanism in Zn//$LiMn_2O_4$ batteries, in which Zn^{2+} cations participate in the cathodic reaction.

One of the ways to control the functional properties of electrode materials is a given change of structural and morphological parameters, achieved by variation of simple synthetic procedures, namely synthesis of manganese oxides with layered structure of different morphology. It is important to create composite materials based on δ-MnO_2 modified by conducting polymer PEDOT or PEDOT:PSS by different methods: addition of polymer to the composite, mechanical application of polymer coating on the surface of MnO_2 particles or electrodeposition of polymer on the as-prepared cathode, as well as to compare their electrochemical properties.

The fundamental part of this work is focused on a more complete study of the electrochemical processes occurring in Zn//MnO_2 cells, including the establishment of potential charge carriers and the role of Zn^{2+} and H^+ cations during charge/discharge. To experimentally investigate the electrochemical processes occurring in the system, an approach with changing the cationic or anionic composition of aqueous zinc-containing electrolyte solutions was used, as well as controlling its acidity, which has a significant effect on the properties and reaction mechanism.

Chapter 2. Experimental part

2.1. Reagents

For the synthesis of manganese dioxide with layered-type morphology potassium permanganate $KMnO_4$ (puriss.) and manganese sulfate monohydrate $MnSO_4 \cdot H_2O$ (JSC LenReactiv, Russia, puriss.) were used.

The chemical synthesis of PEDOT polymer was carried out using EDOT monomer (Aldrich, USA), iron (III) chloride hexahydrate $FeCl_3 \cdot 6H_2O$ (puriss.). Anhydrous acetonitrile (JSC Vekton, Russia, p.a.) was used as solvent.

To prepare electrode materials based on lithiated manganese oxide $LiMn_2O_4$, commercially available LMO powder (LMO, MTI Corp., USA) was used. The compositions of manganese oxide-based cathode materials (LMO or MnO_2) also included carbon black "Super P" (Timcal Inc., Belgium), PVDF binder (Aldrich, USA) and PEDOT:PSS conducting polymer dispersion (1.3 %, Aldrich, USA). N-methyl-2-pyrrolidone (NMP, Aldrich, USA) was used as the solvent to prepare the slurry. Titanium foil (thickness 20 μm) and stainless-steel foil (thickness ≈ 50 μm) were used as a current collector for casting of electrode material mixtures based on MnO_2 and LMO, respectively.

Aqueous electrolyte for zinc-ion batteries were prepared based on the zinc sulfate heptahydrate $ZnSO_4 \cdot 7H_2O$ (JSC LenReactiv, Russia, p.a.), manganese sulfate monohydrate $MnSO_4 \cdot H_2O$ (puriss.), zinc acetate dihydrate $Zn(CH_3COO)_2 \cdot 2H_2O$ (JSC LenReactiv, Russia, puriss.), manganese acetate tetrahydrate $Mn(CH_3COO)_2 \cdot 4H_2O$ (puriss.), anhydrous lithium sulfate Li_2SO_4 (puriss.) and sodium sulfate decahydrate $Na_2SO_4 \cdot 10H_2O$ (JSC LenReactiv, Russia, puriss.).

Deionized water (>18 MΩ·cm) was obtained using the Millipore DirectQ UV system.

2.2. Hydrothermal synthesis of manganese oxide with layered structure

The materials were synthesized using two procedures reported in the literature: coproportionation reaction between potassium permanganate and manganese sulfate (material denoted as MnO_2-I, [11]) and hydrothermal treatment of potassium permanganate aqueous solution (denoted as MnO_2-II, [167]).

For the synthesis of MnO_2-I, 0.948 g of potassium permanganate was dissolved in 50 mL of deionized water to obtain 0.12 M solution, then 0.151 g of manganese sulfate was added in the mixture. The molar ratio of components was 6:1. The obtained solution was stirred during 30 min at the room temperature and then transferred to 100 mL stainless-steel autoclave. Hydrothermal synthesis was carried out during 12 h at 160 °C. The black powder obtained was washed out three times by deionized water using centrifugation (5 min at 4500 rpm) and dried under vacuum at 55 – 60 °C for 18 h.

MnO_2-II material was synthesized by hydrothermal treatment of 0.025 M aqueous solution of potassium permanganate. To obtain this solution, 0.2004 g of $KMnO_4$ was dissolved in 50 mL of deionized water under stirring and then transferred to 100 mL stainless-steel autoclave. Hydrothermal synthesis was carried out during 24 h at 220 °C. The black powder obtained was washed out by deionized water using centrifugation (5 min at 4500 rpm) and dried under vacuum at 55 – 60 °C for 20 h.

2.3. Structural and chemical characterization of samples

The phase composition of synthesized oxides was analyzed by X-ray diffraction (XRD) in the range of 10 – 70 ° using Cu K_α radiation (λ = 0.15418 nm) on a Bruker-AXS D8 DISCOVER diffractometer (Germany) at a scanning step of 0.02 °. The morphology of the obtained particles was investigated by scanning electron microscopy (SEM) on a SUPRA 40VP Carl Zeiss (Germany) electron microscope. Elemental analysis of the surface of the obtained materials was carried out by energy dispersive X-ray analysis (EDX) using the INCAx-act electron microscope attachment (Oxford Instruments plc, UK).

2.4. Preparation of manganese oxide-based cathode materials

LMO-based cathode materials were prepared by conventional technique by mechanical mixing of the components in an agate mortar. Before using, LMO powder was dried under vacuum at 130 °C. The ratio of components was 80 wt.% of electroactive component (LMO), 10 wt.% of carbon black and 10 wt.% of PVDF. First, PVDF powder was dissolved in an appropriate amount of N-methyl-2-pyrrolidone, and then the electroactive material powder and carbon black were added. Mixing was carried out for 1 hour until a completely homogeneous state was achieved. The resulting viscous slurry was cast on the stainless-steel foil (the blade gap height was 200 μm) and dried under vacuum at 80 °C overnight. The resulting electrodes were roll-pressed. The mass loading of electroactive material was 4 – 5 $mg \cdot cm^{-2}$.

To prepare cathode materials based on MnO_2-I and MnO_2-II, another component ratio was applied: 70 wt.% of active material, 20 wt.% of carbon black and 10 wt.% of PVDF. The components were mixed the same way, the resulting slurry was cast on the titanium foil (blade gap height was 150 μm) and dried under vacuum at 50 °C per day. Then the electrodes were roll-pressed to provide better contact between the electrode material and current collector. Mass loading of the electroactive material was ≈ 1 – 1.5 $mg \cdot cm^{-2}$ per electrode.

To prepare PEDOT-modified electrode materials based on MnO_2-I, chemical synthesis of PEDOT polymer was performed by oxidative polymerization. For this, 200 mL of $FeCl_3$ acetonitrile solution prepared by dilution from 7 M salt solution was used as oxidative agent. The synthesis was carried out

in a round-bottom glass flask under stirring at 1000 rpm. To the oxidant solution, 2 mL of 3,4-ethylenedioxythiophene monomer was added and the solution was stirred for 2 h. The resulting product was washed with acetonitrile and deionized water, and dried at 80 °C to constant weight. The resulting polymer powder was added to the cathode material in an amount of 5 wt.% as the fourth component of the slurry.

Modification of MnO_2-I electrode material samples with PEDOT:PSS polymer was carried out by dispersing the active material in aqueous dispersion of PEDOT:PSS under sonification for 30 minutes followed by drying at 70 °C. The ratios of components are given in Table 1.

Table 1. MnO_2-I-based electrode materials composition (in wt.%) with conducting polymer additives.

Sample	δ-MnO_2	C	PVDF	PEDOT	PEDOT:PSS
MnO_2	70	20	10	0	0
MnO_2/PEDOT	68	20	7	5	0
MnO_2/PEDOT:PSS	70	20	8	0	2

After roll-pressing each electrode piece was cut into disks with 12 mm diameter for electrochemical measurements in CR2032 coin-cells with metal Zn anode and glass fiber Whatman GF/A as separator wetted with the appropriate electrolyte solution. Some of the electrodes were cut as thin strips with a width no more than 0.5 cm to assemble three-electrode cells with different types of construction.

2.5. PEDOT electrodeposition on the electrode materials surface and analysis of the coating

The PEDOT electrodeposition was performed on the as-prepared electrode surface in a three-electrode cell, where the foil coated with the cathode material was used as the working electrode (up to 5% of the material was removed from the surface of the titanium foil for connection to the device), the glassy carbon plate was used as the counter electrode, and the silver wire coated with a layer of silver chloride was used as a pseudo reference electrode (the potential shift vs. the standard silver chloride electrode was −0.2 V). The solution used for the electrodeposition was 0.01 M EDOT / 0.1 M LiClO4 / acetonitrile. The deposition was carried out in potentiostatic mode at the E = 1.1 V vs. Ag/AgCl pseudo reference electrode which is correlated to the value $E \approx 1.8$ vs. Zn/Zn^{2+}, the duration was 300 and 600 s. After synthesis, the samples were dried at 70 °C. Surface characterization was performed by EDX and X-ray photoelectron spectroscopy (XPS) methods using a Thermo Fisher Scientific Escalab 250Xi spectrometer (USA).

2.6. Electrochemical measurements

For electrochemical measurements, Autolab PGSTAT12 (Eco Chemie, Netherlands), BioLogic BCS805 (Biologic, France), Elins 20X8 (SmartStat, Russia) potentistats/galvanostats and Neware CT-4008 automatic galvanostatic workstation (Neware Co., China) were used.

The solutions of aqueous zinc-containing electrolytes prepared for the electrochemical tests are summarized in Table 2. For the preparation of all the listed electrolyte solutions, the corresponding amounts of salts were dissolved in 50 mL of deionized water; if necessary, for the preparation of solutions with high salt concentration, heating to 40-45 °C was performed. Some electrolytes prepared from acetates were additionally acidified with 0.25 M acetic acid to a constant pH value.

Table 2. Electrolytes composition for electrochemical tests of manganese oxides–based cathode materials.

Cathode material	Electrolyte compositions
$LiMn_2O_4$	2 M $ZnSO_4$
	1 M $ZnSO_4$ / 2 M Li_2SO_4
	1 M $ZnSO_4$ / 2 M Li_2SO_4 / 0.1 M $MnSO_4$
δ-MnO_2	2 M $ZnSO_4$ / 0.1 M $MnSO_4$
	2 M $ZnSO_4$
	0.1 M $MnSO_4$
	2 M $ZnSO_4$ / 1.0 M Na_2SO_4
	2 M $ZnSO_4$ / 0.1 M $MnSO_4$/ 1.0 M Na_2SO_4
	2 M $ZnSO_4$ / 1.0 M Li_2SO_4
	2 M $ZnSO_4$ / 0.1 M $MnSO_4$/ 1.0 M Li_2SO_4
	1.0 M $Zn(CH_3COO)_2$
	1.5 M $Zn(CH_3COO)_2$
	1.0 M $Zn(CH_3COO)_2$ / 0.2 M $Mn(CH_3COO)_2$
	1.0 M $Zn(CH_3COO)_2$ / 0.05 M $Mn(CH_3COO)_2$ / CH_3COOH
Electrodeposited MnO_2	2 M $ZnSO_4$ / 0.1 M $MnSO_4$
	2 M $ZnSO_4$
	2 M $ZnSO_4$ / 0.1 M $MnSO_4$ / 1.0 M Na_2SO_4
	2 M $ZnSO_4$ / 1.0 M Na_2SO_4
	1.0 M $Zn(CH_3COO)_2$ / 0.2 M $Mn(CH_3COO)_2$
	1.0 M $Zn(CH_3COO)_2$ / 0.05 M $Mn(CH_3COO)_2$ / CH_3COOH
	0.1 M $Mn(CH_3COO)_2$

Electrochemical cells with LMO cathodes were assembled as three-electrode cells using the LMO cathode as the working electrode, zinc foil as both counter and reference electrodes, and two-electrode cells without a counter electrode. MnO_2-based cathodes were assembled in two-electrode coin cells with aqueous electrolyte solution of 2 M $ZnSO_4$ / 0.1 M $MnSO_4$ to study the functional properties of the materials, and other mentioned electrolytes were used to study the electrochemical reaction mechanism in Zn//MnO_2 cells in both two-electrode and three-electrode configurations.

Galvanostatic charge/discharge and cyclic voltammetry measurements for LMO-based cathode materials were performed in the potential range 1.4 – 2.1 V vs. Zn/Zn^{2+} on the Elins 20X8 potentiostat/galvanostat. Charge/discharge measurements were performed in the current range 0.2 – 5 C (1 C current corresponds to 115 $mA \cdot g^{-1}$), CV measurements were performed at the scan rates 0.1 – 0.5 $mV \cdot s^{-1}$. Electrochemical impedance spectra were obtained in the frequency range of 10 kHz – 0.1 Hz with an amplitude of 5 mV in different charge states using a three-electrode scheme on a Biologic BCS-805 potentiostat/galvanostat.

The electrochemical tests of MnO_2-based cathodes by galvanostatic charge/discharge were performed on an automatic galvanostatic workstation CT-4008 in the voltage range of 1.0 – 1.8 V vs. Zn/Zn^{2+} at current densities of 0.1 – 5.0 $A \cdot g^{-1}$. The cyclic stability of the cathode materials was estimated at a fixed current density of 0.3 $A \cdot g^{-1}$. CV and impedance spectroscopy measurements were performed on a Biologic BCS-805 or Autolab PGSTAT12 potentiostat/galvanostat. CV measurements were performed at the scan rates of 0.1 – 0.5 $mV \cdot s^{-1}$ in the potential range E = 1.0 – 1.8 V vs. Zn/Zn^{2+}. Impedance spectra were recorded in the frequency range 10 kHz – 0.1 Hz with an amplitude of 5 mV during the discharge at the potentials E = 1.48, 1.38 and 1.30 V. All measurements were carried out at room temperature ~20 °C with minor seasonal variations.

2.7. Electrochemical quartz crystal microbalance measurements

Electrode mass measurements *in operando* were performed using the electrochemical quartz crystal microbalance (EQCM) technique in combination with CV measurements. A piezoelectric quartz crystal (cut at an angle of 35°) with a sputtered gold layer placed in a holder was used as the working electrode. Titanium or zinc foils were used as the counter electrode and a zinc foil / silver chloride Ag/AgCl electrode filled with saturated NaCl solution (3.5 $mol \cdot L^{-1}$) were used as the reference electrode. All measurements were performed on an Autolab PGSTAT12 potentiostat/galvanostat. The mass of the manganese oxide film was estimated using a QCM200 Quartz Crystal Microbalance Analog Controller + QCM25 Crystal Oscillator (Stanford Research Systems, USA).

The measurements were performed both during the electrodeposition of the MnO_2 coating on the electrode surface and for the previously synthesized MnO_2 film. The potentiodynamic synthesis was

performed by CV at a scan rate of 0.5 $mV \cdot s^{-1}$ in the potential range 0.0 – 0.8 V vs. Ag/AgCl (1.0 – 1.8 V vs. Zn/Zn^{2+}). The preliminary synthesis was carried out in potentiostatic mode at E = 0.7 V in Au / Ti / Ag/Ag/AgCl cell from 0.1 M $Mn(CH_3COO)_2$ electrolyte solution for 50 – 100 s according to the methodology published in [168]. The obtained electrode was washed with deionized water and dried at 70 °C for 24 hours.

Electrochemical tests were performed in the solutions listed in Section 2.6 (Table 2) for electrodeposited MnO_2. Measurements were performed by CV at a scan rate of 0.5 $mV \cdot s^{-1}$ in the potential range of 0.0 – 0.8 V vs. Ag/AgCl or 1.0 – 1.8 V vs Zn/Zn^{2+} for 3 – 5 cycles. During the experiment, the oxide film was electrodeposited on the crystal, which resulted in a change in the resonant frequency of its natural oscillations depending on the mass of the deposited film. The conversion of the frequency measured on the instrument to the mass of the precipitate on the crystal surface was performed according to Sauerbrey equation using OriginPro 2021 software.

$$\Delta f = -C_f \cdot \Delta m \tag{3}$$

where Δf – frequency measured (Hz), C_f – quartz crystal sensitivity factor (56.6 $Hz \cdot cm^2 \cdot g^{-1}$ for the air), Δm – change in the mass of the precipitate on the crystal surface ($\mu g \cdot cm^{-2}$).

2.8. Structural and chemical characterization of electrode materials before and after electrochemical tests

The phase composition and structure of the electrodes after electrochemical tests were characterized by high-resolution X-ray diffractometry (Bruker-AXS D8 DISCOVER, Germany) using Cu K_α-radiation. The morphology of the materials was evaluated by scanning electron microscopy (SUPRA 40VP, Carl Zeiss), the element distribution was studied by EDX analysis. The surface of cathode materials was examined by X-ray photoelectron spectroscopy. Zinc content in MnO_2-cathodes was estimated by X-ray fluorescence analysis of electrode materials in different stages: after 10 and 30 charge/discharge cycles at a current density of 0.1 $A \cdot g^{-1}$ followed by 1 h waiting time in discharge state and after 30 cycles with a waiting time in a fully charged state. The electrodes were washed with deionized water and partially with a solution of 0.25 M acetic acid to remove surface precipitate of basic zinc sulfate $Zn_4(OH)_6SO_4 \cdot nH_2O$.

Chapter 3. Investigation of functional properties of manganese oxide-based cathode materials in aqueous electrolytes

3.1. Study of the properties of $LiMn_2O_4$-based cathodes as a function of the type of electrolyte used

Since it was previously reported in [79–81] that the λ-MnO_2 phase formed by complete delithiation of LMO was electroactive as a cathode for AZIBs, we assumed an electrochemical conversion between $LiMn_2O_4$ and $ZnMn_2O_4$. To verify this hypothesis, LMO-based cathode material was investigated by CV in two electrolytes: aqueous solution of 2 M $ZnSO_4$ and 1 M $ZnSO_4$ / 2 M Li_2SO_4 solution. In the mixed electrolyte containing lithium ions, the CV curve is well correlated with the same literature data in aqueous electrolytes: two pairs of peaks at E = 1.81/1.74 V (first pair) and E = 1.94/1.88 V (second pair) are observed, corresponding to the processes of reversible intercalation/deintercalation of lithium ions into the LMO lattice [166]. The electrode demonstrates high stability over 10 cycles (Figure 14, a) [41].

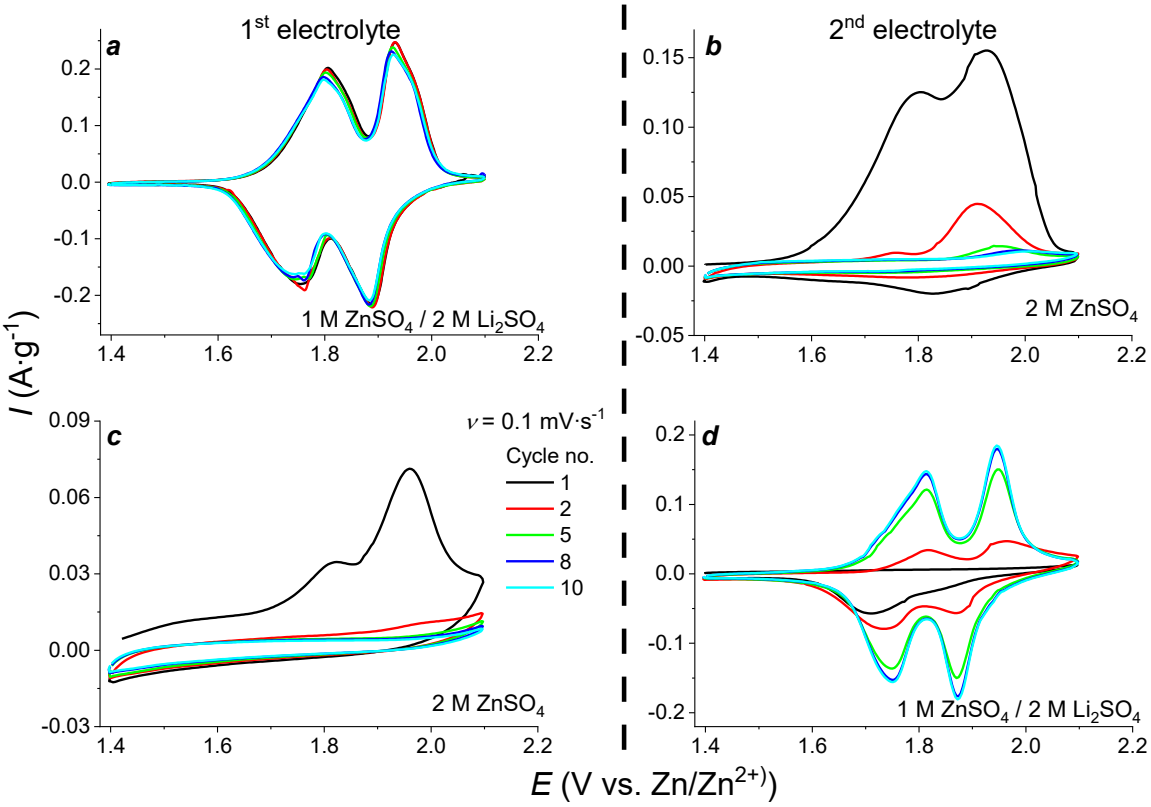

Figure 14. CV curves of LMO-based cathodes, sequentially tested in two types of electrolytes at the scan rate of 0.1 mV·s^{-1}.

When the same electrode is transferred from the mixed solution to 1 M $ZnSO_4$ solution, only two anodic peaks corresponding to the processes of lithium ion deintercalation are observed in the first cycle, while the height of the cathodic peak decreases significantly, then in the second cycle the

currents of the anodic peaks decrease by 5 and more times, and in the fifth cycle they disappear completely (Figure 14, b). Such a significant decrease in currents indicates that in the absence of lithium ions in 2 M $ZnSO_4$ solution, intercalation of Zn^{2+} cations into the lithium-depleted spinel structure (designated as λ-MnO_2) does not occur.

When 2 M $ZnSO_4$ electrolyte was used as the first solution (Figure 14, c), two peaks with very different intensities were observed in the first anodic cycle, while no peaks and zero current density were observed in the cathodic and subsequent cycles. However, after the transfer of the electrode to the mixed electrolyte, a partial "recovery" of the electrochemical activity occurs during the first 5 cycles and by the 8th cycle the anodic and cathodic currents are stabilized (Figure 14, d). At the same time, the capacity of the cathode placed in the 1 M $ZnSO_4$ / 2 M Li_2SO_4 electrolyte after cycling in 2 M $ZnSO_4$ is insignificantly lower than that of the cathode initially placed in the mixed electrolyte: 93 mAh·g^{-1} per the 10th cycle for the electrode firstly cycled in zinc sulfate solution and 119 mAh·g^{-1} per the 10th cycle for the electrode, initially cycled in the mixed electrolyte. Thus, there is almost complete recovery of the cathode capacity, which means that the loss of electroactivity in pure zinc sulfate solution is caused by blocking of electroactive sites – vacancies in the crystalline structure of the material, which can be caused by surface interaction between Zn^{2+} cations and the cathode material.

For a more detailed analysis of the cathode/electrolyte interface, impedance spectra were obtained for the electrode materials after 5 CV cycles in the corresponding electrolyte with their subsequent change. On the spectra of LMO cathodes initially obtained in pure zinc sulfate solution (inset of Figure 15, a), the main component is the pseudo-capacitive response observed as a linear section at an angle close to 90 °, which correlates with the quasi-rectangular shape of the CVA in pure $ZnSO_4$ solution. A semicircle corresponding to the interfacial resistance can be seen on the enlarged graph. The small value of this interfacial impedance (≈ 15 Ohm) can be related to both the zinc counter electrode and the substrate/electrolyte interface (Figure 15, a). The weak dependence of the impedance spectra of the electrodes in zinc sulfate solution on the potential is related to the low current response caused by the almost complete absence of lithium ions in the LMO structure. After changing the electrolyte solution to the one containing lithium ions, the shape of the spectra changes drastically: the second semicircle appears which is the most clearly visible at E = 1.96 V (Figure 15, b, red curve), as well as a linear part in the mid-frequency range at an angle of ≈ 45 ° indicating a diffusion response. Since the zinc electrodeposition/dissolution reaction takes place on the surface and is controlled by the diffusion of Zn^{2+} ions to the anode surface, it can be concluded that the new parts of the spectrum correspond to the LMO/electrolyte interface.

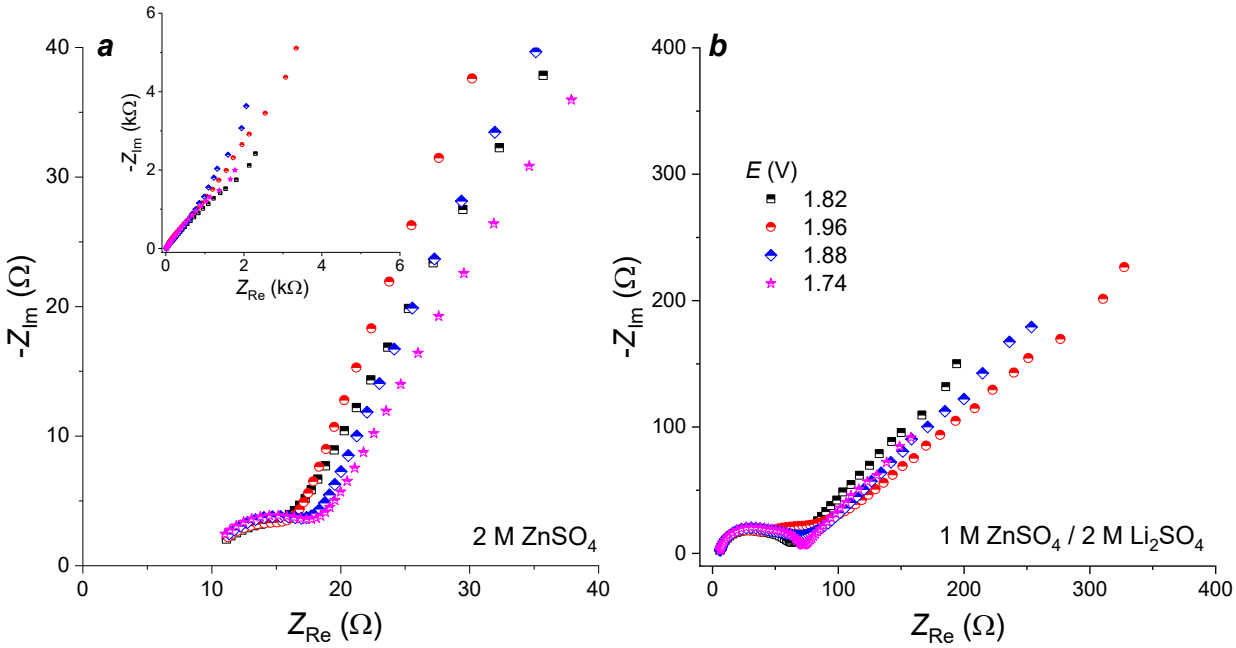

Figure 15. Impedance spectra of LMO cathodes cycled in the 2 M $ZnSO_4$ solution (a) and then transferred to the 1 M $ZnSO_4$ / 2 M Li_2SO_4 solution (b). The inset shows the spectra for LMO cathodes in the full frequency range.

For a detailed study of the ion intercalation process, the impedance spectra were recorded during the discharge of the cell. In the mixed 1 M $ZnSO_4$ / 2 M Li_2SO_4 electrolyte, the shape of the spectra is slightly dependent on the redox potential value and differs significantly only in the fully charged state at $E = 2.1$ V (Figure 16, a). A clearly visible semicircle is observed in all spectra, corresponding to the charge transfer resistance at the LMO/electrolyte interface, and a linear part in the mid-frequency range, corresponding to the diffusion limitations of Li^+-ion transport in the material structure. The R_{ct} value is close to ≈ 65 – 70 Ω. After the transfer of the cathode recharged in mixed electrolyte into the 2 M $ZnSO_4$ solution, a twofold increase in the charge transfer resistance, the appearance of an additional semicircle in the high-frequency region on the spectra, and a pseudo-capacitive response are observed. This indicates the formation of a new interface (Figure 16, b), which could be related to the modification of the cathode surface due to the filling of surface vacancies in the LMO structure with zinc ions, leading to the electrochemical inactivation of the cathode material.

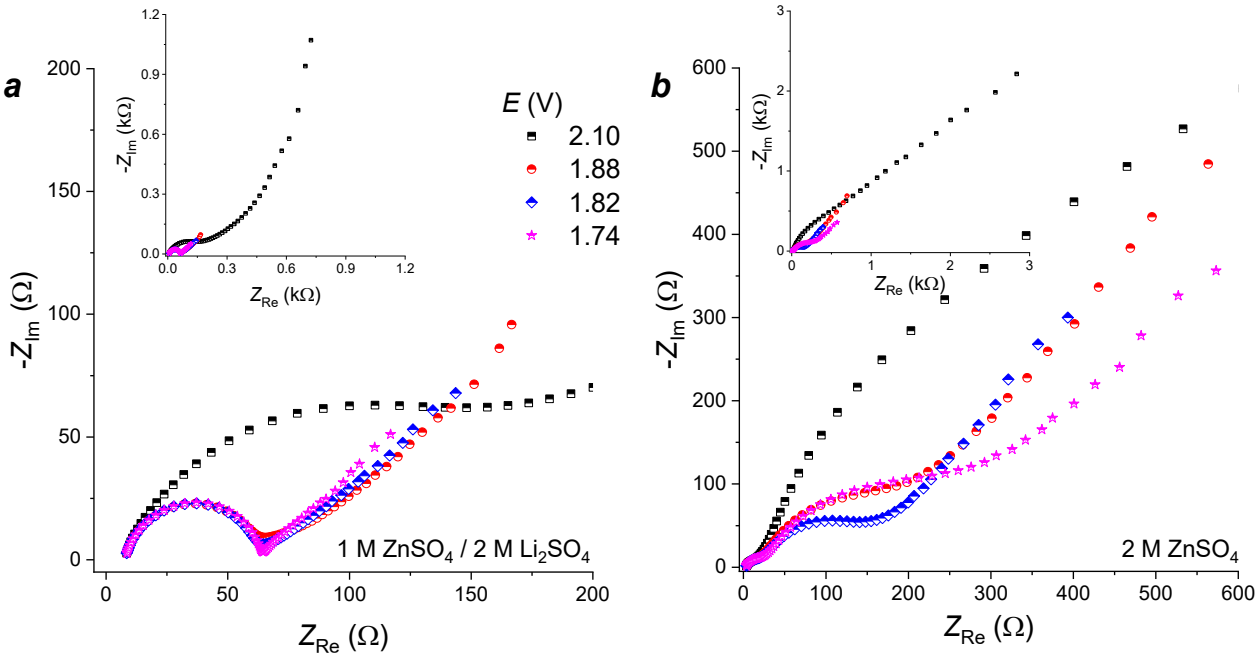

Figure 16. Impedance spectra of LMO cathodes cycled in the 1 M $ZnSO_4$ / 2 M Li_2SO_4 solution (a), and after transferring to the 2 M $ZnSO_4$ solution (b).

To confirm the possible blocking of the cathode surface by Zn^{2+} ions, SEM images of the electrodes after electrochemical tests in two different electrolytes were obtained and EDX analysis with Zn mapping was performed (Figure 17). According to the results of element content calculation from the EDX data, it was found that the surface zinc concentration in the electrode cycled in 2 M $ZnSO_4$ solution was 27 wt.% of the total content, which is 10 times higher than for the electrode after testing in mixed zinc-lithium electrolyte (2 wt.%). It can be clearly seen that zinc in both cases is distributed uniformly over the entire surface of the electrode.

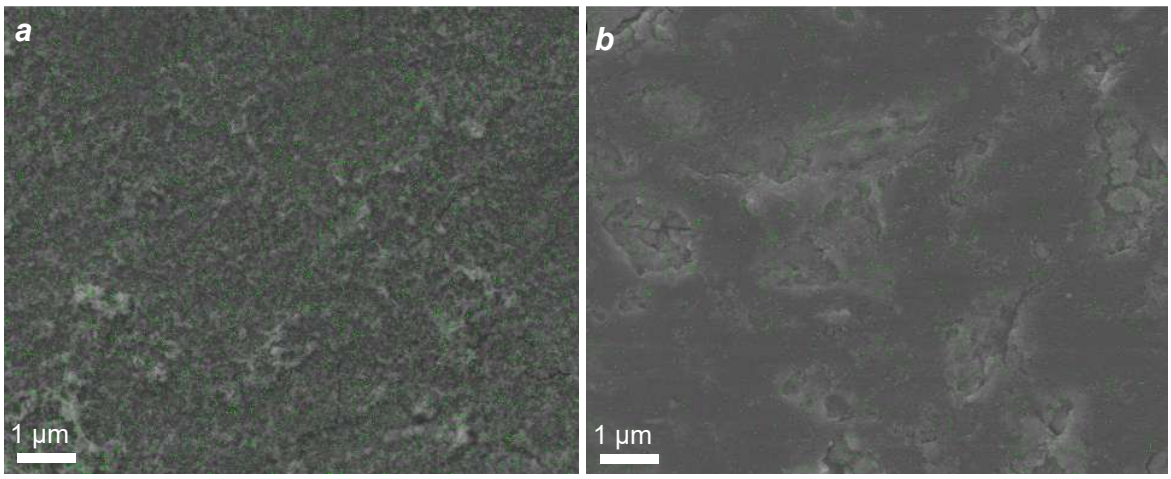

Figure 17. EDX-mapping of the zinc, overlayed on SEM images of LMO cathodes after tests in the 2 M $ZnSO_4$ (a) and 1 M $ZnSO_4$ / 2 M Li_2SO_4 (b) electrolytes.

In addition, the electrode surface after tests in 1 M $ZnSO_4$ / 2 M Li_2SO_4 solution is smoother compared to the sample from 2 M $ZnSO_4$ solution, which shows rough flaky structures probably resulting from the transformation of the surface structure upon insertion of Zn^{2+} ions.

In addition to the *ex situ* morphological analysis of the electrodes, the phase composition of the electrode materials after testing in both types of electrolytes was analyzed by X-ray diffraction. The resulting XRD patterns are shown in figure 18. For the cathode cycled in the mixed aqueous solution of zinc and lithium sulfates, only a phase of $LiMn_2O_4$ (ICCD card #01-070-8343) is observed. Small shifts of the peaks, especially those related to (511), (440), and (531) crystal edges (at 58.34°, 64.09°, and 67.41°, respectively) are associated with the fixed position of the LMO crystals in the composite electrode, which reduces the random distribution of the crystal edge, or may be related to different degrees of lithium intercalation [169].

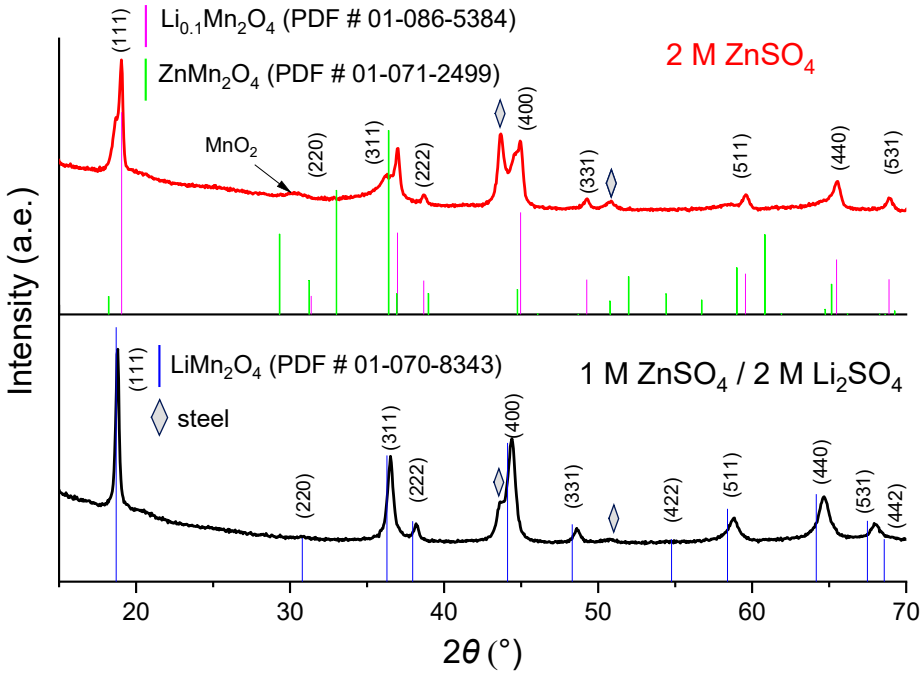

Figure 18. XRD patterns of LMO cathodes after electrochemical tests in two types of zinc-containing electrolytes.

After cycling in the zinc sulfate solution, a delithiated spinel $Li_{0.1}Mn_2O_4$ phase (ICCD card #01-086-5384) is attributed as the main phase with a small admixture of λ-MnO_2 (a weak signal at 30.43°), i.e. products formed by almost complete delithiation of LMO. The diffraction peaks that could be unambiguously attributed to the $Zn_xMn_2O_4$ phase were not detected: the most intense diffraction peaks at 29.32°, 33.01° and 60.83° are missing. However, there is a visible splitting of the (111), (311) and (400) peaks. Thus, complete intercalation of zinc ions into the material structure does not occur, and

phases containing both types of ions, such as $Zn_xLi_yMn_2O_4$, which have no electrochemical activity, are formed [41].

Since the presence of manganese salt in the electrolyte solution for Zn//MnO_2 rechargeable systems leads to the improvement of the functional properties, this additive was used for testing with LMO-based cathode material. figure 19, a – c, shows the comparison of the electrochemical properties of LMO cathode in the presence and absence of manganese sulfate in the electrolyte solution. First of all, the changes in the shape of the CV curves (Figure 19, a), should be noted, in particular, the increase in the peak currents (especially at E = 2.05 V), as well as the appearance of a slight current increase in the potential range close to $E \approx 2.2$ V, which is associated with the competing processes of oxygen evolution and MnO_x precipitation from the electrolyte solution. To avoid these processes and to avoid significant artificial capacity increase, further tests were performed up to the upper limit of the potential E = 2.0 V.

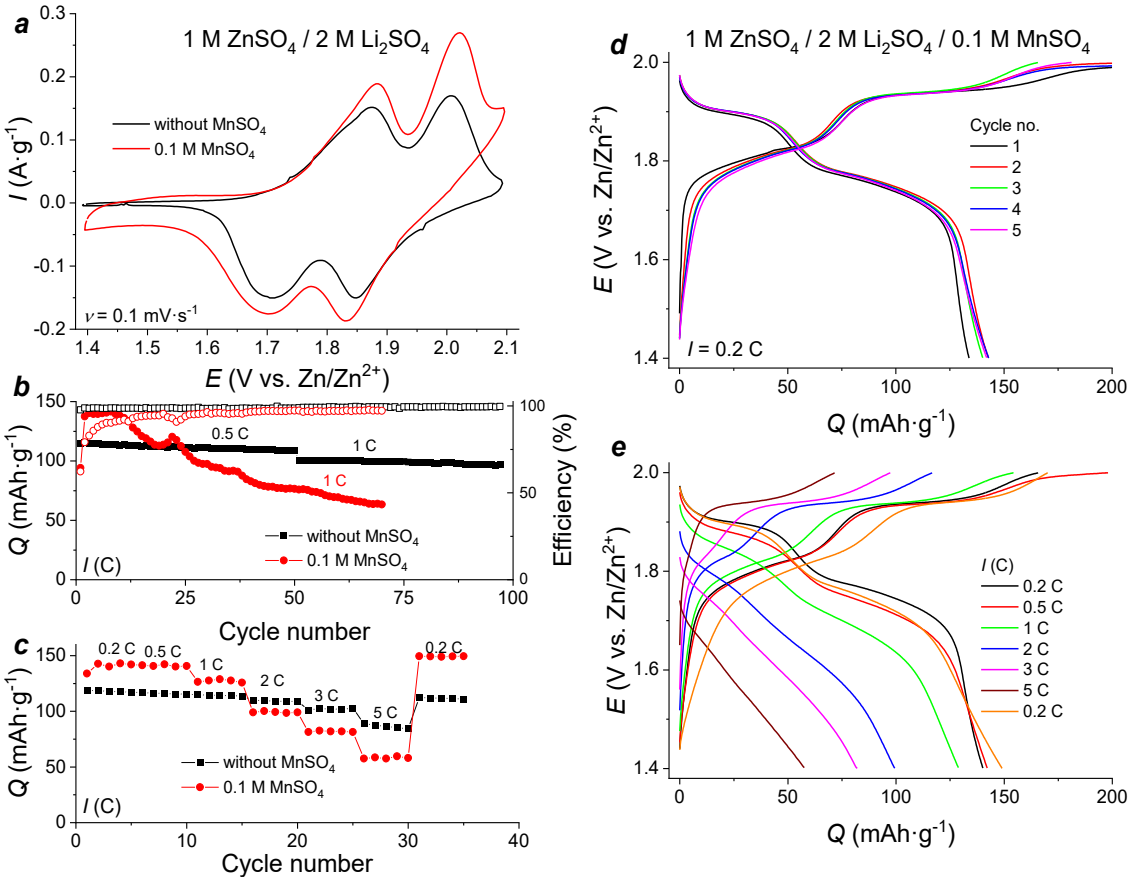

Figure 19. Electrochemical performance of LMO cathodes in in zinc-lithium-manganese sulfate electrolyte solutions: comparison of CVs at 0.1 mV·c^{-1} (a), cyclic stability (b) and C-rate capability (c); charge/discharge profiles in ternary electrolyte at 0.2 C (d), and as function of the discharge current density (e).

In the ternary electrolyte containing 0.1 M $MnSO_4$ the higher initial specific capacity of the materials was observed compared to that in binary 1 M $ZnSO_4$ / 2 M Li_2SO_4 electrolyte regardless of

the charging current: 140 mAh·g^{-1} at a current density of 0.2 C and 137 mAh·g^{-1} at I = 1 C. Despite this, during cycling in ternary electrolyte the capacity of cathode decreases significantly faster than in the binary electrolyte (Figure 19, b, c). For example, at a current density of 5 C the capacity of LMO in the ternary electrolyte is only 56 mAh·g^{-1}, while it reached 86 mAh·g^{-1} in solution of zinc and lithium sulfates at the same current density. During 100 charge/discharge cycles, 85% of the initial capacity was retained for the cathode in the bi-salt electrolyte, while in the 1 M $ZnSO_4$ / 2 M Li_2SO_4 / 0.1 M $MnSO_4$ solution, the capacity dropped by 54% over 80 cycles.

A third plateau appears on the charge/discharge profiles at low current density (0.2 C) in the ternary electrolyte at potentials above 2.0 V, which can be attributed to the process of oxidation of Mn^{2+} cations from the solution on the electrode surface. Since there is no reverse dissolution process of the MnO_x precipitate, the Coulombic efficiency of the electrodes becomes significantly lower than 100% (Figure 19, d). When the current density increases (Figure 19, e) the electrode polarization increases significantly, and the potentials of the redox transitions become almost indistinguishable [41].

In summary, it can be concluded that improving the properties of LMO-based cathode materials by adding manganese salt to the electrolyte composition leads to an increase in specific capacity, possibly in a limited range of current densities. Despite the increase in specific capacity, the stability of such cell is much lower than that of the zinc and lithium sulfate binary electrolyte system due to the intensive deposition of the MnO_x layer on the cathode surface and the high probability of oxygen release reaction.

3.2. Synthesis and study of electrochemical properties of MnO_2-based cathode materials depending on synthetic route

Among many manganese oxide polymorphs, the objectives of the work were to obtain the oxide with layered structure. Therefore, after literature analysis, two techniques were selected for the hydrothermal synthesis of δ-MnO_2, the product of one of which has not been previously studied as a cathode material for AZIBs, namely, the material obtained by hydrothermal treatment of aqueous $KMnO_4$ solution in the absence of other reagents [167]. The synthesis of the initial manganese oxides was carried out according to the following reactions:

Synthetic reaction for MnO_2-I:

$$2\,KMnO_4 + 3\,MnSO_4 + 2\,H_2O \rightarrow 5\,MnO_2 + K_2SO_4 + 2\,H_2SO_4 \quad (4)$$

Synthetic reaction for MnO_2-II:

$$4\,KMnO_4 + 2\,H_2O \rightarrow 4\,MnO_2 + 3\,O_2 + 4\,KOH \quad (5)$$

The primary characterization of synthesized MnO_2-I and MnO_2-II powders was performed by XRD to evaluate the phase composition of the synthesis products. It was found that regardless of the reaction mixture composition and synthesis temperature, we obtained the potassium-doped manganese dioxide with birnessite-type structure (Figure 20). The resulting diffraction patterns are well correlated with the ICCD card #01-086-0666, corresponding to the elemental composition of $K_{0.27}MnO_2 \cdot 0.54H_2O$: there are two intense peaks at 12.3 and 24.7 °, corresponding to the (0,0,3) and (0,0,6) planes, as well as a number of paired peaks characteristic of layered crystal structures. The presence of potassium ions in the structure is related to the excess of $KMnO_4$ in reaction systems; in addition, they keep the manganese dioxide layers at fixed distances [93].

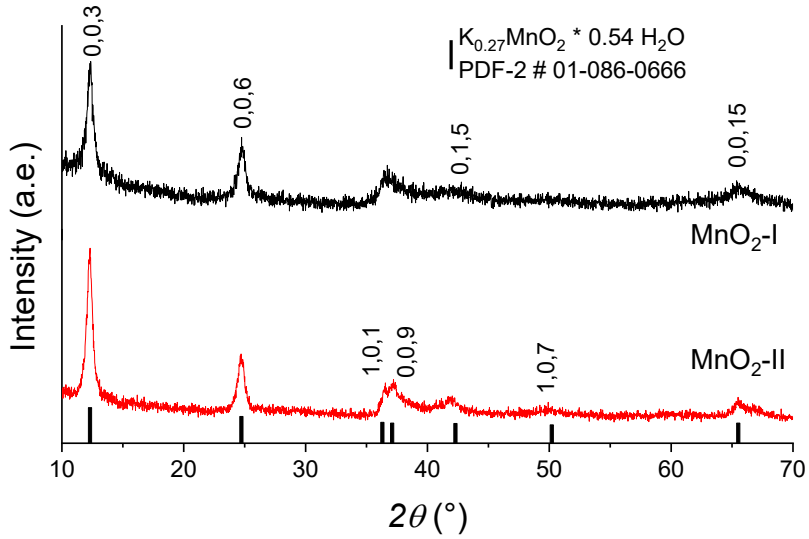

Figure 20. X-ray diffraction patterns of manganese dioxide MnO_2 synthesized by two different ways.

From the XRD data, the crystallite sizes were also estimated, which are slightly different: for MnO_2-I material, crystallites of about 8 nm are observed, for MnO_2-II ≈ 10 nm. The increase in crystallite size is reasonably caused by the increase in the hydrothermal synthesis temperature of the samples in the case of MnO_2-II. In addition, in the MnO_2-I sample, the diffraction maxima are less intense and broader due to a higher degree of amorphous material, confirming the lower crystallinity of the powder.

On the SEM images of MnO_2 powders (Figure 21) some differences in the size of formed agglomerates of particles are observed: for MnO_2-I material there is a trend to the formation of large-size agglomerates (≈90 μm) in which separate crystals are barely discernible (Figure 21, a); when scaling up by 10 times (Figure 21, b), no well pronounced crystal fragments are present, which confirms a more amorphous structure. By contrast, for the MnO_2-II powder it is clearly seen that despite the large agglomerates, they clearly contain smaller particles ranging from 1.5 to 6 μm in size (Figure 21, d) which are clearly distinguishable at higher magnification (Figure 21, e). Together with

the XRD data, it can be concluded that with increasing temperature and synthesis time, there is a tendency for the crystallite size to increase, resulting in an increase in the crystallinity of the sample. At the maximum resolution (Figure 21, c, f) it can be seen that both materials consist of randomly oriented layered structures such as “nanoflowers” or nanosheets. This morphology confirmed the layered structure of the synthesized manganese dioxide for both synthesis methods, while the starting chemicals and the synthesis temperature influenced the micromorphology of the obtained materials.

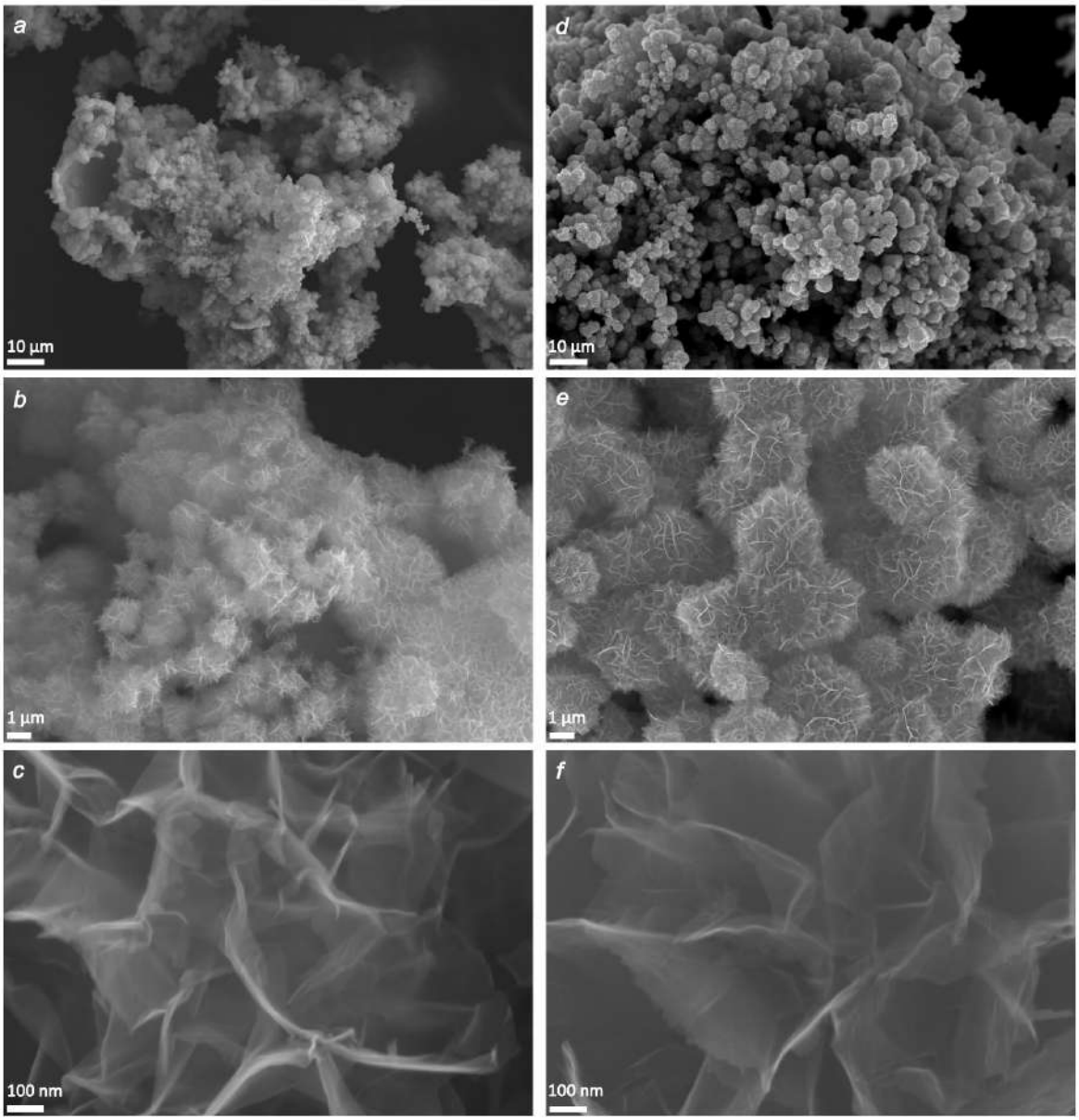

Figure 21. SEM-images of MnO_2-I (a – c) and MnO_2-II (d – f) powders at different resolutions: 10 µm (a, d), 1 µm (b, e) and 100 nm (c, f).

To study the electrochemical properties of the prepared cathode materials, the Zn//MnO_2 two-electrode cells of CR2032 type were assembled with aqueous 2 M $ZnSO_4$ / 0.1 M $MnSO_4$ electrolyte, selected on the basis of literature analysis of electrochemical performance of MnO_2-based cathode

materials. Primary characterization of the properties of the assembled cells was carried out using CV technique at the potential scan rate of 0.1 mV·s^{-1}. Hereinafter, the term "potential" refers to the electrical potential difference between the metal contacts of a two-electrode cell; the term "cell voltage" is commonly used. On the CV curves for both types of materials shown in figure 22, two pairs of peaks at E = 1.57/1.25 V and E = 1.61/1.37 V are observed. Notably, only one peak is present at E = 1.21 V for the MnO_2-I material and at E = 1.18 V for MnO_2-II on the first discharge cycle. This form of the CV curves is in accordance with the dependences reported in the literature [89,92], detailed discussion and correlation of the peaks on the Cv curves and electrochemical reactions in the system with the participation of H^+ and Zn^{2+} cations will be presented further in Chapter 4 and Chapter 5 of this work.

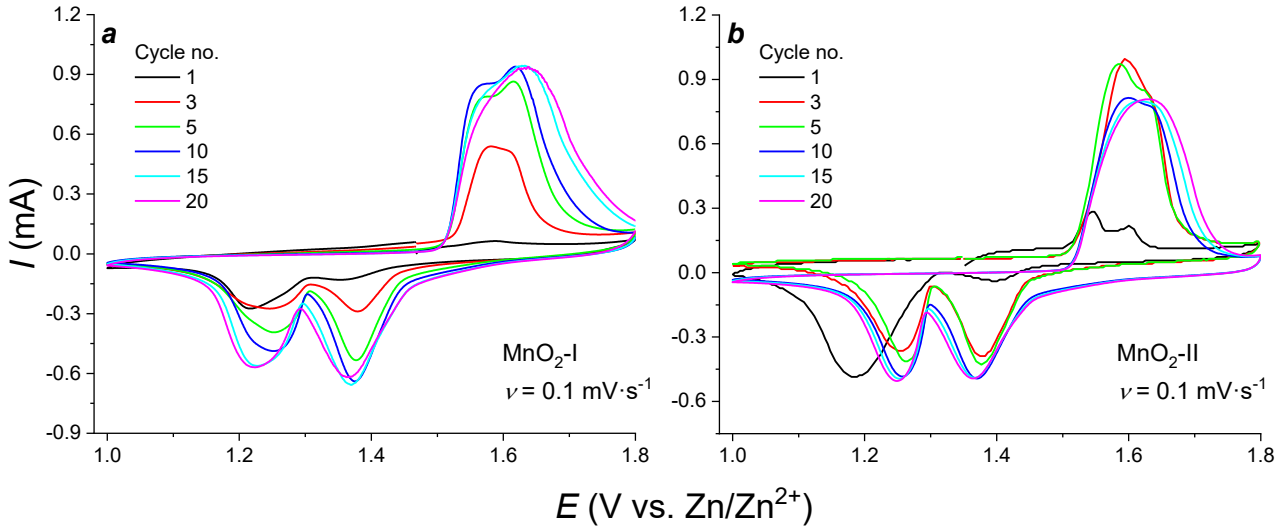

Figure 22. CV curves for MnO_2-based cathodes depending on the cycle number at the scan rate of 0.1 mV·s^{-1} for MnO_2-I (a) and MnO_2-II (b).

From the presented data, the difference in the electrochemical behavior of materials with different degrees of crystallinity can be seen. For the MnO_2-I material, a constant increase in both anodic and cathodic currents is observed from the first to the tenth cycle, followed by a less intense increase in current density with further stabilization of the current response (Figure 22, a). The current growth is explained both by a more complete "utilization" of the electrode material and by the accompanying process of precipitation of the MnO_x phase from the electrolyte solution [17]. The MnO_2-II sample synthesized from the $KMnO_4$ solution in the absence of manganese sulfate shows an increase of the anodic current after the first cathodic cycle, while the cathode current density changes insignificantly. After the fifth cycle, a slight drop in the anodic current and its subsequent stabilization are observed, while the cathodic currents do not increase considerably (Figure 22, b). Such behavior could be explained by the difference in the crystallinity of the electroactive materials: in a more amorphous material, the intercalation processes and the accompanying process of MnO_x deposition on the cathode

surface proceed more easily than in the case of an oxide with higher crystallinity. This effect is widely known for cathode materials based on vanadium oxides [170,171] and was previously shown for MnO_2-based cathodes [92,93]. For both materials, the CV curves show a shift of the anodic peaks to more positive voltages, and of the cathodic peaks to lower voltage values. With increasing number of cycles, the initially well-separated anodic peaks become less pronounced and a single broad anodic peak is observed on the CV curves. Since the masses of electroactive components in the composition of cathode materials are equal, the CV data are given in absolute current values.

The electrochemical performance of the CR2032 cells was studied by galvanostatic charge/discharge. The C-rate capability for both materials is shown in figure 23. It can be observed that the initial capacity of the MnO_2-II based cathode is twice higher – 222 $mAh \cdot g^{-1}$ compared to that of MnO_2-I material – 103 $mAh \cdot g^{-1}$. However, at low currents, an increase in the specific capacity at constant current density is observed for the MnO_2-I cathode, which is caused by additional precipitation of MnO_x from the electrolyte solution (the capacity at 35th cycle at a current density of 0.1 $A \cdot g^{-1}$ was 210 $mAh \cdot g^{-1}$). In the range of current densities 0.5 – 5.0 $A \cdot g^{-1}$, the specific capacities of the materials are comparable (Figure 23, a) [39].

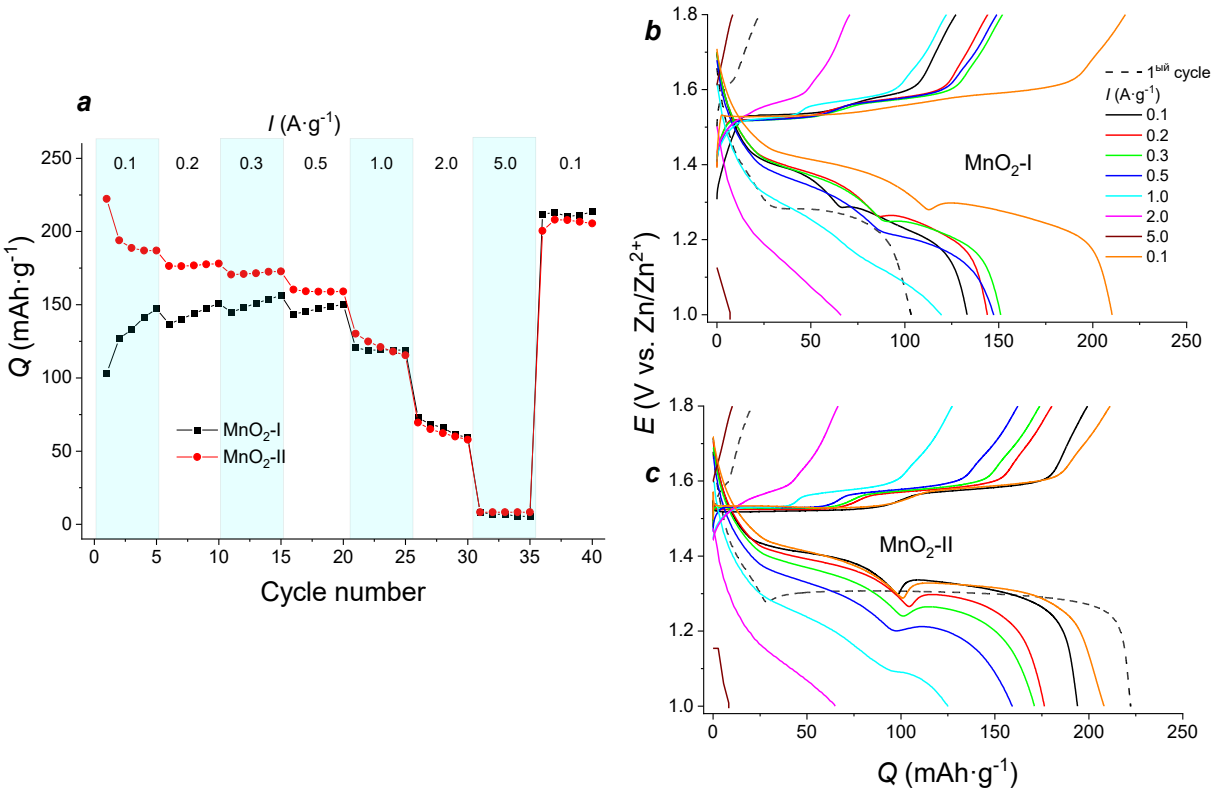

Figure 23. C-rate capability for Zn//MnO_2 cells (a), charge/discharge profiles for MnO_2-I (b) and MnO_2-II (c) cathode materials.

In the first charge/discharge cycle for both types of materials (Figure 23, b,c), there is only one plateau on the discharge curve at E = 1.30 V, which can be compared to the first reduction cycle on CV. In the subsequent cycles, two plateaus are observed on the discharge curve at E = 1.4 V and E = 1.28 V. There is also a characteristic feature on the discharge curve: a slight rise or kink at E = 1.24 – 1.27 V at different discharge current values (indicated by *), which is related to the chemical reaction of precipitation of the basic salt of zinc hydroxide sulfate (ZHS), caused by a local change in the pH of the electrode layer [13,25,143,168,172]. Two plateaus are observed on the charge curve at $E \approx 1.55$ V. The voltage values of the observed plateaus correlate well with the peaks on the CV curves. As the discharge current increases from 1 to 5 $A \cdot g^{-1}$, the plateaus become less pronounced due to the high rate of the processes and the resulting incomplete utilization of cathode material capacity.

The cyclability of cathode materials was studied at a current density of 0.3 $A \cdot g^{-1}$ during 100 cycles (Figure 24). For the amorphous MnO_2-I material the initial capacity was 113.6 $mAh \cdot g^{-1}$, while for the MnO_2-II cathode the initial capacity was 183.3 $mAh \cdot g^{-1}$. During the first 30 cycles, a small capacity growth up to 134.7 $mAh \cdot g^{-1}$ was observed for MnO_2-I, after which the capacity fading was 10% from the maximum value. For MnO_2-II, despite the presence of $MnSO_4$ additive in the electrolyte solution, the MnO_x deposition process did not lead to a significant positive effect: there was at first a sharp (during 25 cycles) and then a more gradual capacity decrease that stabilized after 60 cycles, resulting in only 52% of the initial capacity retained. The Coulomb efficiency for both materials is close to 100% (Figure 24, a). Thus, from the point of view of cyclic stability, the more amorphous material is of interest due to the greater number of internal lattice defects, as discussed previously [92,93].

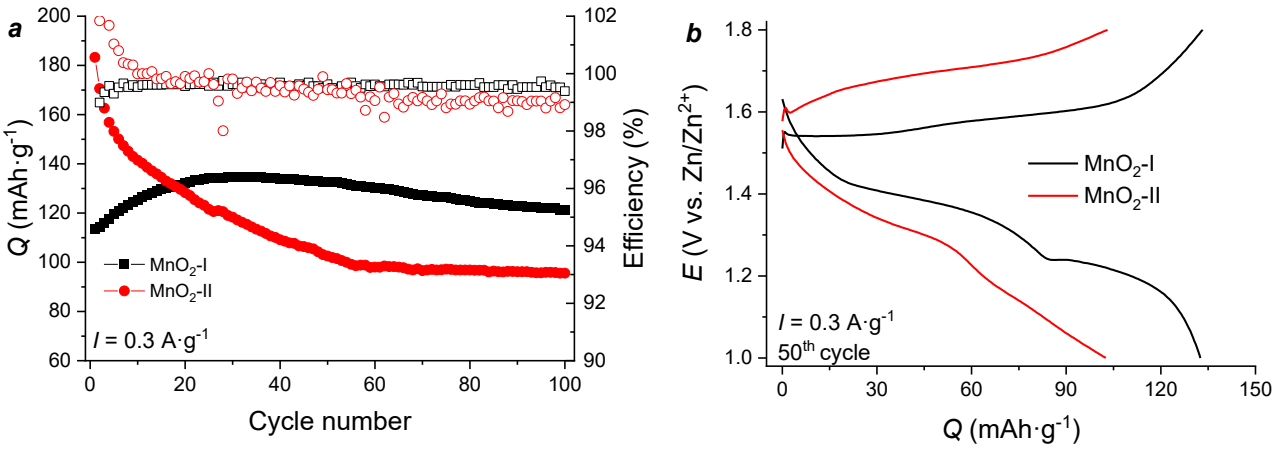

Figure 24. Cyclic stability (a) and charge/discharge profiles (b) for Zn//MnO_2 cells at I = 0.3 $A \cdot g^{-1}$.

The difference of the two materials is clearly seen in the charge/discharge curves. For the amorphous manganese oxide, two poorly resolved plateaus are observed on the charge curve at E = 1.56 V and E = 1.60 V, which are matched by clearly separated discharge plateaus at E = 1.37 V and E = 1.22 V. There is also a kink in the curve at E = 1.26 V described above. For the MnO_2-II

material both charge and discharge plateaus are weakly expressed, the electrode polarization is practically twice as high compared to the MnO_2-I material and the kink in the discharge curve is negligible (Figure 24, b).

Based on the higher polarization of the MnO_2-II cathode during long-term cycling, it can be concluded that the internal ohmic resistance of the cell increases during operation. To test this hypothesis and study the kinetic parameters, electrochemical impedance spectroscopy was applied. The measurements were performed after registration of 20 CV cycles at the scan rate of 0.1 $mV \cdot s^{-1}$ at the voltages values close to the values of the redox-transition potentials: 1.48, 1.38, and 1.30 V, since the spectra at E = 1.8, 1.26, and 1.0 V are uninformative. The obtained data are shown in figure 25.

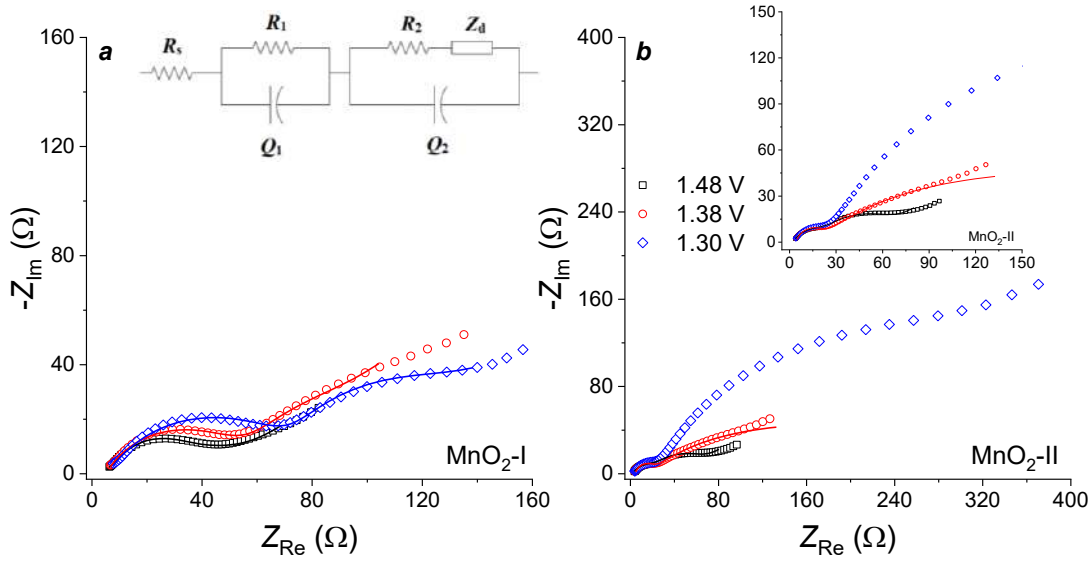

Figure 25. Impedance spectra for Zn//MnO_2 cells based on MnO_2-I (a) and MnO_2-II (b) at different voltage values during the discharge. The inset shows the spectrum for the MnO_2-II-based cell at higher magnification. The figure shows the equivalent circuit, the dots on the graph indicate the experimental data, the lines – the impedance spectra calculated according to the equivalent circuit.

For the Zn//MnO_2-I cell the shape of spectrum was weakly dependent on the voltage value: we observed two semicircles in the high- and mid-frequency regions and a linear part with a slope of 45° in the low-frequency region corresponding to the diffusion limitations of the cell (Figure 25, a). In the case of the MnO_2-II cathode, there is a well-defined semicircle in the high-frequency region coinciding with the resistance value (inset of Figure 25, b), as well as a second semicircle that increases with decreasing cell potential, which is particularly noticeable in the transition from E = 1.38 V to E = 1.30 V. The diffusion part of the spectrum is weakly expressed. All of the above spectra could be described satisfactorily using the equivalent circuit given in the literature for the Zn//MnO_2 cells [13,142,173]. In this circuit, the interphase resistance R_1 corresponds to the zinc anode/electrolyte; the resistance R_2 is formed at the cathode/electrolyte interface or is determined by the combination of zinc anode and

cathode material; the diffusion resistance Z_d corresponds to the ion intercalation into the MnO_2-cathode structure [13].

The analysis of the spectra by the equivalent circuit method showed that for both cathode materials, in all the measured states, the resistance value R_1 corresponding to the first semicircle, varies insignificantly, which allows us to attribute it to a constant interface, i.e., the interface between the zinc anode and the electrolyte solution. For the interfacial resistance R_2, corresponding to the second semicircle, other tendencies are observed: its value does not increase significantly with the change of potential for the MnO_2-I material, while for the MnO_2-II cathode the growth is sharper. The resistance jump at $E = 1.30$ V can be caused by the beginning of the process of formation of a non-conductive phase on the electrode surface – the basic zinc salt ZHS.

In addition, the diffusion regions of the spectra were analyzed in Z_{Re}, $-Z_{Im} - \omega^{-1/2}$ coordinates according to the Mathias-Haas criteria [174]. The values of the Warburg constants σ_W which are related to the diffusion coefficient of the intercalated ions (Zn^{2+} and/or H^+) were calculated from the following equation:

$$D_{Me^{+n}} = \frac{R^2T^2}{2A^2n^4F^4c^2\sigma_W^2} \quad (6)$$

This equation shows an inverse relationship between the diffusion coefficient and the value of the Warburg constant. Quantitative calculation of the D_{Me} value is impossible due to the complexities of the mechanism of Zn//MnO_2 cells operation (possible participation of two types of cations) as well as unknown concentration of the charge transfer ions (Zn^{2+} and H^+) in the MnO_2 crystal lattice.

Based on the Z_{Re}, $-Z_{Im} - \omega^{-1/2}$ dependencies, it follows that the value of the slope of the parallel section, or the Warburg constant value, is lower for the MnO_2-I material which indicates faster ions diffusion in the more amorphous crystal lattice (Figure 26) which was previously observed [92].

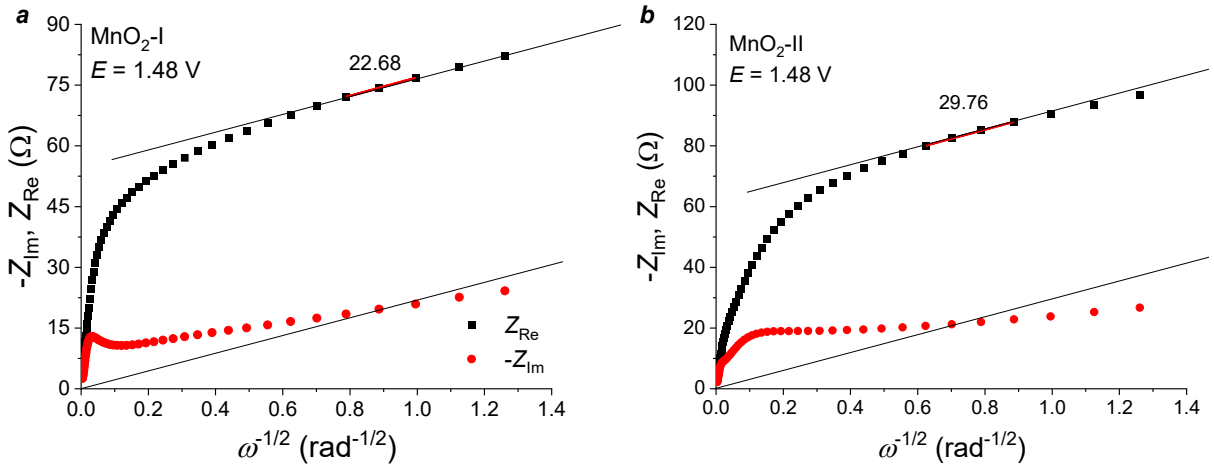

Figure 26. Z_{Re}, $-Z_{Im} - \omega^{-1/2}$ dependencies for Zn//MnO_2 cells obtained at E = 1.48 V for MnO_2-I (a) and MnO_2-II (b).

Thus, depending on the synthetic conditions (reaction mixture composition, time and temperature of hydrothermal synthesis), samples with the same phase composition and nanostructure are obtained, but the differences in micromorphology and degree of crystallinity are observed. These differences have a significant impact on the functional properties of the cathode materials, namely the initial specific capacity value and cyclic stability. In the case of more crystalline MnO_2 oxide, the initial capacity is significantly higher, but during cycling the material loses almost 50% of its initial capacity just over 100 cycles. At the same time, the material with a higher degree of amorphousness (MnO_2-I) has lower capacity values, but due to the increase of the specific capacity during cycling caused by the deposition of additional MnO_x layers, it retains 90% of the maximum capacity after 100 charge/discharge cycles [39], which makes it a more promising material for further study and the creation of cathodes based on it.

3.3. Effect of conducting polymer-based modifier on specific characteristics of δ-MnO_2-based cathode materials

3.3.1. Addition of conducting polymer to the electrode composition

As it has been shown in numerous papers cited in the review of the properties of manganese oxide based cathode materials [40], conducting polymers are promising materials to improve the overall electronic and ionic conductivity of manganese oxides, in addition to having a significant effect on the specific capacity values and cyclability of cathodes. Poly(3,4-ethylenedioxythiophene), including the aqueous dispersion PEDOT:PSS, was chosen to improve the properties of MnO_2-I-based cathode materials (the synthesis designation “I” is omitted in the following text).

The cathode material was modified using two methods: addition of chemically synthesized PEDOT polymer to the electrode composition (the amount of active material and binder was decreased) and dispersing δ-MnO_2 powder in aqueous dispersion of PEDOT:PSS with subsequent evaporation of water to create a polymer shell on the surface of the active component grains. The ratios of components in the electrode composition, as well as the designations of materials are given in table 1.

The PEDOT powder obtained by chemical synthesis was studied by EDX analysis to estimate the element ratios. It was observed that the mass fraction of carbon is close to the theoretical value (56.88 wt.%), while the fraction of oxygen is lower and of sulfur is higher (11.64 wt.% and 31.47 wt.%, respectively). The morphology of the powder was evaluated by SEM (Figure 27). The powder consists of small porous granules, easily agglomerating into particles of ≈ 30 μm in size, with the occurrence of particles of ideal spherical shape, which are uncharacteristic for this polymer, containing 0.1 –

0.2 wt.% of chlorine due to the presence of $FeCl_3$ in the reaction mixture as oxidant. The size of the spheres averages 2 – 5 μm (Figure 27, b).

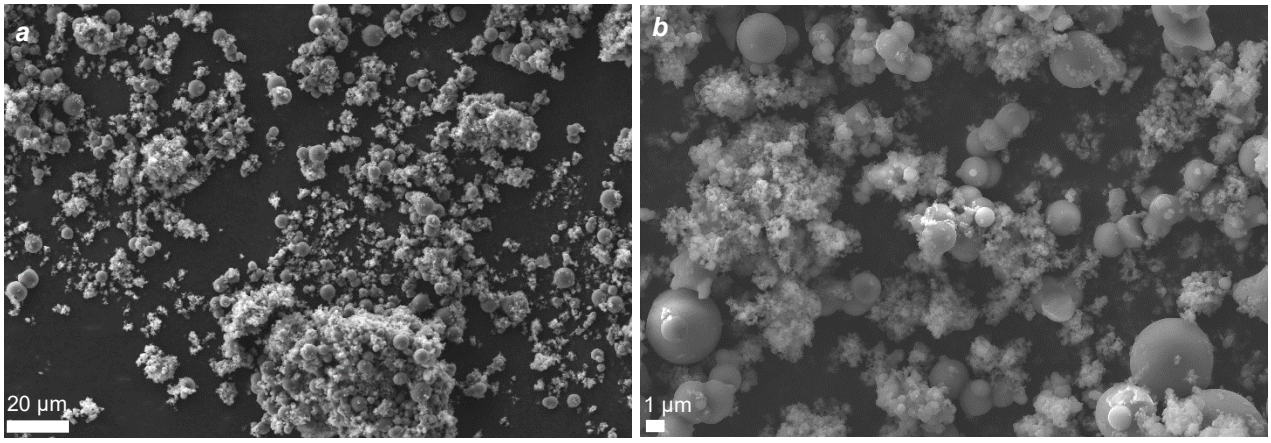

Figure 27. SEM images of PEDOT powder at 20 μm (a) and 1 μm (b).

The morphology of cast electrode materials was also studied by scanning electron microscopy combined with EDX-analysis. The MnO_2 electrode material (Figure 28, a) is characterized by a nonuniform structure in which the grains of the active component agglomerate into large fragments. In contrast, a denser and smoother surface is observed for both types of PEDOT-containing electrodes (Figure 28, b, c).

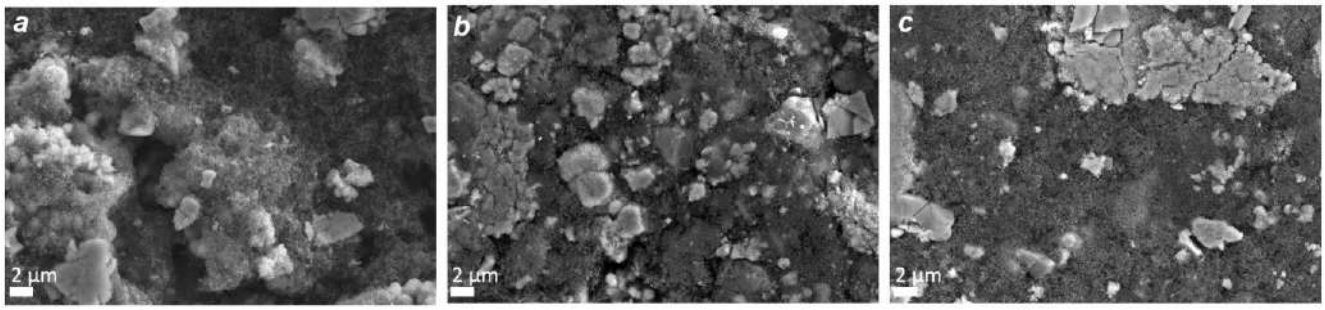

Figure 28. SEM images of MnO_2 (a), MnO_2/PEDOT (b) and MnO_2/PEDOT:PSS (c) cathode materials.

The elemental distribution of the main components of the cathode materials was studied by EDX analysis. In all cases, a complete correlation between the distribution of manganese and oxygen can be seen, confirming the presence of manganese oxide, as well as a uniform distribution of fluorine, confirming the homogeneity of the electrode material (Figure 29).

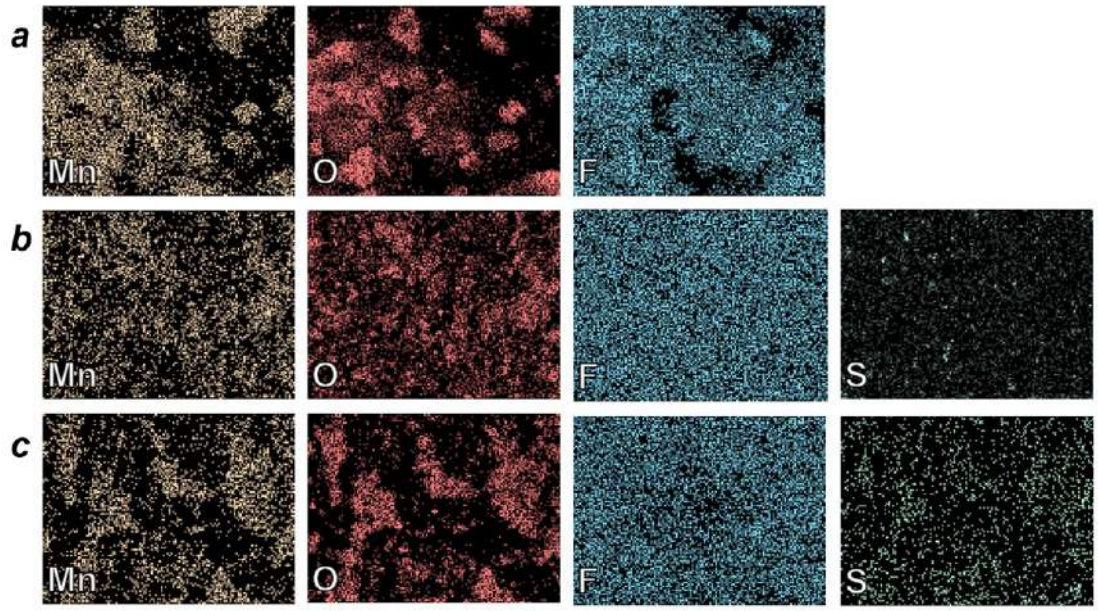

Figure 29. EDX-mapping of the Mn, O, F and S for MnO_2 (a), MnO_2/PEDOT (b) and MnO_2/PEDOT:PSS (c) cathode materials.

After the addition of the conducting polymer, a more uniform distribution of the components on the surface of the electrode material is observed, the polymer particles being linked with most of the grains of the active material (Figure 29, b). In the case of the cathode material with PEDOT:PSS coating, the elemental distribution for sulfur has a higher coincidence with that of manganese, indicating the creation of a polymer coating on the MnO_2 surface (Figure 29, c).

The electrochemical properties of the electrode materials were investigated by CV at the scan rates of 0.1 – 0.5 $mV \cdot s^{-1}$. In general, the CV shapes for different cathodes were very similar and they showed two weakly resolved anodic peaks for MnO_2/PEDOT:PSS electrodes, and two distinct cathodic peaks at E = 1.37 V and E = 1.24 V. The effect of the addition of the conducting polymer is observed in the increase of the anodic current by ≈ 1.5 times for the MnO_2/PEDOT and MnO_2/PEDOT:PSS electrodes, the cathodic currents are slightly higher than for the MnO_2-based electrode. In addition, the cathodic peak at E = 1.24 V is broadened with respect to the unmodified cathode, the so-called “diffusion valleys” are observed, caused by the progressive ZHS precipitation on the more porous surface due to the additional porosity of PEDOT or PEDOT:PSS (Figure 30, a).

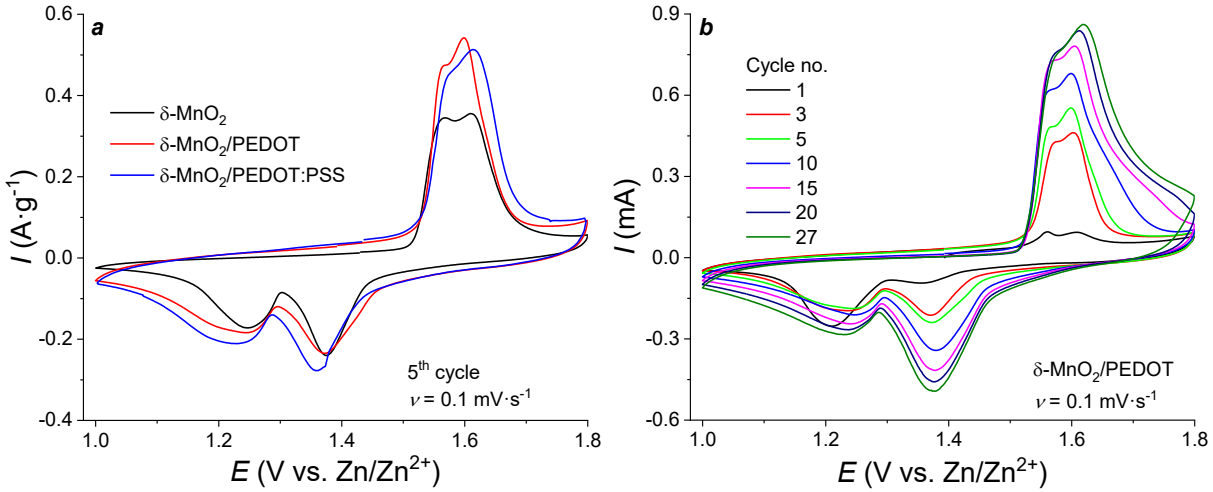

Figure 30. CV curves for MnO_2-cathodes at the scan rate of 0.1 $mV \cdot s^{-1}$: comparison of different cathode materials at 5th cycle (a) and the dependence on the cycle number for MnO_2/PEDOT (b).

As already mentioned, in the electrolyte solution with the addition of manganese sulfate, for all three cathode materials, a gradual growth of currents is observed, as already recorded (see Figure 22, a), due to the formation of the MnO_x layer on the electrode surface, which has its own electroactivity. In particular, for the MnO_2/PEDOT electrode, the capacity growth is observed during 25 CV cycles (Figure 30, b) [38].

In order to evaluate the effect of the conducting polymer on the charge transfer kinetics in modified cathode materials, the nature of the limiting stage was analyzed by the CV at different scan rates. With increasing scan rate (from 0.2 $mV \cdot s^{-1}$ to 0.5 $mV \cdot s^{-1}$) close tendencies are observed for both electrode materials: anodic peaks become practically inseparable and shift to the more positive potentials with increasing scan rate. The cathodic peak at E = 1.24 V almost disappears at high scan rates, while the second one at E = 1.4 V is slightly increased and shifts insignificantly to the more negative potentials (Figure 31, a, c).

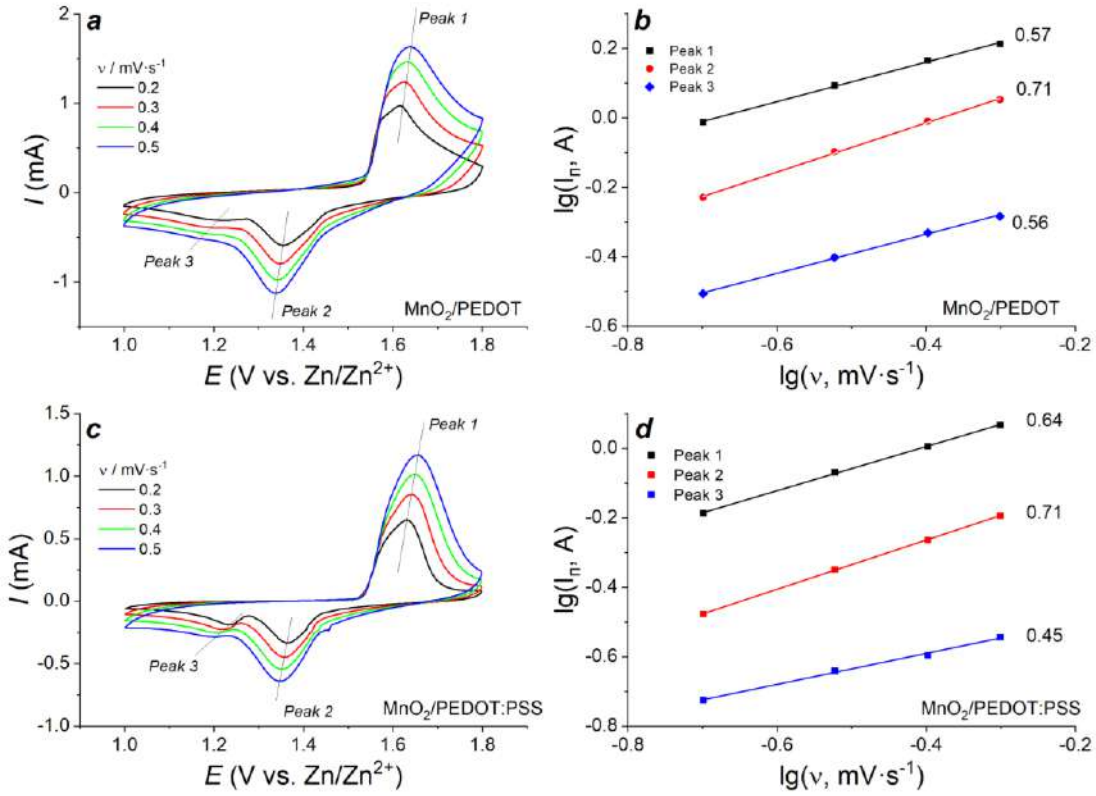

Figure 31. CV curves for MnO_2/PEDOT (a) and MnO_2/PEDOT:PSS (b) cathodes depending on the scan rate; bilogarithmic dependencies of peak current on scan rate for MnO_2/PEDOT (c) and MnO_2/PEDOT:PSS (d) electrodes.

To evaluate the limiting stage of the electrode process, the value of the peak current (anodic or cathodic) was analyzed as a function of the scan rate. This dependence can be described by an empirical equation written in the logarithmic form:

$$(\log I_p) = \log a + b \cdot \log \nu \tag{7}$$

The value of *b*, defined as the tangent of the slope of the logarithmic dependence, is in the range 0.5 – 1.0. When the *b* value is close to 0.5, the limiting stage of the process is mass transfer, and the *b* value close to 1.0 corresponds to the capacitive response. However, due to the complexity of the mechanism and the different nature of the ongoing reactions (both chemical and electrochemical), this analysis to assess the diffusion limitations is only qualitative. For example, for the MnO_2/PEDOT cathode, the values of the slope 0.57, 0.71 and 0.56 were obtained, which correspond to a greater extent to diffusion control in the case of deintercalation processes and the second redox transition at $E \approx 1.2$ V, while for the first cathodic process (E = 1.34 V) we should speak of mixed diffusion-capacitive control (Figure 31, b). For the MnO_2/PEDOT:PSS electrode the *b* values were 0.64, 0.71 and 0.45. The difference of the *b* value for the second cathodic process from the theoretical one

($b < 0.5$) is due to the parallel chemical process of ZHS deposition and, therefore, it is more correct to speak here about the movement of Zn^{2+} ions and hydroxide anions to the cathode surface (Figure 31, d). Thus, to a considerable degree, the rate of the electrochemical process is limited by the ion diffusion.

The electrochemical performance of the cells with three cathode materials was studied by galvanostatic charge/discharge in different modes. It can be seen that at low current densities (0.1 – 0.5 $A \cdot g^{-1}$) the specific capacity of electrodes with conducting polymer additives is much higher than of the unmodified MnO_2-cathode. At a current density of 0.1 $A \cdot g^{-1}$ the specific capacities were 133, 210 and 291 $mAh \cdot g^{-1}$ for MnO_2, MnO_2/PEDOT and MnO_2/PEDOT:PSS electrodes, respectively (Figure 32, a). In the wide current range the specific capacity of PEDOT:PSS-coated electrode material is close to the theoretical value (in the case of one-electron transfer, or Mn^{IV} – Mn^{III} process). For all three cathodes, an increase in the specific capacity at constant discharge current was also observed due to the additional formation of the electroactive precipitate, which could be seen on the surface of a stainless steel disk (spacer) in contact with the electrolyte. At high current densities the capacity of the materials drastically decreased, i.e., at $I = 2.0$ $A \cdot g^{-1}$ the specific capacity was 66, 103 and 133 $mAh \cdot g^{-1}$ for MnO_2, MnO_2/PEDOT and MnO_2/PEDOT:PSS electrodes, respectively, and at further increase of the current up to 5.0 $A \cdot g^{-1}$ the capacity dropped to 6 $mAh \cdot g^{-1}$ for MnO_2-cathode and to 35 – 40 $mAh \cdot g^{-1}$ for the cathodes with conducting polymer.

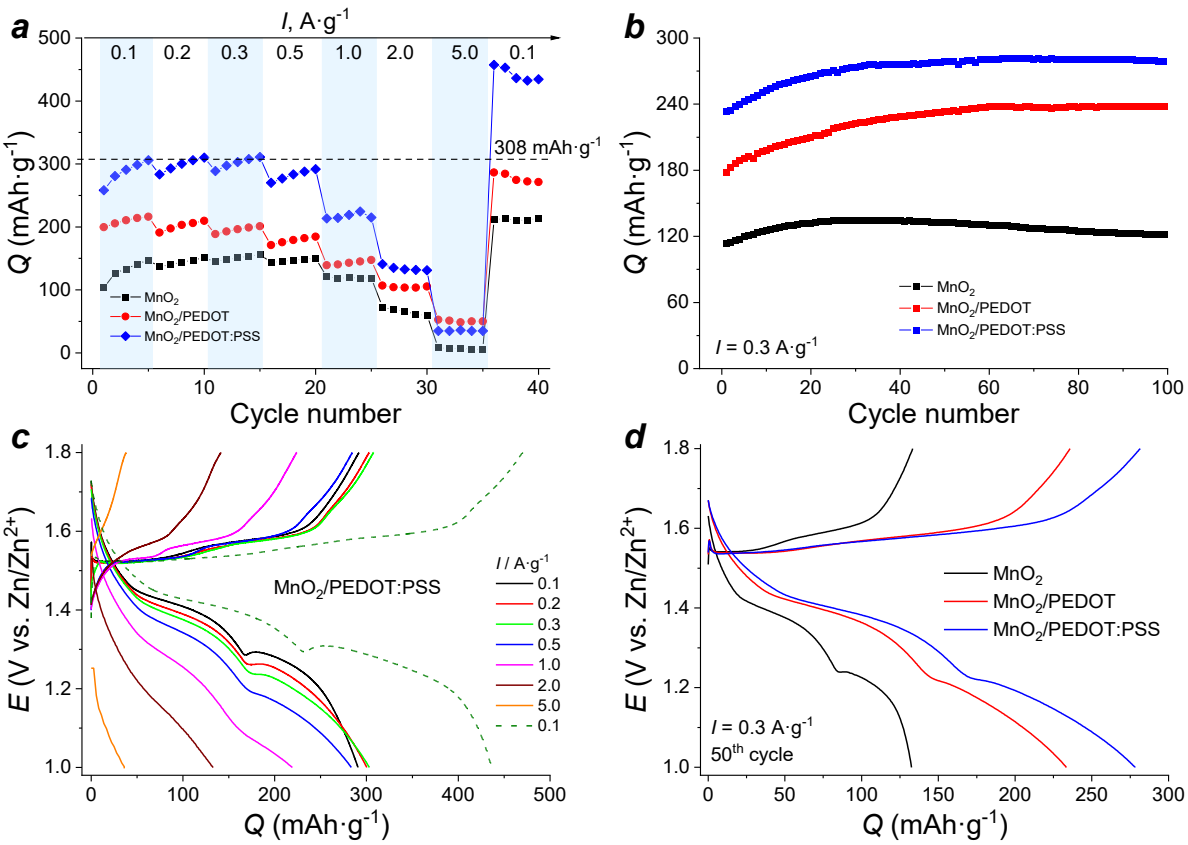

Figure 32. Electrochemical performance of MnO_2-based cathode materials: C-rate capability (a) and cyclic stability at 0.3 A·g^{-1} (b); charge/discharge profiles for MnO_2/PEDOT:PSS cathode (c) and for all cathode materials at 0.3 A·g^{-1} (d).

The cyclic stability of the cathode materials was evaluated at a current density of 0.3 A·g^{-1} during 100 charge/discharge cycles (Figure 32, b.). During the initial 20 – 30 cycles a capacity increase was observed for all three cathodes – 15% for MnO_2, 25% for MnO_2/PEDOT, and 20% for MnO_2/PEDOT:PSS. During further cycling a small capacity fading (10% from the maximum value of 134 mAh·g^{-1}) was observed for the MnO_2-cathode, while no capacity fading occurred for the polymer-modified electrodes, which retained 99% of the maximum value [38].

The shape of the charge/discharge profiles of the MnO_2/PEDOT:PSS electrode is well correlated with that previously observed for the manganese oxide-based cathode (Figure 32, c): two discharge plateaus at E = 1.4 V and E = 1.25 V, and a plateau on the charge curve at E = 1.55 V are observed. The discharge curves clearly show that the plateau at E = 1.4 V is slightly longer than the second one, i.e. this this process is the dominant energy storage reaction. The discharge curves at E = 1.26 – 1.28 V also show a kink in the curve and a slight increase in potential. It corresponds to zinc ion intercalation or/and chemical precipitation of a Zn^{2+}-containing insoluble byproduct zinc hydroxide sulfate ZHS. For the materials with conducting polymer additives the slope of the curve is smoother at the end than for the pristine MnO_2-based cathode (Figure 32, d) which correlates with the shape of CV curves of MnO_2/PEDOT and MnO_2/PEDOT:PSS electrodes in this voltage range.

To examine the surface changes during the cell cycling, the electrode materials before and after 100 charge/discharge cycles were studied by *ex situ* XPS. The survey spectra of electrode materials (Figure 33, a, b) shows the changes in the peak intensities of the main components that occurred after long-term cycling. Thus, there is a sharp increase in the intensity of the oxygen peak and an increase in its surface content almost 7 times (≈ 9% before and ≈ 70% after cycling) which is due to a number of factors like the formation of the basic zinc salt (ZHS) on the electrode surface and partial decomposition of electrode material components due to the overall degradation of the cathode, which is expressed in a decrease in the surface content of carbon, fluorine and manganese, as can be seen from the change in the intensity of their respective peaks. Also new peaks in the range of 1020 – 1050 eV are observed after cycling, which correspond to the presence of zinc ions in the composition of the electrode material, and in the case of pristine MnO_2-cathodes these peaks are more intense than in the case of polymer-modified composite.

Detailed examination of the state of manganese in the composition of the electrode materials is shown in figure 33, c. It can be seen that after cycling there is a slight shift of the peaks by the same fixed value, with the value of the spin-orbit splitting energy being 11.7 eV, which correlates with the data previously obtained for MnO_2 [175]. Depending on the modification strategy, the surface manganese content in the cathode material also changes (Figure 33, c, red curves): in the case of unmodified MnO_2, practically zero intensity of manganese peaks is observed, while for polymer-modified electrodes the intensity is maintained; in the case of MnO_2/PEDOT:PSS cathode, the intensity of peaks before and after the tests is practically the same. This indicates that the PEDOT:PSS coating on the surface of MnO_2 particles prevents the dissolution of the active material during cycling.

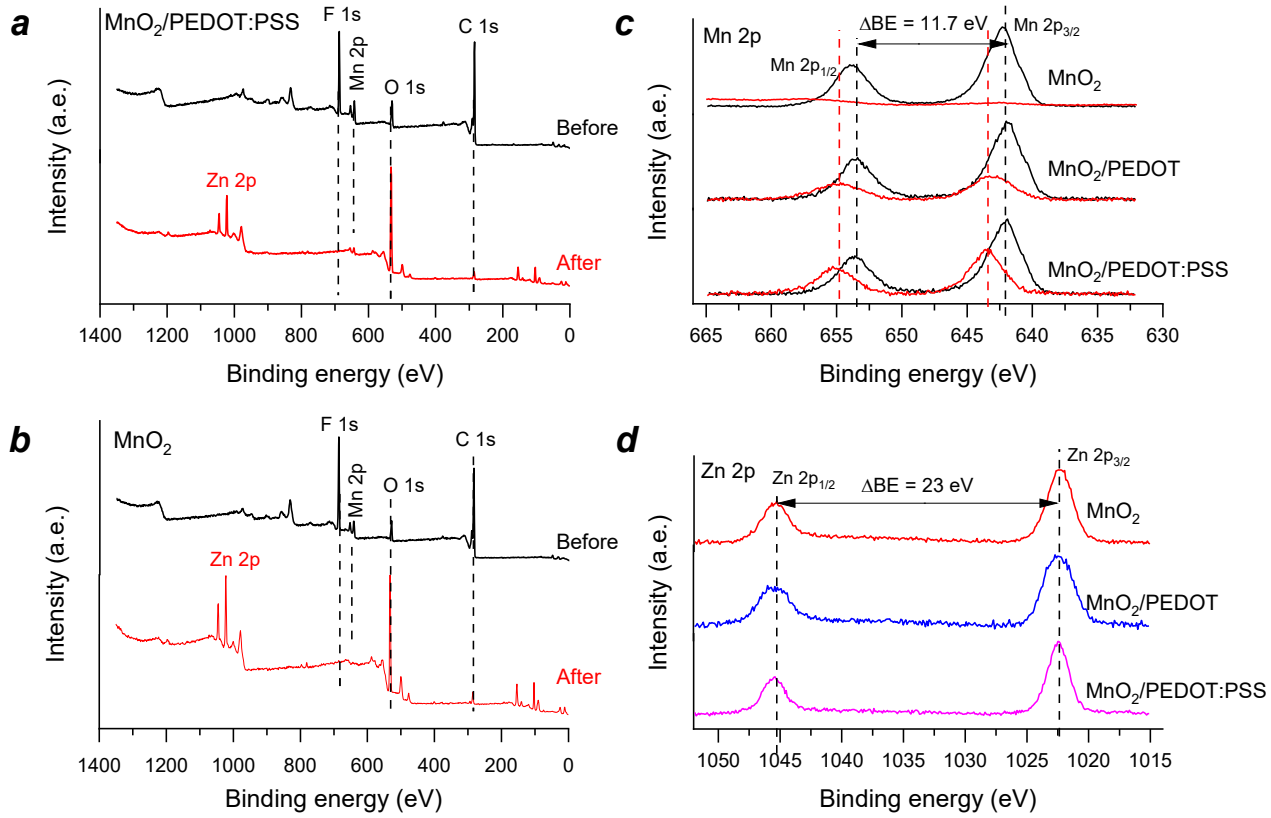

Figure 33. XPS spectra for MnO_2-based cathodes before and after electrochemical tests: survey spectra for MnO_2/PEDOT:PSS (a) and MnO_2-cathodes (b); high resolution XPS spectra of Mn 2p (c) and Zn 2p (d) for all three cathode materials.

After 100 charge/discharge cycles, for all three materials in the discharged state the peaks corresponding to Zn^{2+} cations are observed (Figure 33, d), i.e., there is a surface interaction between zinc ions and the cathode material, including a possible process of intercalation of Zn^{2+} ions into the MnO_2 structure. At the same time, zinc predominates in the ratio of elemental content: for the unmodified oxide, the Mn:Zn ratio was about 1:15 atomic percent, while for the polymer-modified cathodes it was about 1:3. Thus, in the absence of a conducting polymer, there is a significant change in the surface of the cathode material caused by the dissolution of MnO_2, while the use of PEDOT or PEDOT:PSS as part of the electrode material allowed to suppress the dissolution of the cathode and, as a consequence, had a positive effect on the functional properties of the system.

In order to study the composition of the electrodes and the phases formed during discharge and charge under electrochemical tests, the XRD patterns of MnO_2-based cathodes were obtained. The first phase present in the XRD patterns of the electrode materials in the discharged state (Figure 34, a) is δ-MnO_2 ($K_{0.27}MnO_2 \cdot 0.54H_2O$) with no main diffraction maxima for the cathode without conducting polymer (only maxima at 36 and 65° are present), which may be due to both dissolution of the cathode during cycling and to a decrease in the degree of oxidation of manganese in the cathode. However, the maxima of the (0,0,3) and (0,0,6) planes are preserved for the cathodes modified by the conducting

polymer, which proves the protective functions of the polymer as a modifier. The second phase is the zinc-containing manganese oxide $ZnMn_3O_7$-$2H_2O$ (ICCD card #00-047-1825), identified by strong diffraction peaks at 18.55, 33.67, 36.59 and 65.39 °. It should be noted that several peaks (12.35, 25.14, 32.75, 35.12 °) are broader due to the presence of the highly amorphous phase $Zn_4(OH)_6SO_4 \cdot 1.55H_2O$ (ZHS, ICCD card #00-044-0674). For electrodes with conducting polymer, the diffraction peaks of $ZnMn_3O_7$ are fewer and lower in intensity than the peaks of the MnO_2 cathode, while the peaks corresponding to the ZHS phase are clearer. This is the evidence that PEDOT or PEDOT:PSS prevents the active irreversible insertion of zinc ions into the electrode material lattice.

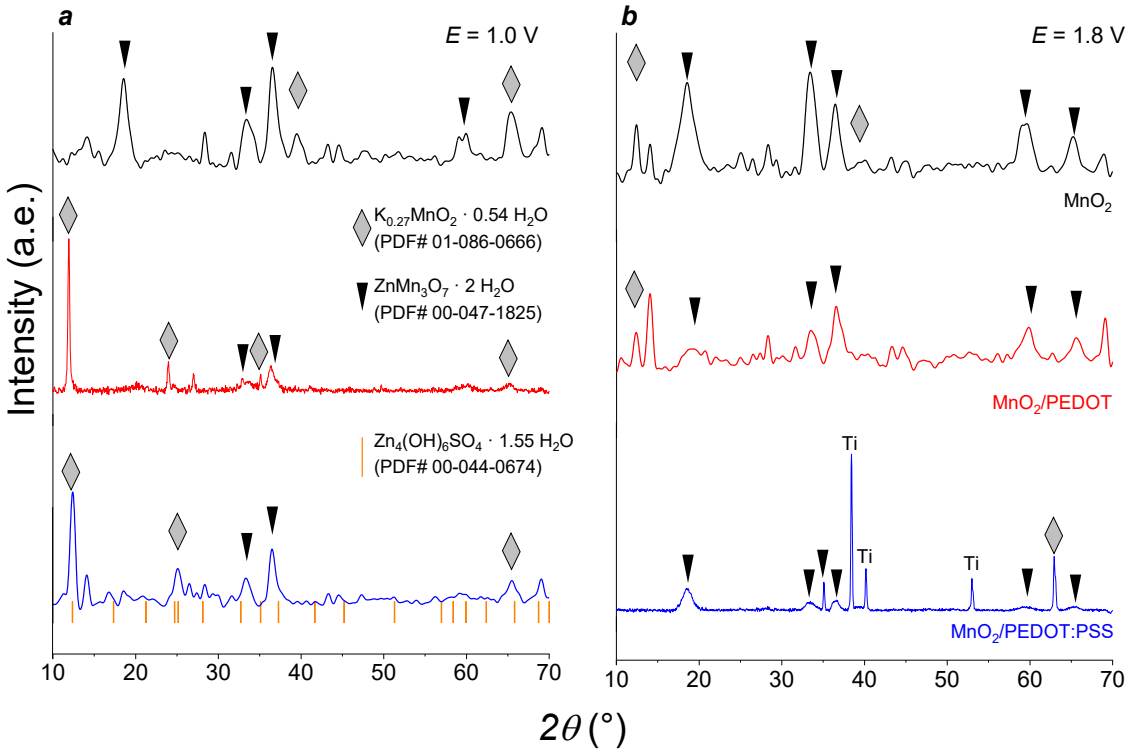

Figure 34. X-ray diffraction patterns of MnO_2-based electrode materials after electrochemical tests in fully discharged (a) and fully charged (b) states.

In the charged state (Figure 34, b), no peaks corresponding to the ZHS phase are observed in the diffractograms for all three materials; therefore, there is a change in the pH of the near-electrode layer during charging, resulting in the dissolution of the additional surface layer of ZHS salt, as previously observed for electrodeposited MnO_2 [168]. The main crystal phases are MnO_2 formed during charging due to the presence of $MnSO_4$ in the electrolyte, and $ZnMn_3O_7$, which has no electrochemical activity and does not participate in the charge/discharge process [38]. The presence of zinc-containing phase of manganese oxide in the charged state may be evidence of irreversible intercalation of zinc ions into the MnO_2 crystal lattice.

3.3.2. Electrodeposition of PEDOT on the prepared MnO_2-cathodes surface

An alternative way to modify the cathode materials is to deposit a polymer coating on the surface as-prepared electrode material, similar to the approach previously used for a mixture of manganese oxides of different morphologies [35]. The synthesis of PEDOT polymer on the surface of the electrode material was carried out in potentiostatic mode at E = 1.1 V vs. Ag/AgCl pseudoreference electrode with varying the deposition time (300 and 600 s). The resulting composite was characterized by scanning electron microscopy and X-ray photoelectron spectroscopy.

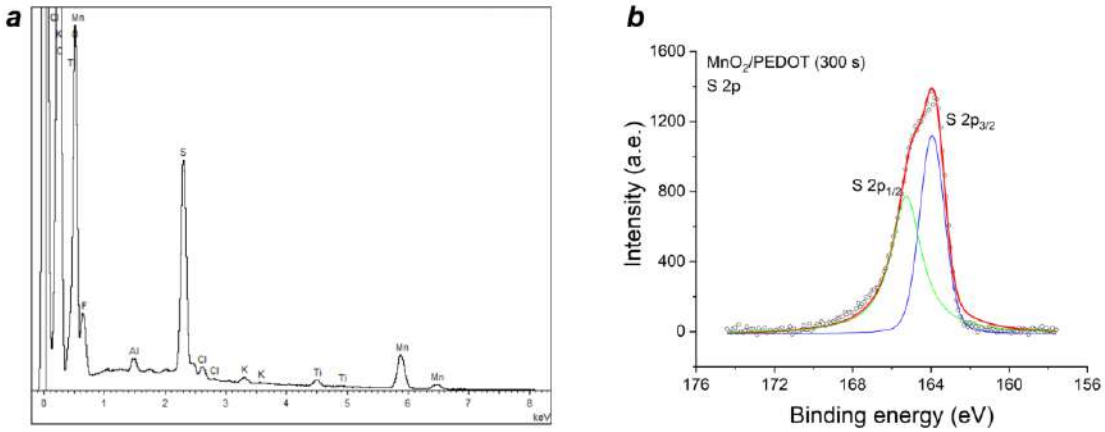

Figure 35. EDX spectrum (a) and XPS spectrum of S 2p (b) for MnO_2/PEDOT electrodes obtained by polymer electrodeposition over 300 s.

The EDX spectra of the samples show Mn and O elements corresponding to the presence of MnO_2, as well as a pronounced sulfur peak at 2.3 keV (Figure 35, a). The XPS spectra of sulfur demonstrate two peaks at 163.9 and 165.1 eV associated with the binding energy of sulfur in the thiophene ring (S $2p_{3/2}$ and S $2p_{1/2}$, respectively) (Figure 35, b) [176]. Thus, during the electrodeposition oligomeric or polymer PEDOT fragments are formed on the surface of the cathode material.

Polymer-modified cathode materials were also studied in the Zn//MnO_2 cells. The specific capacities of the cathode materials at different current densities are shown in Figure 36. At the current density of 0.1 $A \cdot g^{-1}$ the capacity of the polymer-coated electrode is 15% higher (Figure 36, a), while the process of capacity growth during cycling due to MnO_x deposition from the electrolyte solution is weaker for the modified electrodes. The higher value of the specific capacity corresponds to the improved electronic and ionic contact between the active material particles through the additional conductive PEDOT coating on the cathode surface.

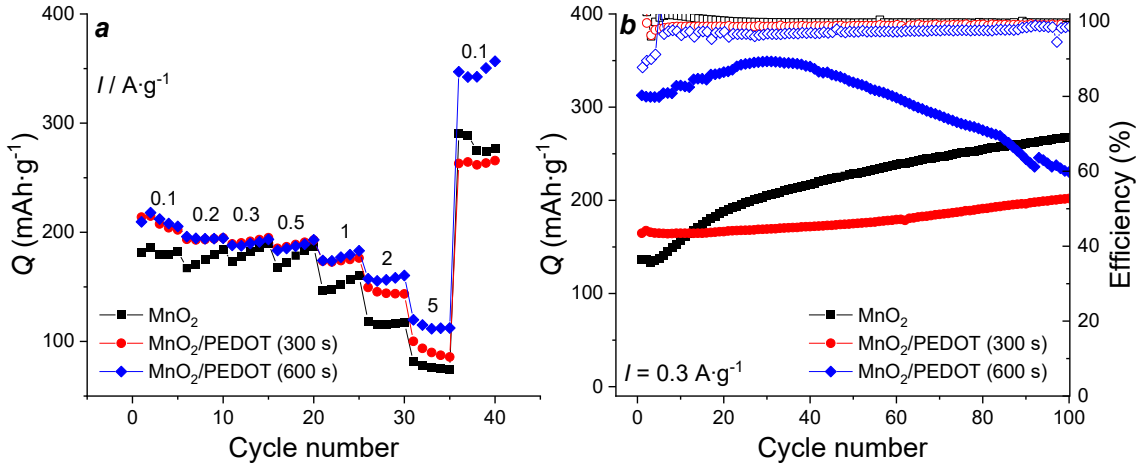

Figure 36. C-rate capability (a) and cyclic stability at $I = 0.3\ A \cdot g^{-1}$ (b) of MnO_2/PEDOT cathode materials

During long-term cycling at a current density of 0.3 $A \cdot g^{-1}$ (Figure 36, b), after several initial cycles the active deposition of MnO_x starts on the unmodified cathode (black curve), while for PEDOT-coated cathodes this process either proceeds to a lesser extent (for t = 300 s, red curve) or is completely suppressed (t = 600 s, blue curve), so, the conducting polymer coating partially blocks the deposition of additional manganese oxide on the electrode surface and prevents the artificial capacity increase.

The electrochemical response of MnO_2/PEDOT cathode material with a modifying PEDOT coating was studied by CV. It is seen that in the first cycle a clear cathodic peak at E = 1.22 V is observed, and in the following cycles two pairs of peaks at E = 1.55/1.25 V and E = 1.60/1.39 V are observed (Figure 37, a).

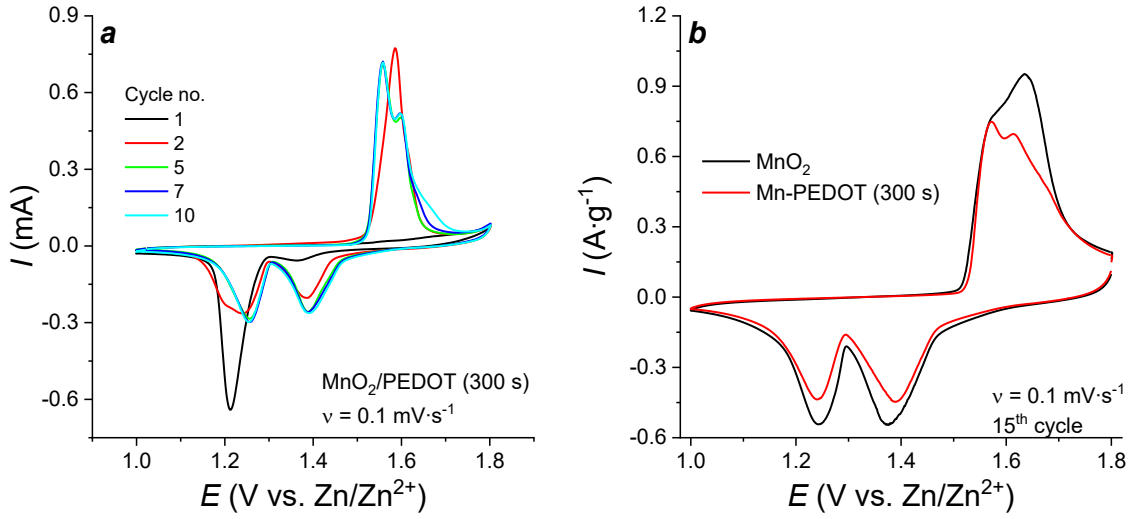

Figure 37. CV curves for MnO_2/PEDOT electrodes depending on the cycle number (a); comparison of CV curves for two types of electrodes normalized to the mass of the active component (b) at the scan rate of 0.1 $mV \cdot s^{-1}$.

The comparative analysis (Figure 37, b) shows that the shape of the CV curves is practically independent of the presence of the conducting polymer, but there is a slight difference in the anodic peaks: for the electrode without conducting polymer, the second peak at E = 1.62 V is more intense and the current intensity of the first anodic peak is low, while for the electrode coated with PEDOT, the first peak at E = 1.56 V is more intense and a clear separation of the peaks is maintained. Due to the previously observed slower capacity growth resulting from suppressed MnO_x deposition for the polymer-coated electrode, a decrease in specific current is observed during cycling, which correlates with the charge/discharge characteristics during long-term cycling.

To investigate the electrode/electrolyte interfaces for cathode materials, the electrochemical impedance spectroscopy was used (Figure 38). For reliable analysis, the spectra were normalized to the mass of the active component in accordance with earlier studies [177]. For the experimental and normalized spectra in the fully charged state (E = 1.8 V), the presence of the polymer coating reduces the charge transfer resistance, which is attributed to the high conductivity of PEDOT. For the coated cathodes the diffusion part in the low-frequency region of the spectrum is more pronounced, which suggests easier ion transport in the composite electrode due to the conductive surface coating.

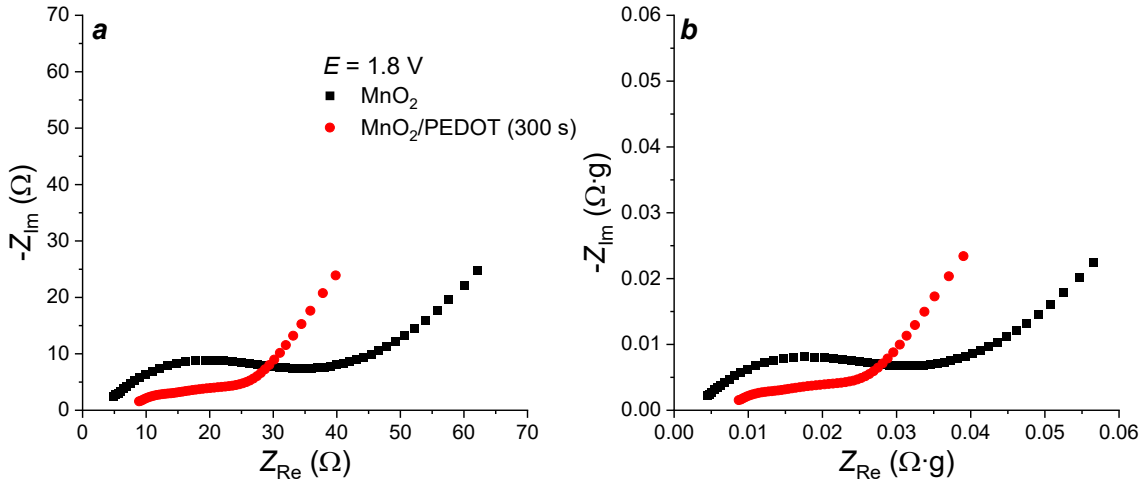

Figure 38. Impedance spectra of MnO_2- and MnO_2/PEDOT-based cathodes after 100 charge/discharge cycles at E = 1.8 V: experimental data (a) and normalized on the MnO_2 mass (b).

Based on the analysis of the electrochemical performance of manganese dioxide-based cathode materials in rechargeable Zn//MnO_2 electrochemical systems, materials with a low crystallinity are required for high reversibility of the specific capacity during long-term cycling. Among the different methods of cathode modification with the conducting polymer PEDOT, the highest specific capacity values were observed in the case of coating MnO_2 grains with a thin layer of PEDOT:PSS (mass loading did not exceed 2%) and in the case of long (t = 600 s) deposition of the PEDOT film on the surface of the as-prepared cathode. Nevertheless, there are still unclear issues about the reaction

behavior in these systems. Since the shape of the curves is practically similar for all cathodes, the reaction mechanism will be considered using the example of the unmodified MnO_2 cathode.

Chapter 4. Investigation of the effect of the electrolyte composition on the electrochemical properties of MnO_2-based cathode materials

4.1. Zinc/manganese sulfate-based electrolytes

An important fundamental issue of the research was to determine the possible electrochemical reactions occurring during charge/discharge processes for MnO_2-based cathodes. Several types of ions: Zn^{2+}, H^+, Mn^{2+} including their hydrated forms could be involved in the electrochemical reaction, the easiest way to study the influence of each ion is to eliminate it or other ions from the electrolyte solution. The most commonly used electrolyte for Zn//MnO_2 cells is an aqueous solution based on zinc and manganese sulfates (2 M $ZnSO_4$ / 0.1 $MnSO_4$, pH ≈ 4.5). The typical feature of the electrochemical behavior of cathodes in this electrolyte, observed by various methods in two-electrode cells, is the increase in electrochemical activity caused by the deposition of an additional surface layer of MnO_x from the electrolyte solution, with a change in the shape of the curves from the first cycle to the next one (Figure 39).

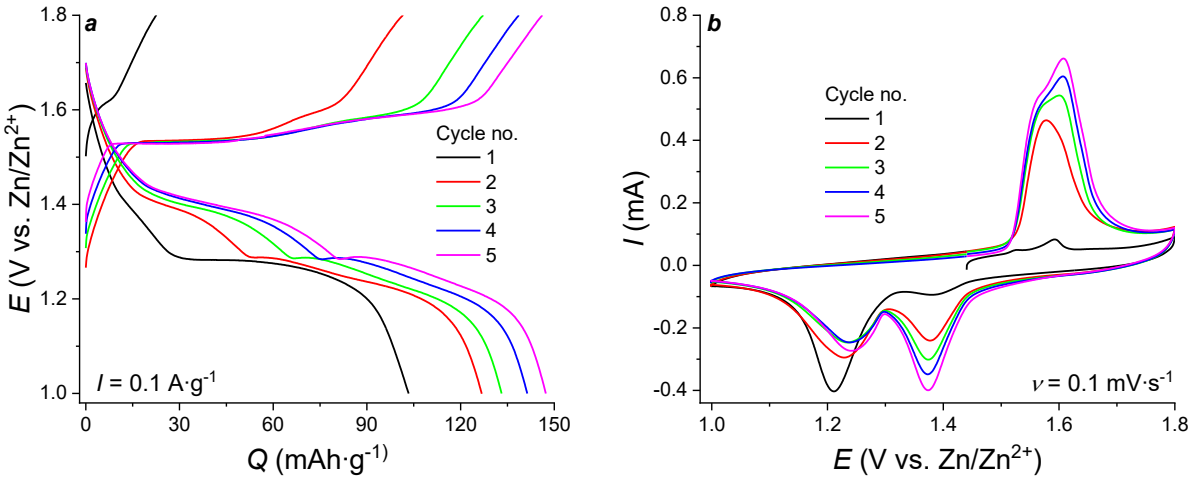

Figure 39. Charge/discharge profiles at $I = 0.1\ A{\cdot}g^{-1}$ (a) and CV curves at $\nu = 0.1\ mV{\cdot}s^{-1}$ (b) for Zn//MnO_2 two-electrode cells in 2 M $ZnSO_4$ / 0.1 M $MnSO_4$ electrolyte.

In particular, on the first cycle (black curve) only one redox transition is present at E = 1.28 V (charge/discharge curve) and E = 1.21 V (CV), the cathodic process at E = 1.38 V (CV) proceeds to a very minor extent, the primary charging process is not pronounced because the MnO_2 phase is already charged. From the second cycle, the shape of curves changes: two well-defined peaks/plateaus appear at E = 1.39 / 1.25 V during discharge, and two weakly separated peaks/plateaus appear at E = 1.56 V during charge. The appearance of the voltage kink on the charge/discharge profiles from the second cycle could be associated with the formation of the basic salt ZHS during discharge [20], which is a competitive chemical process occurring on the surface of the cathode material.

As previously discussed for the LMO-based cathodes (Section 3.1) and for the polymer-modified electrode materials (Section 3.3.1), processes related to the irreversible incorporation of Zn^{2+} cations into the cathode structure were observed. To determine the changes in the electrochemical behavior of manganese oxide depending on the type of electrolyte: in the absence of manganese or zinc ions and in the presence of both, the electrochemical properties of MnO_2 cathodes were tested by the CV method. The compositions of electrolyte solutions used to establish the influence of its nature on the properties of the system, in particular, the shape of CV curves, are given in Section 2.6 (Table 2). To prove the necessity of the presence of zinc ions in the electrolyte solution to ensure the reversibility of Zn//MnO_2 cell, the properties of the MnO_2-electrodes were studied in the absence of a metallic zinc anode in manganese sulfate solution and compared with the response in the binary electrolyte 2 M $ZnSO_4$ / 0.1 M $MnSO_4$. For this, three-electrode cell with separated compartments was assembled. The as-prepared MnO_2 cathode was used as the working electrode, and an aqueous Ag/AgCl electrode filled with 3 M NaCl solution was used as the reference electrode. The first electrolyte applied was aqueous 2 M $ZnSO_4$ / 0.1 M $MnSO_4$ solution, then the cathode was tested in 0.1 M $MnSO_4$ solution, after which the mixed electrolyte was used again. The counter and reference electrodes were connected by a salt bridge to avoid side processes. The resulting CV curves are shown in Figure 40.

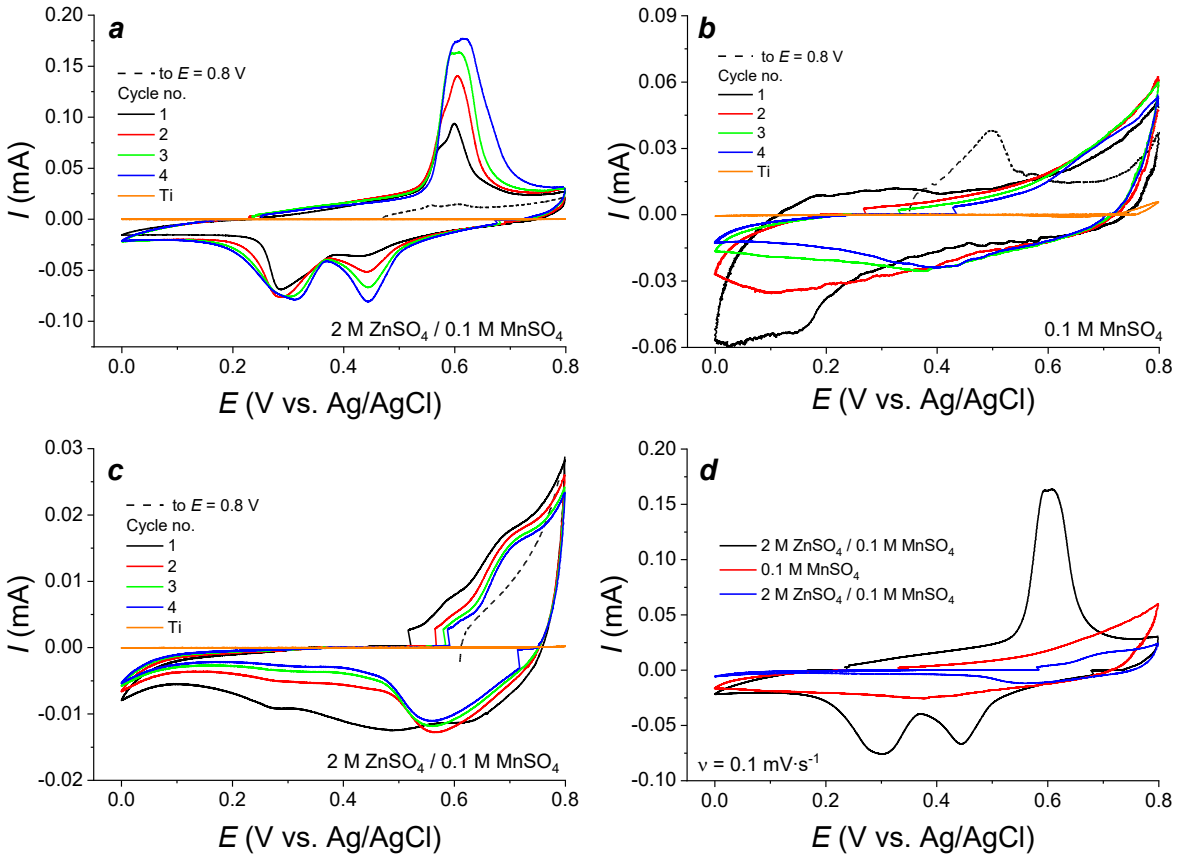

Figure 40. CV curves for MnO_2-cathodes obtained serially in a three-electrode cell in 2 M $ZnSO_4$ / 0.1 M $MnSO_4$ (a), 0.1 M $MnSO_4$ (b), 2 M $ZnSO_4$ / 0.1 M $MnSO_4$ (c) electrolyte solutions at v = 0.1 mV·s^{-1}; comparison of curves obtained in different electrolytes at the third cycle (d).

In conventional 2 M $ZnSO_4$ / 0.1 M $MnSO_4$ electrolyte the shape of CV curve is correlated with the observed earlier (see Section 3.2): on the anodic part a widened peak at E = 0.61 V is observed and on the cathodic one there are peaks at E = 0.44 V and $E \approx 0.3$ V vs. Ag/AgCl (Figure 40, a). However, there are significant changes in the CV curve in 0.1 M $MnSO_4$ solution. During oxidation up to 0.8 V, an anodic peak at E = 0.49 V is observed, which then disappears. On the cathodic curve during the first discharge, a broad peak at E = 0.15 V is observed, which is also extremely weak during the second cycle and completely absent during the following cycles. The shape of the curve is similar to a rectangular one, which indicates the accumulation of charge by the pseudocapacitive mechanism, and at potential values above 0.7 V there is an increase in the current caused by the deposition of MnO_x on the cathode surface (Figure 40, b).

Despite the processes of manganese oxide deposition on the cathode surface from the electrolyte solution, which previously led to an increase in capacity, after transfer of the cathode from the manganese sulfate solution to the mixed electrolyte, there is no recovery of the electroactivity of the material. The CV curves of the material in 2 M $ZnSO_4$ / 0.1 M $MnSO_4$ solution after cycling in $MnSO_4$ pristine solution look quite different: after the first cycle only one cathodic peak at E = 0.56 V is observed, on the anodic curve an intense current increase is observed after reaching the potential value of 0.6 V (Figure 40, c). The current intensity is higher than that of the background (titanium current collector), indicating that the cathode material is retained on the surface. Comparing the data for the same electrode, it can be seen that the current drops several times with the same surface area of the cathode placed in the electrolyte solution: for clarification, the third CV cycle obtained in all three electrolytes is presented (Figure 40, d). Thus, cathode inactivation is observed in manganese sulfate solution in the absence of Zn^{2+} cations.

To evaluate the importance of the combined presence of zinc and manganese cations, following other works [21] we studied the as-prepared MnO_2-cathodes in the same three-electrode cell in solutions of 2 M $ZnSO_4$ and mixed 2 M $ZnSO_4$ / 0.1 M $MnSO_4$ electrolyte (Figure 41). In the pristine $ZnSO_4$ solution gradual electroactivity fading during 5 CV cycles is observed: the intensity of cathodic currents drops more than three times; characteristic peaks are practically absent on the anodic curve. The cathodic curve shows a clear peak at E = 0.31 V and a weakly pronounced peak at E = 0.42 V, which completely disappears by the 5^{th} cycle (Figure 41, a).

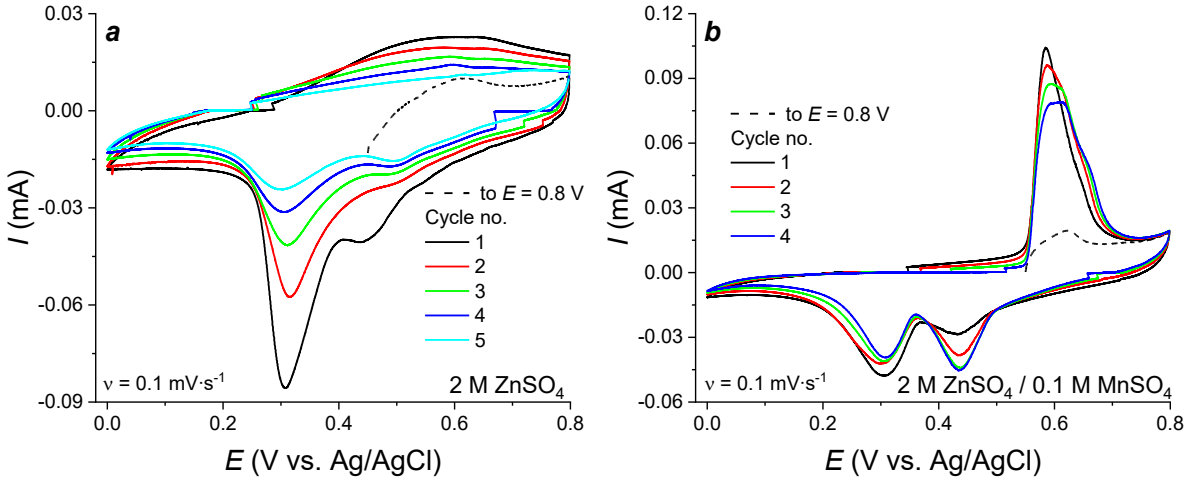

Figure 41. CV curves obtained for MnO_2-cathode in three-electrode cell in 2 M $ZnSO_4$ (a) and 2 M $ZnSO_4$ / 0.1 M $MnSO_4$ (b) electrolytes solutions at $\nu = 0.1\ mV \cdot s^{-1}$.

When changing the electrolyte solution from zinc sulfate to the mixed electrolyte with $MnSO_4$ additive, after the first reduction cycle, the formation of an intense anodic peak at $E = 0.58$ V which broadens during continuous cycling, is observed, as well as the appearance of a cathodic peak at $E = 0.43$ V, which increases from cycle to cycle (Figure 42, b). This effect has been previously observed for $LiMn_2O_4$-based cathode materials, and it is indicative of the recovery of the cathode electroactivity in a mixed solution of zinc and manganese sulfates.

In order to study the mass transfer processes in more detail, experiments were carried out to measure the mass of the electrode material *in operando* using the electrochemical quartz crystal microbalance (EQCM). To perform measurements on a gold-sprayed quartz crystal (hereafter referred to as the gold electrode), manganese dioxide (hereafter referred to as Au-MnO_2) was presynthesized potentiostatically according to the method described in [168] and tested in a 2 M $ZnSO_4$ / 0.1 M $MnSO_4$ solution. It was observed that for electrodeposited manganese oxide the shape of CV curve is close to conventional from the second cycle: two cathodic peaks at $E = 1.37$ V and $E = 1.19$ V are observed as well as an anodic peak splitting into two at $E \approx 1.55$ V (Figure 42, a). During cycling, there is an increase in mass at $E \approx 1.3$ V during reduction (cathodic curve), while during oxidation (anodic curve) there is a sharp decrease in the mass of the precipitate on the gold electrode surface ($E = 1.55$ V) and a slight increase in mass in the region of potentials $E > 1.6$ V (Figure 42, b).

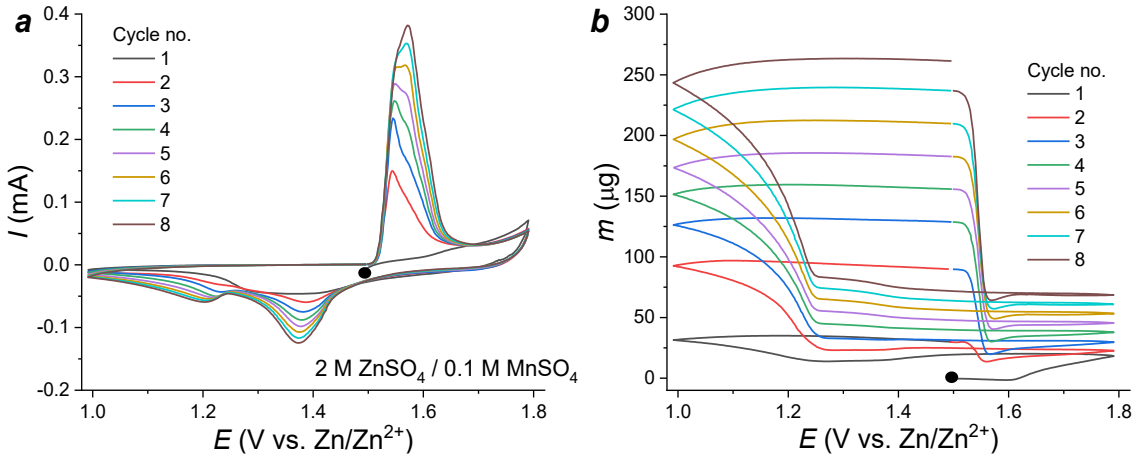

Figure 42. CV curves (a) and mass – potential dependencies (b) for Au-MnO_2 electrode obtained by electrodeposition in 2 M $ZnSO_4$ / 0.1 M $MnSO_4$ solution.

At the first cycle, when moving from the open circuit potential (E = 1.49 V), it can be seen that in the potential area E > 1.6 V a gradual mass increase, which is related to MnO_x deposition on the Au electrode surface, starts. At further cathodic process at the potentials near E = 1.4 V an insignificant mass drop is observed, which is followed by mass intensive growth in the potential range ΔE = 1.05 – 1.25 V. The obtained dependences are in accordance with the data published earlier by the scientific group [168].

The analysis of the mass-charge dependence for the first cycle had shown that three slopes observed on that curve are well-correlated with the mass changes observed. The calculated values of molecular mass for different parts of the cathodic curve according to Faraday's law were 87 $g \cdot mol^{-1}$, 8 $g \cdot mol^{-1}$ and 757 $g \cdot mol^{-1}$ which correspond to the formation of MnO_2 (molar mass 87 $g \cdot mol^{-1}$), transfer of small monovalent ion (probably the transfer of H^+ or H_3O^+ ions), and the formation of an insoluble precipitate of the basic zinc salt (Figure 43, a, b). The values of the number of electrons n were chosen based on the literature analysis, according to which the process at E = 1.4 V is attributed to the participation of a univalent ion (H^+) in the reaction, and the process at E = 1.25 V is attributed to the participation of a divalent ion (Zn^{2+}) [89,90].

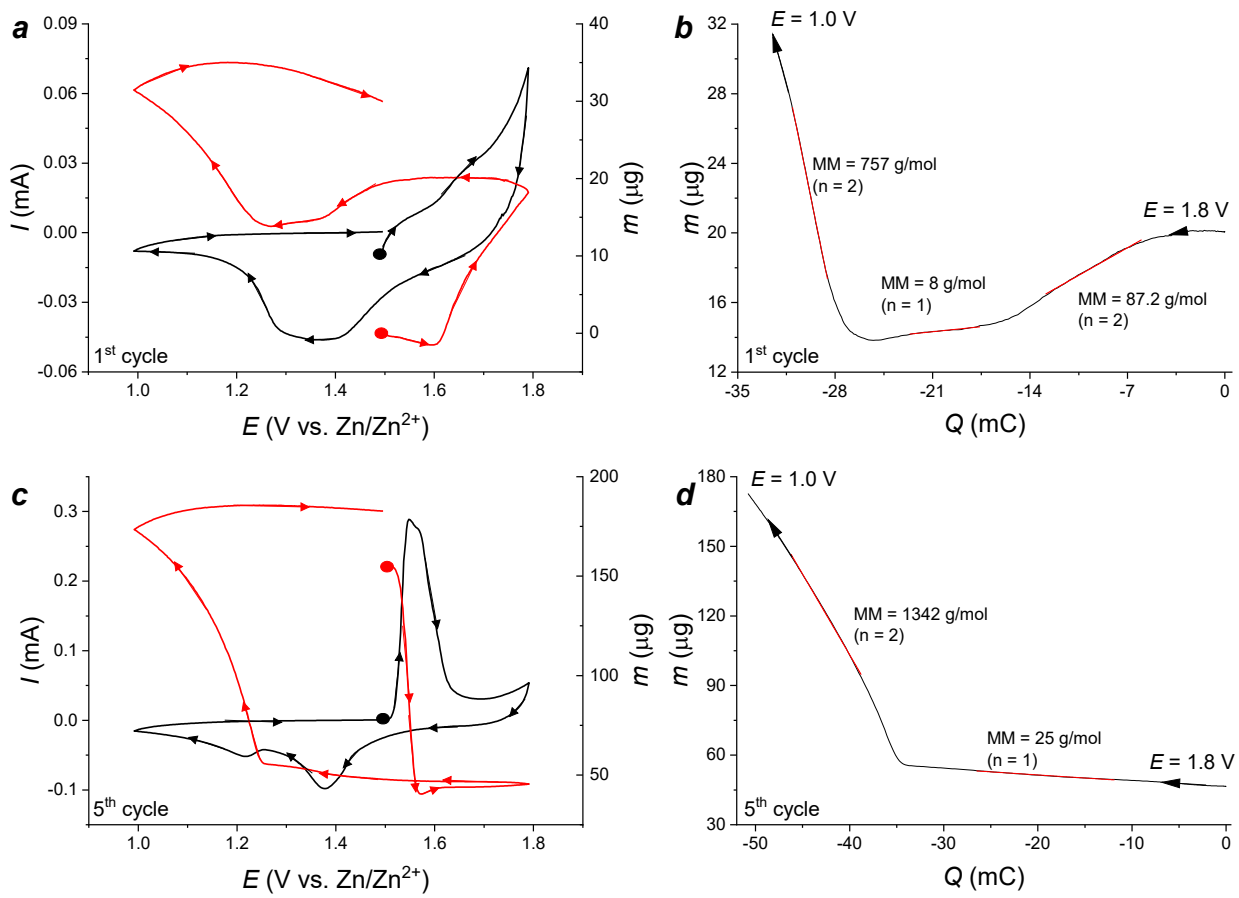

Figure 43. CV curves and m – E dependencies for the first (a) and fifth (c) cycles; the mass-charge dependence of cathodic half-cycle for the first (b) and fifth (d) cycles.

For the fifth CV cycle the mass changes differ from the first cycle: at the anodic peak potential $E = 1.54$ V a sharp mass drop is observed, then it slightly increases at $E = 1.57$ V and during the cathodic process the mass grows smoothly up to $E = 1.25$ V and then drastically increases in the potential range $\Delta E = 1.05 – 1.25$ V. The mass-charge dependence during the cathodic process shows two slopes, which correspond to the processes of ion intercalation (molar mass of particles ≈ 25 g·mol^{-1}) and surface precipitate formation (molar mass 1342 g·mol^{-1}) (Figure 43, c, d). Thus, it is not possible to identify direct intercalation of zinc ions into the structure of materials from the data obtained. Nevertheless, based on the literature analysis, it can be assumed that the cathodic peak at the potential $E \approx 1.4$ V is associated with the participation of the monovalent ion H^+. The experiments carried out in pure zinc sulfate solution for Au-MnO_2 showed that during the first cathodic scan at the potentials $E < 1.3$ V a significant mass increase is observed, which is associated with the process of ZHS formation on the electrode surface [20,168], after which the mass of the cathode remains practically unchanged, i.e. there is a rapid blocking of the electrode surface, due to which further electrochemical reactions do not take place [168].

Thus, it can be concluded that two types of ions (Zn^{2+} and Mn^{2+}) are necessary in the electrolyte composition to ensure the reproducibility and obtain a stable response of the Zn//MnO_2 system.

4.2. Zinc sulfate-based electrolytes with addition of alkali metal ions

As it was shown in the literature review (Section 1.5), H^+ ions are involved in the overall electrochemical reaction, as was confirmed by direct *in operando* pH tracking during CV measurements [22]. However, the form of proton participation – their intercalation into the cathode structure or conversion reaction with oxide fragments – remains not completely clear. To evaluate the intercalation processes involving the monovalent ion, solutions based on zinc sulfate with the addition of alkali metal salts were prepared, containing an excess of metal ions (Li^+, Na^+): 2 mol·L^{-1}. Moreover, solutions with the absence of manganese sulfate were prepared to test the possibility of substitution of Mn^{2+} ions for alkali metal ion in the electrochemical reaction, details of the solution compositions are given in table 2.

In ternary solution in the presence of lithium ions the shape of CV curve is completely similar to those obtained in the conventional 2 M $ZnSO_4$ / 0.1 M $MnSO_4$ solution: at the first cycle, a pronounced cathode peak at E = 1.20 V is observed, and at subsequent cycles, two pairs of peaks are observed at E = 1.60 / 1.24 V and E = 1.64 / 1.36 V (Figure 44, a). After the second cycle the CV curve is almost unchanged, which indicates stabilization of the electrochemical response. In the absence of manganese salt in the electrolyte composition, a different behavior during cycling is observed: after the first reduction cycle the cathodic peak at E = 1.39 V stabilizes up to the fifth cycle, and then the current response becomes stable. The intensity of the second cathodic peak at E = 1.24 V gradually decreases, which indicates the difficulties arising in this reaction (Figure 44, b).

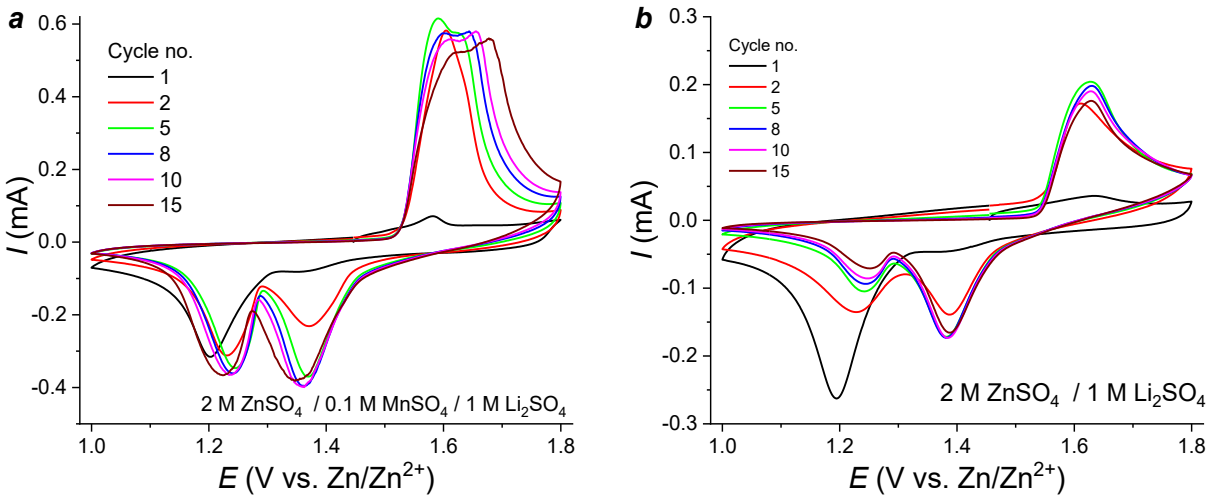

Figure 44. CV curve for MnO_2-cathodes in ternary solution 2 M $ZnSO_4$ / 0.1 M $MnSO_4$ / 1.0 M Li_2SO_4 (a) and in binary solution 2 M $ZnSO_4$ / 1.0 M Li_2SO_4 (b) at v =0.1 mV·s^{-1}.

Completely identical dependences are observed when Li^+ cations are replaced by Na^+ cations, while in the ternary solution the current response does not change after the fifth cycle (Figure 45, a), indicating high reversibility of this system. In the binary electrolyte solution, the cathodic peak at

E = 1.21 V also strongly decreases in intensity relative to the peak at E = 1.4 V (Figure 45, b). Thus, in the absence of manganese salt in solution, the cathodic peak at E = 1.21 V shifts to more positive values of the potential, and its intensity decreases, which indicates a decrease in the proportion of intercalated Zn^{2+} ions and suppression of the reaction of formation of the basic zinc salt, while the current value of the second peak remains stable, i.e. in this range of potentials the intercalation of single-charged ions (Li^+/Na^+) takes place, which are present in excess of the concentration of free H^+ cations by 3–4 orders of magnitude.

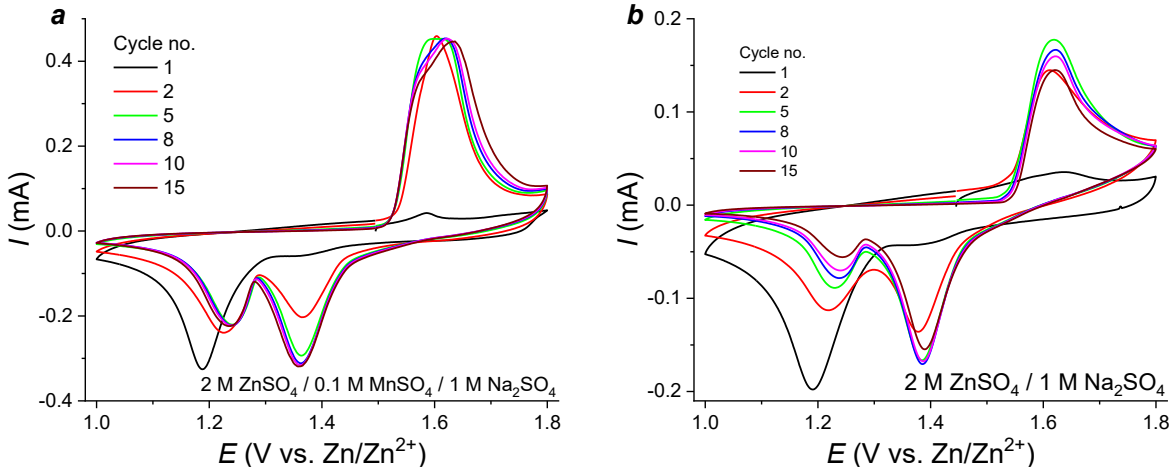

Figure 45. CV curves for MnO_2-cathodes in ternary solution 2 M $ZnSO_4$ / 0.1 M $MnSO_4$ / 1.0 M Na_2SO_4 (a) and in binary solution 2 M $ZnSO_4$ / 1.0 M Na_2SO_4 (b) at v =0.1 mV·s^{-1}.

The C-rate capability tests in binary and ternary electrolyte solutions (Figure 46, a, b) show that the initial specific capacity of cathode materials is similar (for the solution with Li^+ ions Q_{in} ≈ 165 mAh·g^{-1}, for the Na-containing electrolyte Q_{in} ≈ 140 mAh·g^{-1}). During the tests in binary solutions, regardless of the nature of the alkali metal cation, a gradual drop in the specific capacity of cathodes is observed, there is no increase in capacity due to the absence of $MnSO_4$ in the electrolyte solution. In the case of ternary solutions at low current densities (0.1 – 0.5 A·g^{-1}) the capacity of MnO_2 cathodes increases slightly from cycle to cycle, which correlates well with our earlier data on the cycling of cathodes in a solution containing 0.1 M $MnSO_4$. Cathode materials cycled in Li-containing electrolyte show a higher specific capacity compared to the same materials cycled in Na-containing solutions which could be related to the difficulty of insertion/extraction of Na^+ due to its larger ionic radius than that of Li^+ in dehydrated state.

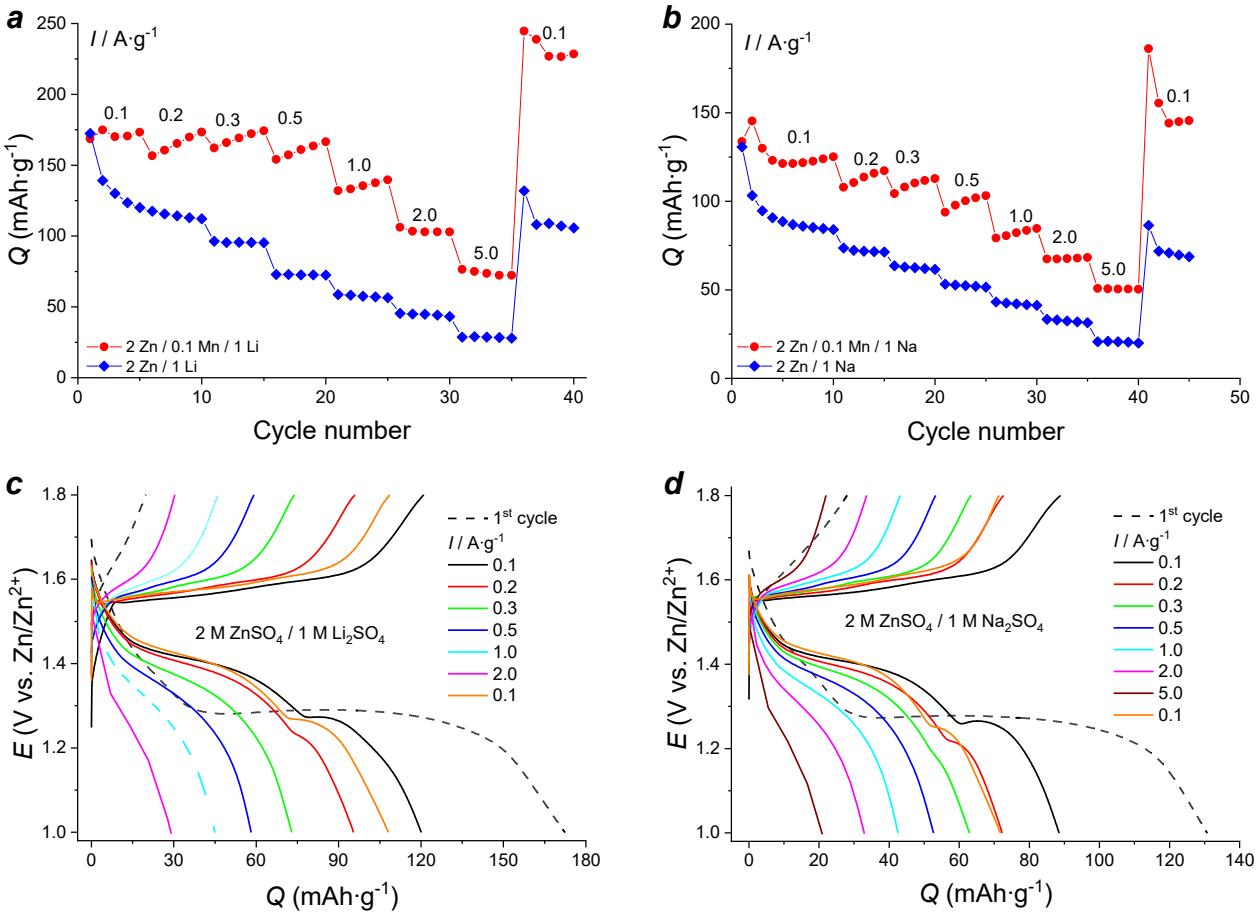

Figure 46. C-rate capabilities of MnO_2-cathodes in the solutions with Li^+ (a) or Na^+ (b) additives; charge/discharge profiles of the cathode materials cycled in the binary solutions containing Li^+ (c) or Na^+ (d) ions.

The charge/discharge profiles for the cathode materials cycled in the binary solutions are similar to the CV data: during the cycling process, the plateau in the potential region E = 1.24 V, which dominates at the first discharge cycle, practically disappears with increasing number of cycles, even when returning to the initial current density (Figure 46, c, d). Thus, replacement of Mn^{2+} cation by M^+ cation (M = Li, Na) in this system does not lead to a significant improvement of electrochemical properties, on the contrary, one of the cathodic processes is completely suppressed, despite the presence of Zn^{2+} cations.

Complex CV measurements with registration of the mass changes of the electrode by EQCM were performed to find out the charge carriers during the cycling process in binary solutions. Au-MnO_2 electrode was previously synthesized, Na-containing solution was used due to Na^+ higher molar mass in comparison with H^+ or Li^+ ions. In the first cycle, a distinct cathode peak at E = 1.20 V is observed. From the second cycle, the shape of the CV curve is similar to that observed in $ZnSO_4$ solutions: almost complete absence of cathode electroactivity, insignificant cathodic and anodic currents (Figure 47, a).

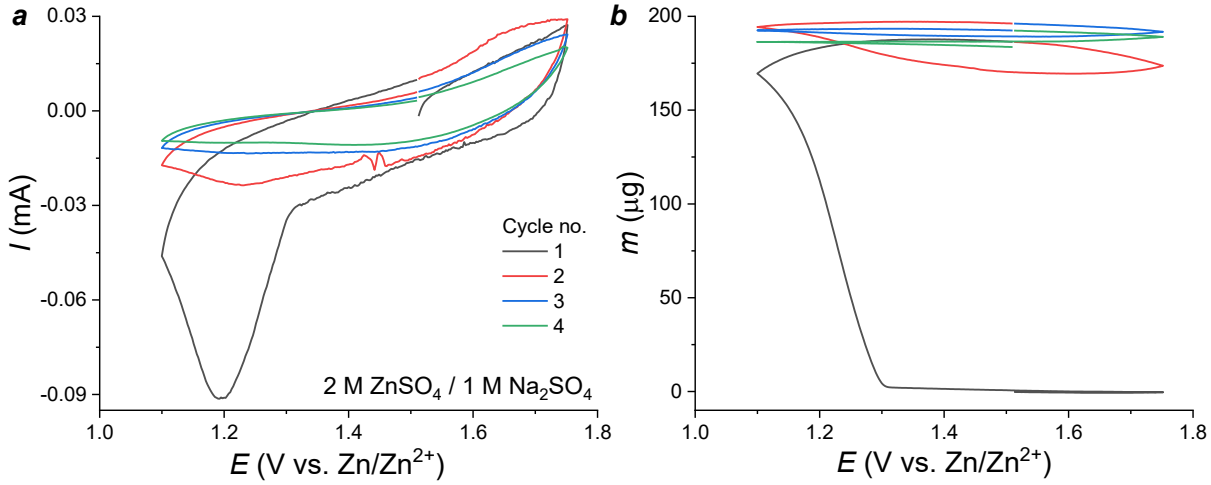

Figure 47. CV curves (a) and mass – potential dependencies (b) for Au-MnO_2 electrode obtained by electrodeposition in 2 M $ZnSO_4$ / 1.0 M Na_2SO_4 solution.

During the first CV cathodic scan, a sharp and significant mass increase is observed in the potential range ΔE = 1.05 – 1.25 V, corresponding to the redox transition, which was previously observed in $ZnSO_4$-based solutions and corresponding to the primary process of deposition of the basic zinc salt on the cathode surface. In the following cycles, the mass change is practically not observed, which leads to the conclusion that there is no dissolution of ZHS from the surface during the charging of the cell, resulting in the blocking of the cathode surface (Figure 47, b).

To minimize the deposition of ZHS on the electrode surface and, as a consequence, blocking the electrode surface, *in situ* deposition of the cathode material on the gold electrode was performed by potentiodynamic method, for which ternary solutions were applied because of the need of the presence of Mn^{2+} ions. First of all, it is worth noting that the mass accumulation of the precipitate in this solution is extremely low, hence very thin, close to monolayer, films of cathode material were obtained. The main deposition process occurs at the potentials $E > 1.7$ V which correspond to a sharp increase in anodic currents and an increase in the mass of the precipitate in this range (Figure 48). Moreover, the shape of CV curve differs significantly in the thin-layered cathode: on the first discharge cycle three different processes at E = 1.53, 1.40 and 1.20 V are observed, and at the second and following cycles only one peak at E = 1.4 V is retained (Figure 48, a). During discharge of the cell at potentials 1.35 – 1.45 V, a mass drop begins which was not previously observed in sulfate solutions, and the mass of the precipitate decreases by ≈ 40% of the maximum value per cycle (Figure 48, b).

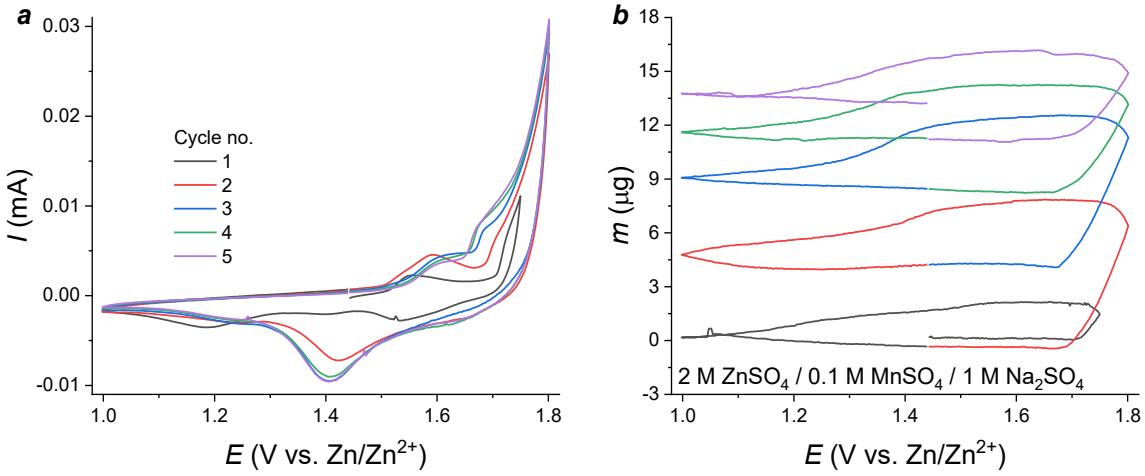

Figure 48. CV curves (a) and mass – potential dependencies (b) for in situ deposited Au-MnO_2 electrode in 2 M $ZnSO_4$ / 0.1 M $MnSO_4$ / 1.0 M Na_2SO_4 solution.

A detailed study of the current and mass dependence on the potential shows that the mass loss is observed in the initial and final stages of charging, precisely in the redox transition region corresponding to ion deintercalation. Then the cathode mass increases at the MnO_2 deposition potential, and after the first cathodic peak at the CV curve, the cathode mass starts a slow decrease (Figure 49, a). From the mass-charge dependence of the cathodic cycle it was found that this curve has two slopes, which correspond to molecular mass values of 29 g·mol^{-1} and 107 g·mol^{-1} for single-charged particles. The first slope correlates with the position of the peak at E = 1.4 V, and is also close to the molecular mass of the Na^+ ion (23 g·mol^{-1}), deviations may be related to the presence of the hydrate shell of the Na^+ ion. Thus, the intercalation of the monovalent ion during the cathodic process at E = 1.4 V is noticeable (Figure 49, b).

Similar dependencies were found for solutions containing Li^+ ions: the CV curves for *in situ* deposited cathode material show comparable shape, the anodic process at E = 1.65 V is more clearly expressed, which is associated with ion deintercalation, the cathodic cycle also shows only one peak at E = 1.36 V. The cathode mass trends are similar to those observed in solutions with Na^+ ions (Figure 49, c). The slopes on the mass-charge dependence of the cathode cycle in Li-containing solution analyzed according to Faraday's law show that two of the observed slopes (18 g·mol^{-1} and 45 g·mol^{-1}) can be related to the participation of Li^+ ions (7 g·mol^{-1}) in the reaction; the larger mass values can be explained by the movement of Li^+ cations with hydrate shell (Figure 49, d).

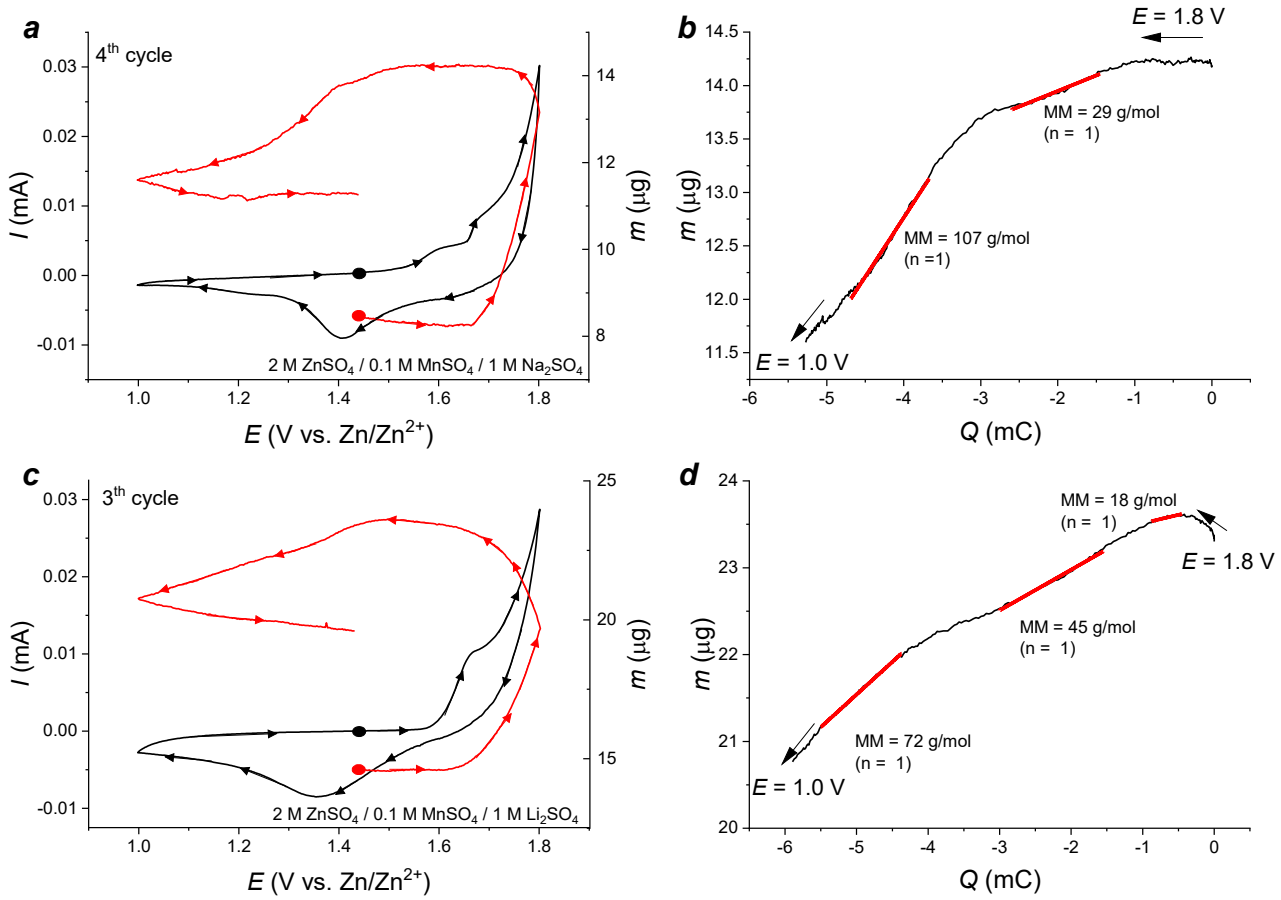

Figure 49. CV curves and m – E dependencies for the Au-MnO_2 electrodes obtained by in situ electrodeposition from the ternary solutions containing Na^+ (a) and Li^+ (c) ions; cathodic mass-charge dependencies for Au-MnO_2-electrodes in presence of Na^+ (b) and Li^+ (d) ions.

Thus, studies of the cathode mass change during cycling of MnO_2 thin films, for which insignificant changes in the pH of both the solution and the near-electrode layer allowed to avoid the formation of the basic salt on the cathode surface and to detect the intercalation processes taking place. The introduction of a high concentration of monovalent ions made it possible to suppress the injection of H^+ ions, which occurs at the same potentials, and to detect the intercalation of alkali metal ions.

However, despite the high stability of MnO_2 properties in sulfate solutions, several works reported that zinc acetate $Zn(CH_3COO)_2$ based solutions would be more suitable for Zn//MnO_2 cells, since they would have a weaker contribution of H^+ ions to the overall reaction, as well as a reduced MnO_2 precipitation potential [37]. Therefore, to confirm or disprove the participation of Zn^{2+} cations in the overall reaction and to determine the influence of protons on the overall electrochemical process, it is necessary to study the properties of MnO_2-based cathodes in acetate electrolytes.

4.3. Zinc/manganese acetate-based electrolytes

The investigations were carried out in different solutions based on zinc acetate $Zn(CH_3COO)_2$ (further acetate ion CH_3COO^- denoted as Ac) with compositions given in table 2. Since zinc acetate is

a salt formed by a weak cation and a weak anion, the media of this solution are close to neutral, which was confirmed by direct measurement of the pH of the solutions prepared (pH ≈ 6). To compare the results with those obtained with zinc and manganese sulphate solutions, some solutions were acidified to a pH of ≈4.5 with a 0.25 M acetic acid solution.

From the C-rate capability data in the pure zinc acetate solutions with different concentrations (1.0 M and 1.5 M), we concluded that the functional properties are slightly higher for the less concentrated solution: i.e. the initial specific capacity of the cathode in 1.0 M $ZnAc_2$ reached app. 280 $mAh \cdot g^{-1}$ at $I = 0.1$ $A \cdot g^{-1}$, while in the concentrated electrolyte it was only 200 $mAh \cdot g^{-1}$ (Figure 50, a). However, regardless of the type of electrolyte used and the current applied, a sharp capacity decrease is observed, which is most evident for cells with 1.5 M $ZnAc_2$ electrolyte: at a current density of 0.3 $A \cdot g^{-1}$, the specific capacity of the cathode decreases for 5 – 10 $mAh \cdot g^{-1}$ during 10 cycles, while for 1.0 M $ZnAc_2$ solution the same processes occur during 30 cycles (Figure 50, b). This instability has previously been observed in aqueous solutions of zinc acetate and has been associated with incomplete dissolution of the $Zn_5(OH)_8(CH_3COO)_2 \cdot nH_2O$ salt and stronger binding of acetate ions to Zn^{2+} cations [178]. At higher electrolyte concentrations, this basic salt is formed more rapidly and a lower mobility of the ions in solution is observed.

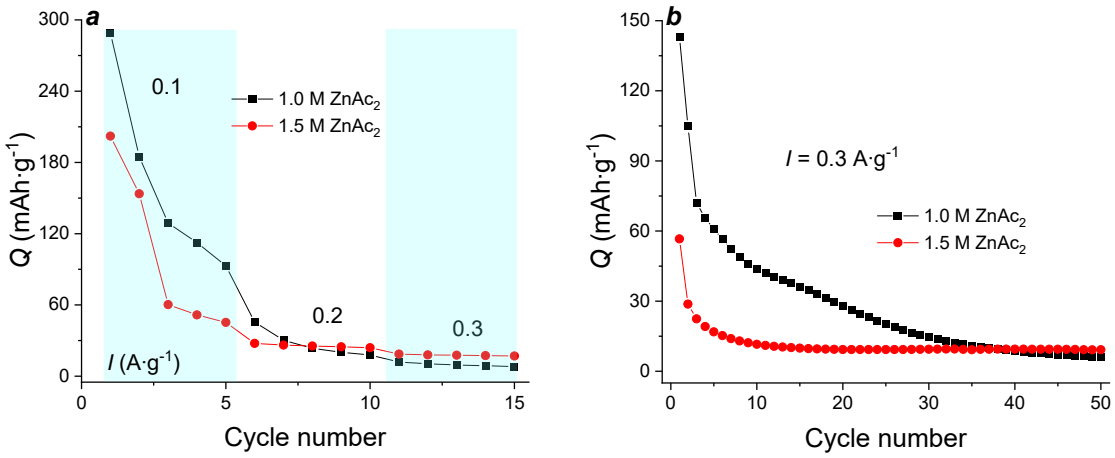

Figure 50. C-rate capability (a) and cyclic stability at a current density of 0.3 $A \cdot g^{-1}$ (b) for Zn//MnO_2 cells with zinc acetate-based electrolytes.

The data on the degradation of the MnO_2-based cathode in the electrolyte without the addition of Mn^{2+} salt correlate with the observed dependencies in the pure 2 M $ZnSO_4$ solution, so for further investigations solutions based on 1.0 M $ZnAc_2$ with the addition of 0.2 M $MnAc_2$ and 0.05 $MnAc_2$ were prepared, some of which were also acidified with acetic acid to lower the pH of the solution. Based on the charge/discharge profiles in mixed 1 M $ZnAc_2$ / 0.2 M $MnAc_2$ solution in the presence or absence of acetic acid (Figure 51), it was observed that without the addition of CH_3COOH (pH = 6.0) a

well resolved plateau at E = 1.16 V and slight changes in the slope at E = 1.38 V are observed and a redox process at E = 1.63 V is visible at the first charge. In the second cycle, the charge plateau potential drops to E = 1.54 V and rises further due to increasing polarization, while the discharge curves show a plateau at E = 1.43 V (Figure 51, a). In acidified acetic solution (pH = 4.5), a sloping plateau at E = 1.55 V is observed on the first and subsequent discharge cycles, while on the charge curve of the first cycle the value of the redox transition potential was 1.70 V and from the second cycle E = 1.62 V (Figure 51, b).

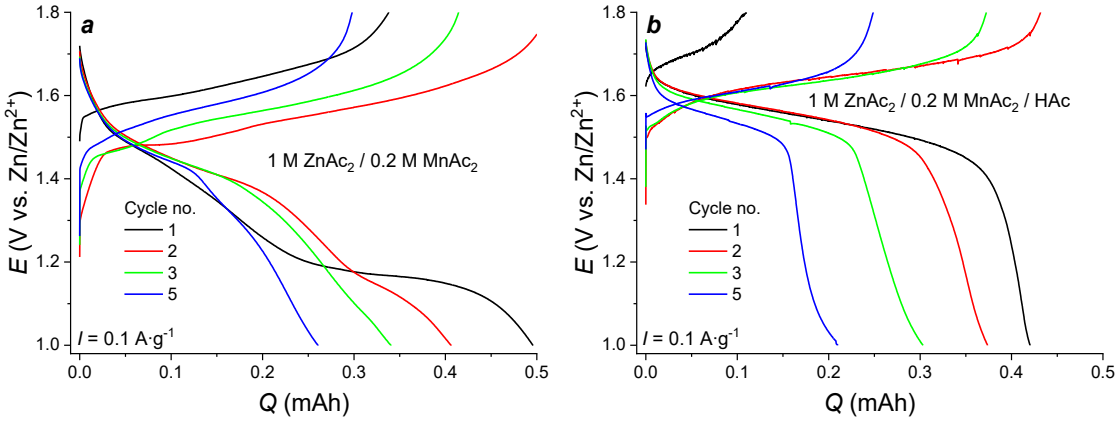

Figure 51. Charge/discharge profiles for Zn//MnO_2 cells at a current density of 0.1 $A \cdot g^{-1}$ in the 1.0 M $ZnAc_2$ / 0.2 M $MnAc_2$ solution: unacidified (a) and acidified with acetic acid (b).

Thus, the complete loss of functional properties of cathode materials occurs regardless of the composition of the electrolyte solution, even when manganese salt is added to the electrolyte, which proves the failure of pure acetate solutions as electrolytes for Zn//MnO_2 cells. This effect is explained by the high coordination ability of acetates to Zn^{2+} and Mn^{2+} cations, which reduces the proportion of free cations and prevents their participation in the electrochemical reaction [179]. The actively forming layer of the basic zinc salt, which does not dissolve completely, plays no small part in the overall process [178]. Nevertheless, the acidity of the medium has an important influence on the electrochemical reaction, especially on the first cycle. Such a dependence of the mechanism on pH also confirms, if not directly, then indirectly, the involvement of H^+ cations in the electrochemical reactions of rechargeable Zn//MnO_2 systems.

For the detailed study of the electrochemical behavior of the cathode materials, the EQCM technique was applied to the gold crystal electrode. The synthesis of manganese oxide was carried out *in situ* with simultaneous measurement of the precipitate mass on the crystal. In the case of electrolyte solution with pH = 4.5, a stable current response was observed on the CV curve, a broad cathodic peak is observed at E = 1.51 V, on the anodic curve a current increase is detected in the potential region E > 1.7 V, which corresponds to a gradual deposition of MnO_2 on the electrode surface (Figure 52, a). The

mass-potential dependencies show a slight increase in mass after each cycle, which is associated with the gradual deposition of MnO_2 on the cathode surface. Nevertheless, a mass decrease is observed in the potential region E = 1.4 V, which correlates with the cathode peak on the CV curve (Figure 52, b). Thus, it can be assumed that part of the manganese oxide deposited on the electrode surface during charge is dissolved during discharge, and this process provides a certain fraction of the electrochemical reaction capacity due to the intercalation of H^+ cations, which entail the conversion of MnO_2 and, as a consequence, the spontaneous reduction of Mn^{3+} to Mn^{2+}.

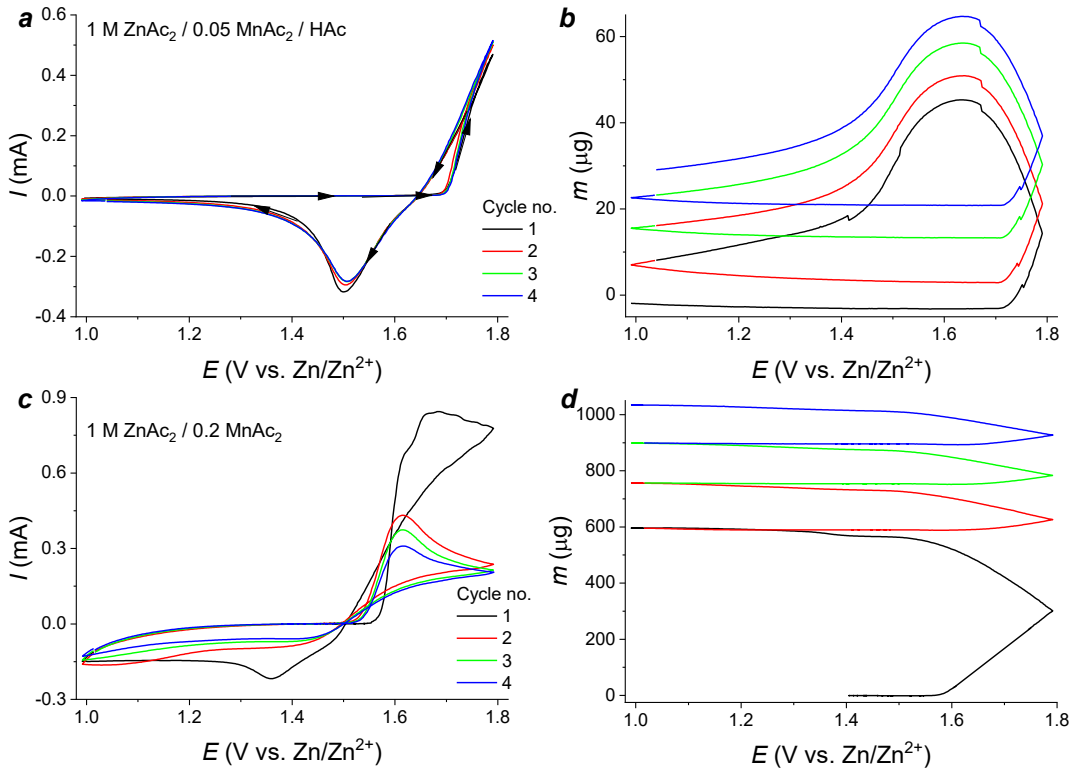

Figure 52. CV curves (a, c) and mass – potential dependencies (b, d) for Au electrodes in 1.0 M $ZnAc_2$ / 0.05 M $MnAc_2$ / Hac (a, b) and 1.0 M $ZnAc_2$ / 0.2 M $MnAc_2$ (c, d) electrolyte solutions.

On the other hand, in the absence of acetic acid in the electrolyte solution, the current response on the CV curve is maximum for the first cycle and then decreases until the third cycle, after which it stabilizes (Figure 52, c). On the cathode curve there is no peak in the potential range 1.45 – 1.55 V, but on the first cycle there is a peak at E = 1.36 V, which disappears in the following CV cycles. The mass of the precipitate on the electrode increases throughout the cycle, and the mass increase occurs in two potential ranges: in the range of potentials 1.7 – 1.8 V, which corresponds to the deposition of MnO_2, and at a potential of 1.34 V, where the cathodic peak is observed (Figure 52, d). Therefore, it can be assumed that during cycling there is no dissolution of MnO_2 and the peak is associated with mass growth due to the formation of an electrochemically inactive compound. The accumulation of this compound on the surface of the gold electrode leads to the blocking of its surface [135].

In summary, the shape of the voltammetric response of the Zn//MnO_2 electrochemical system is strongly dependent on the acidity of the electrolyte, which could be related to different electrochemical reaction mechanisms. At pH = 4.5, regardless of the nature of the anion, a reproducible response is observed due to the active participation in the general reaction of H^+ cations, the concentration of which is extremely small in solutions with pH = 6.0. Consequently, the overall electrochemical reaction can proceed in forward and reverse direction only with the participation of H^+ cations in the process.

Chapter 5. Interpretation of electrochemical reaction mechanism in Zn//MnO_2 rechargeable cells

Despite the large number of studies on the electrochemical properties of Zn//MnO_2 rechargeable cells using aqueous mildly acidic electrolyte carried out in the last 7 years, the key and controversial issue still remains the understanding of the electrochemical reaction mechanism. Due to the complex electrolyte composition containing several types of ions (Zn^{2+}, Mn^{2+}, H^+) as well as their different forms of presence in aqueous solution, the full disclosure of the charge storage mechanism in such systems seems to be an ambitious task that has not been solved yet. The data obtained and discussed in this work and the following discussion should be considered as an attempt to bring more clarity to the understanding of the charge transfer processes in the Zn//MnO_2 cell, to verify and systematize already proposed hypotheses, but they are not comprehensive.

To date, the following variants of the reaction mechanism have been proposed at different stages of the study of aqueous zinc-ion systems [6,37]:

- Reversible intercalation of Zn^{2+} ions;
- Reversible co-intercalation of Zn^{2+} and H^+ ions;
- Conversion reaction with participation of H^+ ions;
- Electrolytic deposition/dissolution of MnO_2.

A number of works studying this problem emphasize a single factor or detail of the mechanism (evolution of crystal phases, changes in the pH of the electrolyte solution, changes in the concentration of ions in solution during cycling). However, all these changes are in fact complementary, and, although the data of different methods may testify in favor of one or another hypothesis, they collectively reflect the course of the same chemical and electrochemical reactions.

Although there are different polymorphic modifications of manganese oxide, their electrochemical behavior is much the same [76,78], the shape of both the first cycle and the subsequent ones is slightly dependent on the MnO_2 crystal lattice. Differences are observed only in the value of the initial specific capacity [77]. It can be concluded that changes in the cathode material during cycling are only indirectly related to intercalation processes, since surface reactions (precipitation of precipitates on the cathode surface, formation of additional MnO_2 layers) become more important [76]. Thus, the crucial role in the electrochemical reaction mechanism is attributed to the electrolyte solution, primarily its cationic composition and acidity (pH). An important factor is the dynamic process of formation and dissolution of surface precipitates of both the basic zinc salt and new layers of manganese oxide during charge and discharge, which regulates the concentrations of ions – participants of the reaction in the near-electrode layer.

It is well known that in order to suppress the disproportionation process of MnO_2 cathodes during cycling, manganese (II) salt is added to the electrolyte solution in low (0.1 – 0.5 M) concentration [16–18]. However, it has been shown that the addition of $Mn2^+$ ions to the electrolyte is much more important than just preventing the cathode dissolution. To verify this influence, tests were performed in solution without the co-presence of Zn^{2+} and Mn^{2+} ions (see Section 4.1).

From the experiments carried out in the absence of Mn^{2+} cations in the solution composition, it is shown that the electroactivity of the material in zinc sulfate electrolyte practically disappears after the third cycle (Figure 41, a). During the first cathodic cycle, an intense peak at E = 0.31 V is observed, as well as a weak peak at E = 0.42 V, which disappears during the second cycle. The absence of anodic peaks during the oxidation process and the corresponding loss of electroactivity of MnO_2 indicate the blocking of the deintercalation of zinc ions into the solution, which means the irreversibility of the process during the first discharge cycle. Direct measurements of mass changes by EQCM for Au-MnO_2 electrode in 2 M $ZnSO_4$ showed that during the first discharge process active mass increase is observed in the potential range $E \approx 1.2$ V, after which no mass changes were detected [168]. Thus, electrochemical inactivation of the cathode takes place in pure zinc sulfate solution. The obtained results are well correlated with those previously reported in [21], where the similar trends were observed in studies by galvanostatic charge/discharge (Figure 53, a).

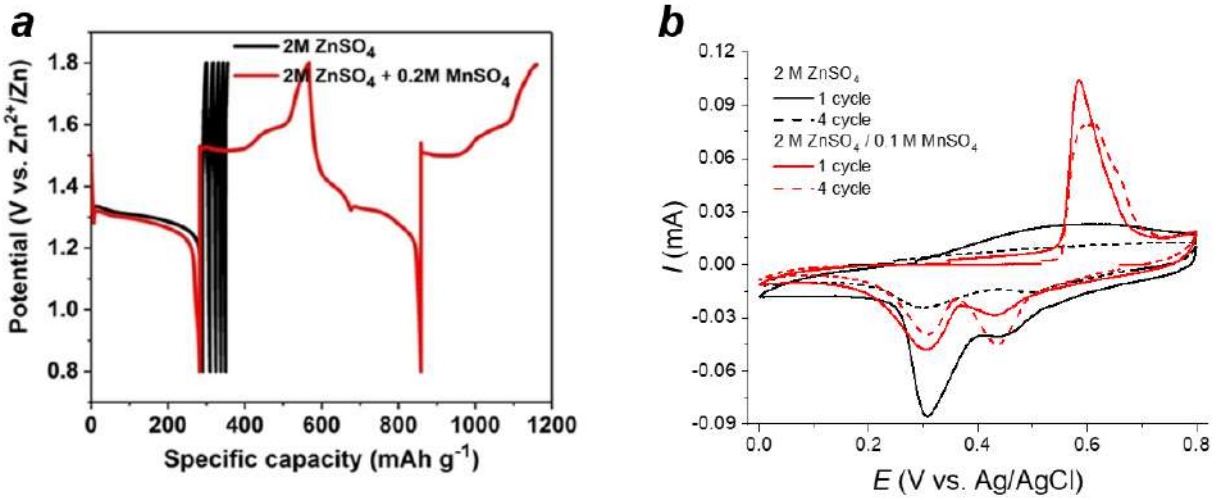

Figure 53. Charge/discharge profiles for MnO_2-cathodes obtained in the solutions based on $ZnSO_4$ and $MnSO_4$ [21] *(a); CV curves for MnO_2-cathodes obtained in the solutions based on $ZnSO_4$ and $MnSO_4$ obtained in this work (b).*

Another confirmation of the blocking of the cathode surface is the decrease in electroactivity of $LiMn_2O_4$-based cathodes in zinc sulfate solution, for which irreversible surface introduction of zinc cations was shown by EDX analysis of the electrodes after cycling (Figure 17). Therefore, the

mechanism of intercalation/deintercalation of Zn^{2+} ions only was not accepted for MnO_2 cathodes, which is confirmed by most of the publications. As a result, the Zn//MnO_2 electrochemical system can only be indirectly called a "zinc-ion battery" in the classical meaning (by the rocking chair mechanism). After adding the manganese salt to the electrolyte solution, the cathodes regain their electroactivity (Figure 53, b).

It has been shown in this work that during the electrochemical tests in $MnSO_4$ solution, which does not contain zinc cations, at pH values ≈ 4 the loss of electroactivity of the MnO_2 cathode is also observed. During charging at E > 1.7 V, the deposition process of MnO_2 on the cathode surface is observed, but the cathodic dissolution process of the oxide is not (Figure 40, b). Thus, the deposition of the amorphous layer of manganese oxide is not dominant in the overall charge/discharge process and charge storage of the MnO_2 electrode. The mass-potential dependencies were obtained in 0.1 $MnSO_4$ solution [179], where after the first cycle during oxidation there is an increase in the electrode mass at the potentials E > 0.5 V, and then during reduction there is a decrease in the mass, which is associated with the process of dissolution of the oxide (Figure 54, a). The mass-potential dependencies obtained by EQCM for Au-MnO_2 electrodes in 0.1 M manganese acetate solution are similar to those previously discussed [179]: there is an increase in mass during oxidation in the range of high positive potentials, which is replaced by a sharp decrease in mass during cell reduction at E= 0.34 V, and then the mass decreases smoothly to zero value (Figure 54, b). As in the case of the manganese sulfate solution, there is almost complete dissolution of the oxide film from the surface of the gold electrode.

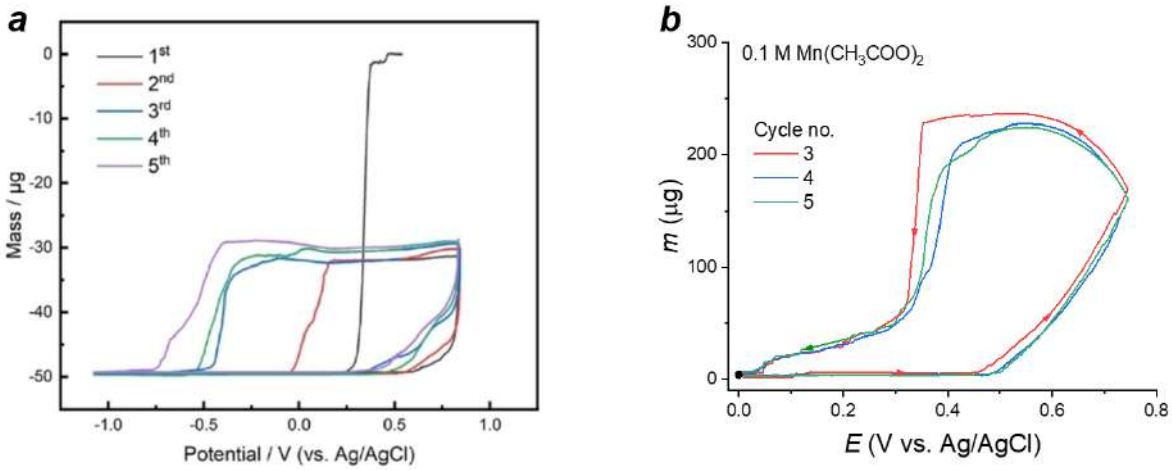

Figure 54. The mass-potential dependencies for Au-MnO_2 electrodes obtained in 0.1 M $MnSO_4$ [179] *(a) and 0.1 M $Mn(CH_3COO)_2$ (this work, b) solutions.*

To summarize the results obtained, we can conclude that the electroactivity of MnO_2-cathodes in sulfate-based solution is provided by the simultaneous presence of Zn^{2+} and Mn^{2+} ions. It is also worth noting that different forms of I – E dependences are observed for MnO_2 in the first CV cycle

depending on the electrolyte composition (Figure 55). In manganese sulfate solution (pH ≈ 4), no cathodic and anodic peaks are observed on the CV for the MnO_2 cathode, confirming the conclusion about the absence of electroactivity of cathodes in this solution. In zinc sulfate-based solutions: 2 M $ZnSO_4$ and 2 M $ZnSO_4$ / 0.1 M $MnSO_4$, two cathode peaks are observed at E = 1.44 V and E = 1.29 V, whereas the intensity of the first peak is significantly lower than that of the second one, respectively. The presence of two clearly separated peaks on the cathodic curve indicates that two different energy processes occur during the discharge, apparently due to the intercalation of particles of different nature present in the electrolyte solution, or they may be associated with the formation of additional barriers on the electrode surface, leading to a change in the conditions of charge transfer.

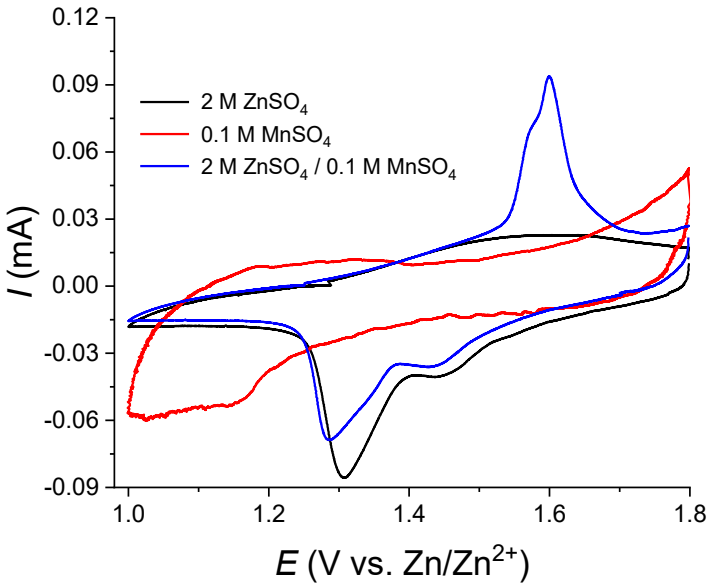

Figure 55. First CV cycle for MnO_2 -cathodes obtained in the three types of zinc and manganese sulfate electrolytes considered.

For the first cathodic cycle at E ≈ 1.44 V vs. Zn/Zn^{2+}, the low intensity of the current response can be related to the low concentration of intercalated particles, which can be the free hydrogen ions present in the electrolyte solution. Moreover, in accordance to the direct measurements of the cathode mass during cycling (Figure 43, a, b) and analysis of electrochemical properties of MnO_2 cathodes in the solutions with excess of alkali ions concentration (Section 4.2), the processes involving the monovalent ions occur in this potential range. In the mixed 2 M $ZnSO_4$ / 0.1 M $MnSO_4$ electrolyte solution this monovalent ion is H^+ or H_3O^+ ion. At pH = 4.5 its concentration is $[H^+] \approx 0.000032$ M, which causes a low intensity of peak currents during the cathodic process, so at E ≈ 1.44 V H^+ ions contained in the electrolyte solution due to hydrolysis of zinc and/or manganese salts participate in the cathodic reaction, let us call them “free H^+ ions”. This observation correlates well with the change in the electrochemical response of $Zn//MnO_2$ in $ZnSO_4$ solution, where the pH was fixed by the addition

of acetic acid [76]. At pH = 4.0, the peak at $E \approx 1.5$ V was practically the only one observed on the CV curve; as the pH of the solution increased, its intensity decreased, which correlates with a decrease in the concentration of free H^+ ions contained in the solution. The process of intercalation of H^+ ions is associated with a decrease in the degree of oxidation of manganese to Mn^{3+}, so one of the phases formed in this case is MnOOH [142,180,181]. In particular, the formation of Mn–O–H bonds has been demonstrated by *ex situ* XPS [181], from which it has been concluded that H^+ ions intercalate. Apparently, the formation of MnOOH phase in this case does not occur in the whole volume of the electroactive material due to the small amount of H^+ ions.

It is seen for the cathode process occurring at the potential values $E \approx 1.29$ V, based on the intensity of currents at the first cycle, that the concentration of redox centers participating in the electrochemical process, in which there is a simultaneous intercalation of ions – participants of the reaction should be higher than during the redox process at $E \approx 1.44$ V. Considering that zinc ions maintain the high currents of this peak in the first cycle, it could be assumed that intercalation of zinc ions occurs with their subsequent transformations in the solid phase of manganese oxide. Moreover, from the changes of the electrode mass it is clearly seen that in this potential range the most intense growth of the precipitate mass on the Au electrode is observed, which is associated with the intercalation of zinc ions and the formation of zinc basic salt precipitate (Figure 42, b). Thus, the electrochemical process involves the desolvation and intercalation of zinc ions, their partial dissociation and the process of chemical precipitation of the basic salt $Zn_4(OH)_6SO_4 \cdot nH_2O$ (ZHS), the presence of which has been repeatedly confirmed in various publications [182,183], as well as in our X-ray diffraction data. At the same time, there is a periodic pH change in the near-electrode region, which has been estimated to a first approximation using *in operando* pH measurements [22]. The pH shift to 5.0 is due to the release of OH^- ions which promotes the formation of ZHS. This process could be generally described by the following equation [37]:

$$4Zn^{2+} + SO_4^{2-} + (6 + x)H_2O \rightarrow Zn_4(OH)_6SO_4 \cdot xH_2O + 6H^+ \quad (8)$$

Based on this form of the equation, the second cathodic process involves Zn^{2+} ions, which could be present in solution, for example, in the aqua complex $[Zn(H_2O)_6]^{2+}$. The deposition of ZHS on the MnO2 cathode surface occurs due to a chemical process associated with the pH changes. It should be noted that when the cell is discharged, part of the charge (equivalent to 0.77 mAh) is spent on the ZHS formation process, so additional electrochemical reactions occur during the ZHS formation process that contribute to the capacity.

When the cell is charged in the potential range $\Delta E = 1.0 – 1.2$ V, the insignificant mass increase is observed on the $m – E$ dependence, which is related to the continuous chemical process of ZHS

formation, further at $E \approx 1.5$ V, where anodic peaks are present on the CV curves, the electrode mass decreased sharply. After this loss of mass, a slight increase begins, which is particularly noticeable in the following cycles (Figure 42, b). So, two parallel processes: ZHS dissolution and Mn^{2+} oxidation with MnO_2 deposition take place as follows:

$$Mn^{2+} + 2H_2O - 2\bar{e} \rightarrow MnO_2 + 4H^+ \quad (9)$$

According to this equation, during Mn^{2+} oxidation, the large amount of free protons in the solution leads to the acidification of the near-electrode layer, which may contribute to a more efficient dissolution of the surface ZHS precipitate. Therefore, the equilibrium between MnO_2 formed on the cathode surface and ZHS ensures a constant acidity of the electrolyte solution in the absence of additional buffering agents [136]. Furthermore, it has been demonstrated that the presence of ZHS in the system reduces the potential of oxidation of Mn^{2+} to MnO_2. A higher oxidation potential ($E > 1.7$ V) is required for the primary assembled cell compared to the charged cell while after achieving $E = 1.0$ V during charge the deposition process of manganese oxide on the surface is reduced to $E = 1.55$ V [20,184]. Hence, the presence of ZHS layer is crucial for the electrodeposition of new MnO_2 layers and these processes are inverse in terms of their charge/discharge. The dependence between ZHS dissolution and Mn^{2+} oxidation was proven during synthesis of the cathode material, which employed a carbon paper substrate coated with a layer of chemically synthesized ZHS rather than manganese oxide. *In situ* measurements revealed that during the charge process, ZHS undergoes dissolution while MnO_2 is deposited on the surface of the current collector, in accordance with the following equation [185]:

$$3Mn^{2+} + 2Zn_4(OH)_6SO_4 \cdot 5H_2O - 6\bar{e} \rightarrow 3MnO_2 + 8Zn^{2+} + 2SO_4^{2-} + 16H_2O \quad (10)$$

The formation of manganese dioxide with birnessite structure has been proved by scanning and transmission electron microscopy with elemental analysis, and it has also been shown that Zn^{2+} ions are injected into the interlayer spaces of the cathode structure, indicating the formation of zinc-containing Zn_xMnO_2 phases [183]. Thus, ZHS is an electrochemically inactive participant in the reaction, but its presence in combination with the presence of Mn^{2+} ions in the solution allows the processes of precipitation and dissolution of manganese oxide to proceed efficiently.

The formation of the basic salt is reversible only in solutions containing Mn^{2+} ions and irreversible in pristine zinc sulfate electrolytes. This leads to the conclusion that the reaction of ZHS formation and dissolution is a consequence of the participation of H^+ in the oxidation process of Mn^{2+} ions which is supported by previous studies [20,181].

However, in the second cathodic process at $E \approx 1.29$ V, not only H^+ cations but also Zn^{2+} cations are involved (Figure 55). Moreover, following the initial intercalation phase at $E \approx 1.44$ V, the proton concentration in the solution is relatively low. This indicates that the primary process should be the intercalation of Zn^{2+} cations into the electrode structure. The accumulation of phases of zinc-containing manganese compounds, Zn_xMnO_2 [186] or $Zn_xMnO(OH)_y$ [187] in the electrode provides clear evidence of this intercalation. During the following cycling process, the accumulation of $ZnMn_3O_7$ (woodruffite), which is non-electroactive, begins. In addition to X-ray diffraction data and analysis of the cathode phase composition, it is possible to estimate the content of Zn^{2+} cations in the cathode structure in the fully charged and fully discharged states by elemental analysis in order to determine the presence of intercalated cations in the cathode structure. We used X-ray fluorescence analysis to determine the zinc content in the cathode materials in discharged state after 10 and 30 charge/discharge cycles and in the charged state after 30 cycles. The samples were washed by deionized water and 0.25 M solution of acetic acid to completely or partially remove surface compounds. In all three states, manganese and zinc were the main components of the material, impurity amounts of potassium were also detected, consistent with the initial structure of the synthesized birnessite, as well as traces of sulfur indicative of sulfate residues on the surface or in the volume. The data on the quantitative content of elements was used to obtain the ratios of Mn:Zn per one manganese atom, which are presented in the table 3.

Table 3. Mn:Zn ratio in the electrode materials after electrochemical tests based on the X-ray fluorescence analysis data.

	Before CH_3COOH treatment	After CH_3COOH treatment
10 cycles (*E* = 1.0 V)	1 : 1.4	1 : 0.2
30 cycles (*E* = 1.0 V)	1 : 1.5	1 : 1.05
30 cycles (*E* = 1.8 V)	1 : 0.4	1 : 0.3

These data indicate that zinc is present in the composition of the cathode material in both the discharged (E = 1.0 V) and charged (E = 1.8 V) states, so, zinc is inserted into the cathode material at discharge and that its extraction is incomplete at charge. In the discharged state, zinc cations exist in two forms: the surface precipitate of the basic salt and zinc ions intercalated into the MnO_2 lattice. After the acidic treatment of the cathode the fraction of zinc decreases, indicating dissolution of ZHS. The remaining fraction of zinc is Zn^{2+} ions intercalated in the crystal lattice of the material. As the number of cycles increases, the zinc content increases in a manner that is consistent with the accumulation of zinc-containing manganese oxide detected from XRD or high-resolution transmission electron microscopy data [20], indicating that electroactive sites in the cathode structure are blocked due to the strong binding of Zn^{2+} ions and the cathode material. This is also supported by the fact that

zinc is present in the fully charged state of the cathode material, and its concentration is weakly dependent on the treatment with acetic acid solution.

Nevertheless, the process of Zn^{2+} ion injection into the MnO_2 structure is not the only reaction occurring at the potential E = 1.2 V and requires more detailed consideration. In particular, a number of authors claim that H^+ ions are also involved in this process [181], which correlates well with alkalinization of the near-electrode layer of the solution for the efficient course of the parallel reaction of ZHS formation. In this case, the question arises about the source of protons involved both in co-intercalation and in the surface reaction. The most probable source of protons near the particles of the electroactive material in this case are the $[Zn(H_2O)_6]^{2+}$ ions adsorbed on the surface or located in the near-electrode layer. This cation exhibits weak Brønsted acidity, as indicated by a pKa value of 8.96 in the first step [188,189]. If we consider that the dissociation of the intra-sphere water molecule in the coordination sphere of the $[Zn(H_2O)_6]^{2+}$ ion is essentially a hydrolysis process of the Zn^{2+} ion, the value of the hydrolysis constant will be determined as a value of 14 – 8.96 = 5.04 which correlates with the acidity range of the electrolyte solution 2 M $ZnSO_4$ / 0.1 M $MnSO_4$ for processes at $E \approx 1.29$ V, confirmed by *in operando* pH measurements [22]. Hydrolysis of zinc ions, or dissociation of hexaaquozinc cations, can be described by the following equations:

$$[Zn(H_2O)_6]^{2+} \leftrightarrow [Zn(H_2O)_5(OH)]^+ + H^+ \quad (11)$$

$$[Zn(H_2O)_6]^{2+} + H_2O \leftrightarrow [Zn(H_2O)_5(OH)]^+ + H_3O^+ \quad (12)$$

In order to distinguish the nature of the as-generated H^+ particles, let us denote the ones formed in this reaction “bound H^+ ions”, hydrated zinc ions act as a source of H^+ ions. The H^+ ions, which are formed as a result of the dissociation of the water molecule within the hydrate shell of the Zn^{2+} ion, are more strongly repelled by the resulting positive cation. As a result, they are effectively transported both deep into the cathode and from the near-electrode layer into the electrolyte solution. The formed $[Zn(H_2O)_5)OH)]^+$ ion, in turn, acts as a precursor for the synthesis of ZHS on the surface of the electroactive material. This explains the fact that as the degree of discharge of the Zn//MnO_2 system and the number of charge/discharge cycles increase, the accumulation of the basic salt proceeds more intensively [135]. Further evidence that ZHS formation is dependent on “bound” rather than “free” H^+ ions is provided by studies of MnO_2 cathodes in binary solutions containing alkali metal ions. During the initial cycle, the formation of ZHS on the surface of MnO_2 particles is observed, followed by the absence of dissolution (Figure 47, b). Subsequently, the primary process is the intercalation of alkali metal ions, with the process of Zn^{2+} injection and the formation of new ZHS layers becoming significantly challenging (Figure 45, b).

To summarize, the electrochemical reaction in the Zn//MnO_2 electrochemical cell in sulfate-based solutions involves both H^+ cations associated with the processes of dynamic precipitation/dissolution of both the ZHS precipitate and additional MnO_2 layers. In addition, Zn^{2+} cations are also involved, resulting in an accumulation of cathode capacity. This confirms the term "co-intercalation of Zn^{2+} and H^+ ions" used repeatedly in the literature for the mechanism in MnO_2 cathodes. In this case, the H^+ cations have two different formation pathways. The first type are the ions initially present in solution either as a result of hydrolysis of zinc and manganese salts (in the first cycle) or as a result of oxidation of Mn^{2+} to MnO_2 (subsequent cycles). The second type of H^+ ions is formed as a result of the dissociation of $[Zn(H_2O)_6]^{2+}$ ions in the reaction zone, which is located in close proximity to the surface of the electroactive material particles. The formation and dissolution of ZHS, along with the electrolytic deposition and dissolution of MnO_2, regulate the concentration of H^+ ions in the near-electrode layer, thus maintaining the equilibrium within the system (Figure 56).

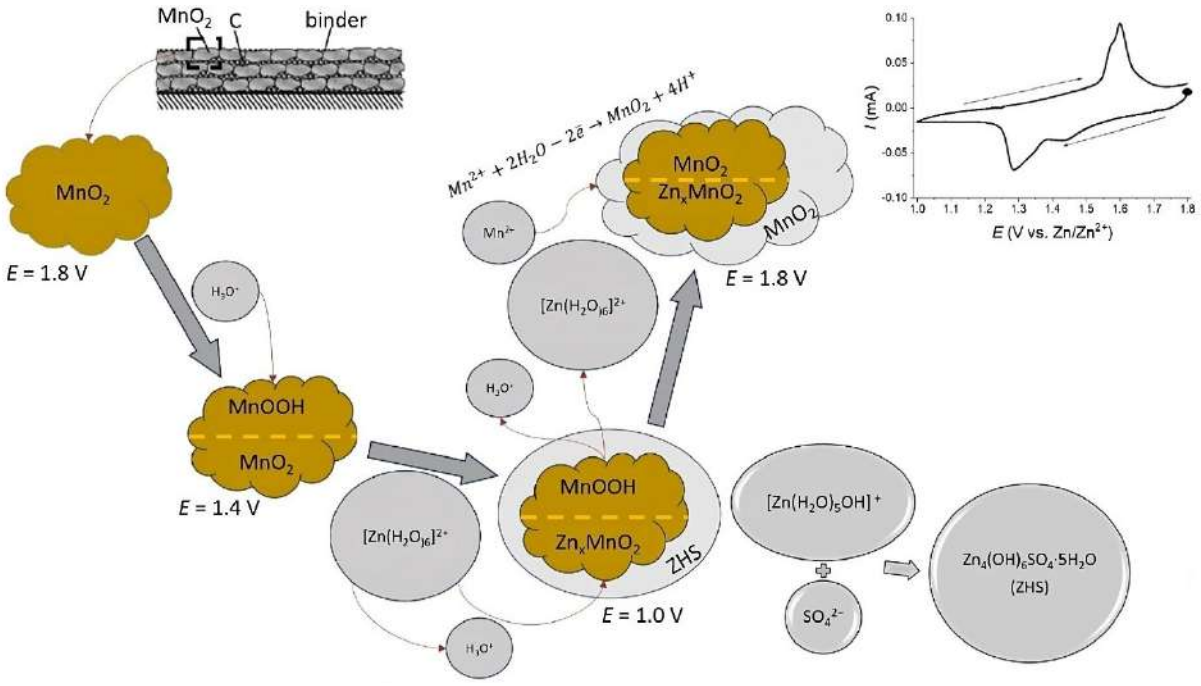

Figure 56. Schematic representation of the electrochemical reaction realized in the Zn//MnO_2 system in a solution of zinc and manganese sulfates.

In addition, it should be noted that controlling the acidity of the solution can lead to a change in the reaction mechanism. The tests carried out with the CV and EQCM in acetate-based solutions with a constant pH of 4.5 showed that the formation of the basic salt did not occur. Consequently, the oxidation potential of MnO_2 remained within the initial potential range (Figure 52, a, b). In addition, these data confirm that the main variant of the mechanism under these conditions is electrolytic precipitation/dissolution of MnO_2, which has been shown by other authors [76,135,145]. This is in good agreement with the conclusions of [179], where the impact of an acetic acid buffer solution on

the electrochemical reaction mechanism was examined. In contrast, the use of a non-acidified zinc acetate-based electrolyte solution results in the formation of a surface precipitate, which explains the mass increase on the gold electrode (Figure 52, c, d). At the same time, there is no reverse dissolution process of this precipitate, in contrast to sulfate-based electrolyte solutions. Despite the occurrence of intensive processes of MnO_2 deposition on the cathode surface during charging, the extremely low concentration of H^+ ions in the solution precludes the possibility of ensuring the dissolution of precipitates from the surface of grains of electroactive material. This results in a loss of electroactivity and a reduction in current response.

Conclusions

A systematic study of the properties of cathode materials based on manganese oxide with layered structure and spinel structure in aqueous zinc-ion and zinc-hybrid battery test cells has been conducted. The influence of the electrolyte composition, the structure and the composition of the cathode material on their functional properties has been established.

For the $LiMn_2O_4$-based cathode materials, the necessity of the presence of lithium salt in the electrolyte solution was established. In solutions containing only Zn^{2+} ions, the irreversible introduction of these ions into the material structure is observed, resulting in a deterioration of the electrochemical properties of $LiMn_2O_4$. However, this structural transformation is reversible. Therefore, reactions involving H^+ ions present in the aqueous electrolyte solution are practically non-existent. The presence of Mn^{2+} ions in the mixed electrolyte (zinc and manganese sulfates) results in an artificial increase in the specific capacity, which is subsequently offset by its sharp decrease during long-term cycling due to competing processes of deposition of an additional phase, blocking the surface of the material for ionic transport, as well as the competing process of oxygen evolution reaction. The dependence of the functional properties and kinetic parameters of cathode materials for aqueous zinc-ion batteries based on manganese oxide with a layered structure on the synthesis procedure has been established. It was observed that with increasing amorphousness of the synthesized manganese oxide, there was a corresponding decrease in the initial specific capacity, accompanied by an increase in the cyclic stability of the capacity. In addition, the resistance to charge transfer was found to be lower, which can be attributed to the preservation of the bonds between the fragments of the cathode material.

Among the various methods of modification of MnO_2-based cathodes by conducting polymer PEDOT, considered in this research, the best electrochemical performance and kinetic parameters were obtained for the MnO_2 cathodes coated by PEDOT:PSS. Due to the reduced direct contact area of the electroactive material and electrolyte, as well as the conductivity of the polymer coating, the best specific capacity values during cycling were achieved (291 $mAh \cdot g^{-1}$ and 276 $mAh \cdot g^{-1}$ at current densities of 0.1 and 0.3 $A \cdot g^{-1}$, respectively). In the case of the MnO_2/PEDOT:PSS composite electrode, the processes of MnO_x deposition from the electrolyte solution occur on the surface of the polymer rather than the electroactive material. This results in an increase in the amount of material deposited and a stabilization of the specific capacity of the material.

Investigations of the dependence of the electrochemical properties of MnO_2 on the electrolyte composition have shown the necessity of the presence of two cations (Zn^{2+} and Mn^{2+}) in the electrolyte solution, because in the absence of one of the cations the degradation of the properties occurs. The widely discussed but elusive involvement of H^+ ions in the electrode reaction was indirectly

demonstrated by the addition of a monovalent ion in an excess concentration to the solution, with Na^+ ions serving as an illustrative example. According to the measured *in operando* mass changes of MnO_2 precipitate on the quartz crystal surface in thin films, at the potential E = 1.4 V at discharge, the monovalent ion is identified as the primary contributor to the capacity.

In zinc acetate-based electrolyte solutions, the main proposed mechanism for manganese oxide is proton intercalation initiating the processes of electrolytic precipitation/dissolution of additional MnO_x layers. The direct dependence of the electrochemical process on the pH value of the solution allows us to state that the processes of formation of basic salts on the surface of the cathode material are practically suppressed in the case of acidic electrolyte solutions, this leads to a change in the reaction mechanism and suppression of the participation of Zn^{2+} ions in the overall electrochemical process.

A new hypothesis is proposed to explain the mechanism of electrochemical processes in MnO_2-cathodes in mixed zinc- and manganese-containing sulfate electrolyte solutions. The electrochemical reaction mechanism involves the co-intercalation of Zn^{2+} ions and H^+ ions, which proceeds with the dissociation of a water molecule within the hydrate shell of the zinc cation injected into the oxide structure. This results in the occurrence of free hydrogen ions H^+ and a reduction in the charge of the cation, leading to the formation of $[Zn(H_2O)_5)OH)]^+$ ion. The latter acts as a precursor for the subsequent precipitation/dissolution reaction of the basic salt $Zn_4(OH)_6SO_4 \cdot nH_2O$ on the surface of manganese oxide particles within the composite cathode. However, the question of the contribution of each ion to the total cathode capacity remains unanswered, as does the chemical state of the H^+ ion in the MnO_2-cathode structure.

Acknowledgements

I would like to express my gratitude to everyone who supported, guided and helped me during the realization of my dissertation research. First of all, I would like to thank my supervisors: Prof. V. V. Kondratiev and Assist. Prof. S. N. Eliseeva, for careful supervision of the experimental work, including regular discussions of both the obtained results and literature data. I am also grateful the staff and students of the Department of Electrochemistry including graduate students for their assistance in obtaining and analysis of the results: F. S. Volkov, A. Yu. Popov, Yu. D. Salnikova, Ph.D. A. O. Efremova, Ph.D. A. I. Volkov and Assist. Prof., Ph.D. E.G. Tolstopjatova for consultative assistance both in setting up the experiment and in analyzing the text of the work.

I would like to express my special gratitude to my family members, especially to my wife E. A. Kamenskaya, for moral support during the implementation and writing of the work.

The data obtained using the Research Park of Saint Petersburg State University equipment listed below were used in this work:

1. Centre for X-ray Diffraction Studies – X-ray powder diffraction and high-resolution X-ray diffraction.
2. Interdisciplinary Resource Centre for Nanotechnology – scanning electron microscopy and energy dispersive X-ray analysis.
3. Centre for Physical Methods of Surface Investigation – X-ray photoelectron spectroscopy.
4. Chemical Analysis and Materials Research Centre – X-ray fluorescence analysis.

I express my gratitude to the Russian Foundation for Basic Research (project No. 21-53-53012) for financial support.

List of abbreviations

AZIBs – aqueous zinc-ion batteries

CV – cyclic voltammetry

EDOT – 3,4-ethylenedioxythiophene

EDX – energy dispersive X-ray analysis

EQCM – electrochemical quartz crystal microbalance

LMO – lithium manganese spinel $LiMn_2O_4$

PANI – polyaniline

PEDOT – poly(3,4-ethylenedioxythiophene)

PPy – polypyrrole

PSS – polystyrene sufonate

PVDF – polyvinylidene fluoride

SEM – scanning electron microscopy

XPS – X-ray photoelectron spectroscopy

XRD – X-ray diffraction

ZHS – $Zn_4(OH)_6SO_4 \cdot nH_2O$ – zinc hydroxide sulfate

References

[1] X. Zeng, J. Hao, Z. Wang, J. Mao, Z. Guo, Recent progress and perspectives on aqueous Zn-based rechargeable batteries with mild aqueous electrolytes, Energy Storage Mater. 20 (2019) 410–437. https://doi.org/10.1016/j.ensm.2019.04.022.

[2] J. Huang, Z. Guo, Y. Ma, D. Bin, Y. Wang, Y. Xia, Recent Progress of Rechargeable Batteries Using Mild Aqueous Electrolytes, Small Methods. 3 (2019) 1800272. https://doi.org/10.1002/smtd.201800272.

[3] M.B. Lim, T.N. Lambert, B.R. Chalamala, Rechargeable alkaline zinc–manganese oxide batteries for grid storage: Mechanisms, challenges and developments, Mater. Sci. Eng. R Reports. 143 (2021) 100593. https://doi.org/10.1016/j.mser.2020.100593.

[4] V. Mathew, N.B. Schorr, B. Sambandam, T.N. Lambert, J. Kim, A Critical Comparison of Mildly Acidic versus Alkaline Zinc Batteries, Accounts Mater. Res. 4 (2023) 299–306. https://doi.org/10.1021/accountsmr.2c00221.

[5] L. Sun, Z. Song, C. Deng, Q. Wang, F. Mo, H. Hu, G. Liang, Electrolytes for Aqueous Zn-Ion Batteries Working in Wide-Temperature Range: Progress and Perspective, Batteries. 9 (2023) 386. https://doi.org/10.3390/batteries9070386.

[6] A. Zhou, R. Chi, Y. Shi, X. Zhao, X. Li, Z. Kou, Z. Zhang, X. Zhang, G. Nie, Manganese-based cathode materials for aqueous rechargeable zinc-ion batteries: recent advance and future prospects, Mater. Today Chem. 27 (2023) 101294. https://doi.org/10.1016/j.mtchem.2022.101294.

[7] L. Kang, M. Cui, Z. Zhang, F. Jiang, Rechargeable Aqueous Zinc-Ion Batteries with Mild Electrolytes: A Comprehensive Review, Batter. Supercaps. 3 (2020) 966–1005. https://doi.org/10.1002/batt.202000060.

[8] C. Xu, B. Li, H. Du, F. Kang, Energetic zinc ion chemistry: The rechargeable zinc ion battery, Angew. Chemie - Int. Ed. 51 (2012) 933–935. https://doi.org/10.1002/anie.201106307.

[9] J.E. Post, Manganese oxide minerals: Crystal structures and economic and environmental significance, Proc. Natl. Acad. Sci. 96 (1999) 3447–3454. https://doi.org/10.1073/pnas.96.7.3447.

[10] X. Jia, C. Liu, Z.G. Neale, J. Yang, G. Cao, Active Materials for Aqueous Zinc Ion Batteries: Synthesis, Crystal Structure, Morphology, and Electrochemistry, Chem. Rev. 120 (2020) 7795–7866. https://doi.org/10.1021/acs.chemrev.9b00628.

[11] Y. Jin, L. Zou, L. Liu, M.H. Engelhard, R.L. Patel, Z. Nie, K.S. Han, Y. Shao, C. Wang, J. Zhu, H. Pan, J. Liu, Joint Charge Storage for High-Rate Aqueous Zinc–Manganese Dioxide Batteries, Adv. Mater. 31 (2019) 1900567. https://doi.org/10.1002/adma.201900567.

[12] M.H. Alfaruqi, S. Islam, D.Y. Putro, V. Mathew, S. Kim, J. Jo, S. Kim, Y.-K. Sun, K. Kim, J. Kim, Structural transformation and electrochemical study of layered MnO_2 in rechargeable aqueous zinc-ion battery, Electrochim. Acta. 276 (2018) 1–11. https://doi.org/10.1016/j.electacta.2018.04.139.

[13] G. Li, Z. Huang, J. Chen, F. Yao, J. Liu, O.L. Li, S. Sun, Z. Shi, Rechargeable Zn-ion batteries with high power and energy densities: A two-electron reaction pathway in birnessite MnO_2 cathode materials, J. Mater. Chem. A. 8 (2020) 1975–1985. https://doi.org/10.1039/c9ta11985j.

[14] A.R. Mainar, E. Iruin, J.A. Blázquez, New Insights of Zn^{2+}/Li^{+} Hybrid Aqueous Batteries, Energy Technol. 8 (2020) 2–8. https://doi.org/10.1002/ente.202000476.

[15] Y. Xu, G. Zhang, J. Liu, J. Zhang, X. Wang, X. Pu, J. Wang, C. Yan, Y. Cao, H. Yang, W. Li, X. Li, Recent Advances on Challenges and Strategies of Manganese Dioxide Cathodes for Aqueous Zinc-Ion Batteries, Energy Environ. Mater. 6 (2023) e12575. https://doi.org/10.1002/eem2.12575.

[16] M. Chamoun, W.R. Brant, C.W. Tai, G. Karlsson, D. Noréus, Rechargeability of aqueous sulfate Zn/MnO2 batteries enhanced by accessible Mn^{2+} ions, Energy Storage Mater. 15 (2018) 351–360. https://doi.org/10.1016/j.ensm.2018.06.019.

[17] V. Soundharrajan, B. Sambandam, S.S. Kim, S. Islam, J. Jo, S.S. Kim, V. Mathew, Y. Kook Sun, J. Kim, The dominant role of Mn^{2+} additive on the electrochemical reaction in $ZnMn_2O_4$ cathode for aqueous zinc-ion batteries, Energy Storage Mater. 28 (2020) 407–417. https://doi.org/10.1016/j.ensm.2019.12.021.

[18] C. Qiu, X. Zhu, L. Xue, M. Ni, Y. Zhao, B. Liu, H. Xia, The function of Mn^{2+} additive in aqueous electrolyte for Zn/δ-MnO_2 battery, Electrochim. Acta. 351 (2020) 136445. https://doi.org/10.1016/j.electacta.2020.136445.

[19] Z. You, W. Hua, N. Li, H. Liu, J.-G. Wang, An in-depth mechanistic insight into the redox reaction and degradation of aqueous Zn-MnO_2 batteries, Chinese Chem. Lett. 34 (2023) 107525. https://doi.org/10.1016/j.cclet.2022.05.039.

[20] I. Aguilar, P. Lemaire, N. Ayouni, E. Bendadesse, A. V. Morozov, O. Sel, V. Balland, B. Limoges, A.M. Abakumov, E. Raymundo-Piñero, A. Slodczyk, A. Canizarès, D. Larcher, J.-M. Tarascon, Identifying interfacial mechanisms limitations within aqueous Zn-MnO_2 batteries and means to cure them with additives, Energy Storage Mater. 53 (2022) 238–253. https://doi.org/10.1016/j.ensm.2022.08.043.

[21] J. Yang, J. Cao, Y. Peng, W. Yang, S. Barg, Z. Liu, I.A. Kinloch, M.A. Bissett, R.A.W. Dryfe, Unravelling the Mechanism of Rechargeable Aqueous Zn–MnO_2 Batteries: Implementation of Charging Process by Electrodeposition of MnO_2, ChemSusChem. 13 (2020) 4103–4110. https://doi.org/10.1002/cssc.202001216.

[22] O. Fitz, C. Bischoff, M. Bauer, H. Gentischer, K.P. Birke, H.M. Henning, D. Biro, Electrolyte Study with in Operando pH Tracking Providing Insight into the Reaction Mechanism of Aqueous Acidic Zn//MnO_2 Batteries, ChemElectroChem. 8 (2021) 3553–3566. https://doi.org/10.1002/celc.202100888.

[23] F. Rossi, E. Marini, M. Boniardi, A. Casaroli, A.L. Bassi, A. Macrelli, C. Mele, B. Bozzini, What Happens to MnO_2 When It Comes in Contact with Zn^{2+}? An Electrochemical Study in Aid of Zn/MnO_2-Based Rechargeable Batteries, Energy Technol. 10 (2022) 2200084. https://doi.org/10.1002/ente.202200084.

[24] J. Huang, J. Tu, Y. Lv, Y. Liu, H. Huang, L. Li, J. Yao, Achieving mesoporous MnO_2@polyaniline nanohybrids via a gas/liquid interfacial reaction between aniline and $KMnO_4$ aqueous solution towards Zn-MnO_2 battery, Synth. Met. 266 (2020) 116438. https://doi.org/10.1016/j.synthmet.2020.116438.

[25] J. Huang, Z. Wang, M. Hou, X. Dong, Y. Liu, Y. Wang, Y. Xia, Polyaniline-intercalated manganese dioxide nanolayers as a high-performance cathode material for an aqueous zinc-ion battery, Nat. Commun. 9 (2018) 2906. https://doi.org/10.1038/s41467-018-04949-4.

[26] N. Li, Z. Hou, S. Liang, Y. Cao, H. Liu, W. Hua, C. Wei, F. Kang, J.-G. Wang, Highly flexible MnO_2@polyaniline core-shell nanowire film toward substantially expedited zinc energy storage, Chem. Eng. J. 452 (2023) 139408. https://doi.org/10.1016/j.cej.2022.139408.

[27] J. Huang, X. Tang, K. Liu, G. Fang, Z. He, Z. Li, Interfacial chemical binding and improved kinetics assisting stable aqueous Zn–MnO_2 batteries, Mater. Today Energy. 17 (2020) 100475. https://doi.org/10.1016/j.mtener.2020.100475.

[28] X. Liao, C. Pan, Y. Pan, C. Yin, Synthesis of three-dimensional β-MnO_2/PPy composite for high-performance cathode in zinc-ion batteries, J. Alloys Compd. 888 (2021) 161619. https://doi.org/10.1016/j.jallcom.2021.161619.

[29] J.W. Xu, Q.L. Gao, Y.M. Xia, X. Sen Lin, W.L. Liu, M.M. Ren, F.G. Kong, S.J. Wang, C. Lin, High-performance reversible aqueous zinc-ion battery based on iron-doped alpha-manganese dioxide coated by polypyrrole, J. Colloid Interface Sci. 598 (2021) 419–429. https://doi.org/10.1016/j.jcis.2021.04.057.

[30] Y. Zhang, G. Xu, X. Liu, X. Wei, J. Cao, L. Yang, Scalable In Situ Reactive Assembly of Polypyrrole-Coated MnO_2 Nanowire and Carbon Nanotube Composite as Freestanding Cathodes for High Performance Aqueous Zn-Ion Batteries, ChemElectroChem. 7 (2020) 2762–2770. https://doi.org/10.1002/celc.202000253.

[31] T. Niu, J. Li, Y. Qi, X. Huang, Y. Ren, Preparation and electrochemical properties of α-MnO_2/rGO-PPy composite as cathode material for zinc-ion battery, J. Mater. Sci. 56 (2021) 16582–16590. https://doi.org/10.1007/s10853-021-06266-6.

[32] J. Mao, F.-F. Wu, W.-H. Shi, W.-X. Liu, X.-L. Xu, G.-F. Cai, Y.-W. Li, X.-H. Cao, Preparation of Polyaniline-coated Composite Aerogel of MnO_2 and Reduced Graphene Oxide for High-performance Zinc-ion Battery, Chinese J. Polym. Sci. 38 (2020) 514–521. https://doi.org/10.1007/s10118-020-2353-6.

[33] P. Ruan, X. Xu, X.X. Gao, J. Feng, L. Yu, Y. Cai, X.X. Gao, W. Shi, F. Wu, W. Liu, X. Zang, F. Ma, X. Cao, Achieving long-cycle-life Zn-ion batteries through interfacial engineering of MnO_2-polyaniline hybrid networks, Sustain. Mater. Technol. 28 (2021) e00254. https://doi.org/10.1016/j.susmat.2021.e00254.

[34] Y. Ma, M. Xu, S. Huang, L. Wang, H. Xiao, L. Chen, Z. Zhang, R. Liu, G. Yuan, Conformal poly (3,4-ethylenedioxythiophene) skin stabilized ε-type manganese dioxide microspheres for zinc ion batteries with high volumetric energy density, J. Colloid Interface Sci. 649 (2023) 996–1005. https://doi.org/10.1016/j.jcis.2023.06.172.

[35] N. Fu, Q. Zhao, Y. Xu, H. Wang, J. Hu, Y. Wu, L. Yang, X. Wu, X. Zeng, Exploiting the synergistic effect of multiphase MnO_2 stabilized by an integrated conducting network for aqueous zinc-ion batteries, Mater. Chem. Front. 6 (2022) 1956–1963. https://doi.org/10.1039/D2QM00254J.

[36] J. Chen, J. Liang, Y. Zhou, Z. Sha, S. Lim, F. Huang, Z. Han, S.A. Brown, L. Cao, D. Wang, C.H. Wang, A vertical graphene enhanced Zn–MnO_2 flexible battery towards wearable electronic devices, J. Mater. Chem. A. 9 (2021) 575–584. https://doi.org/10.1039/D0TA08775K.

[37] N. Zhang, Y.R. Ji, J.C. Wang, P.F. Wang, Y.R. Zhu, T.F. Yi, Understanding of the charge storage mechanism of MnO_2-based aqueous zinc-ion batteries: Reaction processes and regulation strategies, J. Energy Chem. 82 (2023) 423–463. https://doi.org/10.1016/j.jechem.2023.03.052.

[38] M.A. Kamenskii, F.S. Volkov, S.N. Eliseeva, R. Holze, V.V. Kondratiev, Comparative Study of PEDOT- and PEDOT:PSS Modified δ-MnO_2 Cathodes for Aqueous Zinc Batteries with Enhanced Properties, J. Electrochem. Soc. 170 (2023) 010505. https://doi.org/10.1149/1945-7111/acabec.

[39] M.A. Kamenskii, A.Y. Popov, S.N. Eliseeva, V. V Kondratiev, The Effect of the Synthesis Method of the Layered Manganese Dioxide on the Properties of Cathode Materials for Aqueous Zinc-Ion Batteries, Russ. J. Electrochem. 59 (2023) 1092–1101. https://doi.org/10.1134/S1023193523120066.

[40] M.A. Kamenskii, F.S. Volkov, S.N. Eliseeva, E.G. Tolstopyatova, V.V. Kondratiev, Enhancement of Electrochemical Performance of Aqueous Zinc Ion Batteries by Structural and Interfacial Design of MnO_2 Cathodes: The Metal Ion Doping and Introduction of Conducting

Polymers, Energies. 16 (2023) 3221. https://doi.org/10.3390/en16073221.

[41] M.A. Kamenskii, S.N. Eliseeva, A.I. Volkov, V.V. Kondratiev, Electrochemical Performance of $LiMn_2O_4$ Cathodes in Zn-Containing Aqueous Electrolytes, J. Electrochem. Sci. Technol. 13 (2022) 177–185. https://doi.org/10.33961/jecst.2021.00689.

[42] J. Biemolt, P. Jungbacker, T. van Teijlingen, N. Yan, G. Rothenberg, Beyond Lithium-Based Batteries, Materials. 13 (2020) 425. https://doi.org/10.3390/ma13020425.

[43] Y. Tian, G. Zeng, A. Rutt, T. Shi, H. Kim, J. Wang, J. Koettgen, Y. Sun, B. Ouyang, T. Chen, Z. Lun, Z. Rong, K. Persson, G. Ceder, Promises and Challenges of Next-Generation "beyond Li-ion" Batteries for Electric Vehicles and Grid Decarbonization, Chem. Rev. 121 (2021) 1623–1669. https://doi.org/10.1021/acs.chemrev.0c00767.

[44] Y. Gao, Z. Pan, J. Sun, Z. Liu, J. Wang, High-Energy Batteries: Beyond Lithium-Ion and Their Long Road to Commercialisation, Nano-Micro Lett. 14 (2022) 94. https://doi.org/10.1007/s40820-022-00844-2.

[45] J.-Y.Y. Hwang, S.-T.T. Myung, Y.-K.K. Sun, Sodium-ion batteries: Present and future, Chem. Soc. Rev. 46 (2017) 3529–3614. https://doi.org/10.1039/c6cs00776g.

[46] K. Kubota, M. Dahbi, T. Hosaka, S. Kumakura, S. Komaba, Towards K-Ion and Na-Ion Batteries as "Beyond Li-Ion," Chem. Rec. 18 (2018) 459–479. https://doi.org/10.1002/tcr.201700057.

[47] J. Zheng, C. Hu, L. Nie, H. Chen, S. Zang, M. Ma, Q. Lai, Recent Advances in Potassium-Ion Batteries: From Material Design to Electrolyte Engineering, Adv. Mater. Technol. 8 (2023) 2201591. https://doi.org/10.1002/admt.202201591.

[48] J. Xie, Q. Zhang, Recent Progress in Multivalent Metal (Mg, Zn, Ca, and Al) and Metal-Ion Rechargeable Batteries with Organic Materials as Promising Electrodes, Small. 15 (2019) 1805061. https://doi.org/10.1002/smll.201805061.

[49] M.A. Schroeder, L. Ma, G. Pastel, K. Xu, The mystery and promise of multivalent metal-ion batteries, Curr. Opin. Electrochem. 29 (2021) 100819. https://doi.org/10.1016/j.coelec.2021.100819.

[50] Z. Pan, X. Liu, J. Yang, X. Li, Z. Liu, X.J. Loh, J. Wang, Aqueous Rechargeable Multivalent Metal-Ion Batteries: Advances and Challenges, Adv. Energy Mater. 11 (2021) 2100608. https://doi.org/10.1002/aenm.202100608.

[51] B. John, V. Anoopkumar, T.D. Mercy, Potassium-ion batteries: Key to future large-scale energy storage?, ACS Appl. Energy Mater. 3 (2020) 9478–9492. https://doi.org/10.1021/acsaem.0c01574.

[52] P. He, Q. Chen, M. Yan, X. Xu, L. Zhou, L. Mai, C.-W. Nan, Building better zinc-ion batteries: A materials perspective, EnergyChem. 1 (2019) 100022.

https://doi.org/10.1016/j.enchem.2019.100022.

[53] Y. Shi, Y. Chen, L. Shi, K. Wang, B. Wang, L. Li, Y. Ma, Y. Li, Z. Sun, W. Ali, S. Ding, An Overview and Future Perspectives of Rechargeable Zinc Batteries, Small. 16 (2020) 2000730. https://doi.org/10.1002/smll.202000730.

[54] N. Borchers, S. Clark, B. Horstmann, K. Jayasayee, M. Juel, P. Stevens, Innovative zinc-based batteries, J. Power Sources. 484 (2021) 229309. https://doi.org/10.1016/j.jpowsour.2020.229309.

[55] X. Zhang, L. Wang, H. Fu, Recent advances in rechargeable Zn-based batteries, J. Power Sources. 493 (2021) 229677. https://doi.org/10.1016/j.jpowsour.2021.229677.

[56] H. Liu, J.G. Wang, Z. You, C. Wei, F. Kang, B. Wei, Rechargeable aqueous zinc-ion batteries: Mechanism, design strategies and future perspectives, Mater. Today. 42 (2021) 73–98. https://doi.org/10.1016/j.mattod.2020.08.021.

[57] Q. Zhang, Z. Yang, H. Ji, X. Zeng, Y. Tang, D. Sun, H. Wang, Issues and rational design of aqueous electrolyte for Zn-ion batteries, SusMat. 1 (2021) 432–447. https://doi.org/10.1002/sus2.20.

[58] D. Deng, Li-ion batteries: basics, progress, and challenges, Energy Sci. Eng. 3 (2015) 385–418. https://doi.org/10.1002/ese3.95.

[59] T. Yamamoto, T. Shoji, Rechargeable Zn|$ZnSO_4$|MnO_2-type cells, Inorganica Chim. Acta. 117 (1986) L27–L28. https://doi.org/10.1016/S0020-1693(00)82175-1.

[60] C. Xu, H. Du, B. Li, F. Kang, Y. Zeng, Reversible Insertion Properties of Zinc Ion into Manganese Dioxide and Its Application for Energy Storage, Electrochem. Solid-State Lett. 12 (2009) A61. https://doi.org/10.1149/1.3065967.

[61] N. Liu, B. Li, Z. He, L. Dai, H. Wang, L. Wang, Recent advances and perspectives on vanadium- and manganese-based cathode materials for aqueous zinc ion batteries, J. Energy Chem. 59 (2021) 134–159. https://doi.org/10.1016/j.jechem.2020.10.044.

[62] F. Lanlan, L. Zhenhuan, D. Nanping, Recent advances in vanadium-based materials for aqueous metal ion batteries: Design of morphology and crystal structure, evolution of mechanisms and electrochemical performance, Energy Storage Mater. 41 (2021) 152–182. https://doi.org/10.1016/j.ensm.2021.05.004.

[63] L. Chen, Q. An, L. Mai, Recent Advances and Prospects of Cathode Materials for Rechargeable Aqueous Zinc-Ion Batteries, Adv. Mater. Interfaces. 6 (2019) 1900387. https://doi.org/10.1002/admi.201900387.

[64] B. Tang, L. Shan, S. Liang, J. Zhou, Issues and opportunities facing aqueous zinc-ion batteries, Energy Environ. Sci. 12 (2019) 3288–3304. https://doi.org/10.1039/c9ee02526j.

[65] Y. Kim, Y. Park, M. Kim, J. Lee, K.J. Kim, J.W. Choi, Corrosion as the origin of limited

lifetime of vanadium oxide-based aqueous zinc ion batteries, Nat. Commun. 13 (2022) 2371. https://doi.org/10.1038/s41467-022-29987-x.

[66] W. He, S. Zuo, X. Xu, L. Zeng, L. Liu, W. Zhao, J. Liu, Challenges and strategies of zinc anode for aqueous zinc-ion batteries, Mater. Chem. Front. 5 (2021) 2201–2217. https://doi.org/10.1039/D0QM00693A.

[67] J. Shin, J. Lee, Y. Park, J.W. Choi, Aqueous zinc ion batteries: Focus on zinc metal anodes, Chem. Sci. 11 (2020) 2028–2044. https://doi.org/10.1039/d0sc00022a.

[68] J. Huang, X. Qiu, N. Wang, Y. Wang, Aqueous rechargeable zinc batteries: Challenges and opportunities, Curr. Opin. Electrochem. 30 (2021) 100801. https://doi.org/10.1016/j.coelec.2021.100801.

[69] T. Zhang, Y. Tang, S. Guo, X. Cao, A. Pan, G. Fang, J. Zhou, S. Liang, Fundamentals and perspectives in developing zinc-ion battery electrolytes: A comprehensive review, Energy Environ. Sci. 13 (2020) 4625–4665. https://doi.org/10.1039/d0ee02620d.

[70] S. Guo, L. Qin, T. Zhang, M. Zhou, J. Zhou, G. Fang, S. Liang, Fundamentals and perspectives of electrolyte additives for aqueous zinc-ion batteries, Energy Storage Mater. 34 (2021) 545–562. https://doi.org/10.1016/j.ensm.2020.10.019.

[71] W. Kao-ian, A.A. Mohamad, W. Liu, R. Pornprasertsuk, S. Siwamogsatham, S. Kheawhom, Stability Enhancement of Zinc-Ion Batteries Using Non-Aqueous Electrolytes, Batter. Supercaps. 5 (2022) e202100361. https://doi.org/10.1002/batt.202100361.

[72] V. Mathew, B. Sambandam, S. Kim, S. Kim, S. Park, S. Lee, M.H. Alfaruqi, V. Soundharrajan, S. Islam, D.Y. Putro, J.-Y. Hwang, Y.-K. Sun, J. Kim, Manganese and Vanadium Oxide Cathodes for Aqueous Rechargeable Zinc-Ion Batteries: A Focused View on Performance, Mechanism, and Developments, ACS Energy Lett. 5 (2020) 2376–2400. https://doi.org/10.1021/acsenergylett.0c00740.

[73] D. Selvakumaran, A. Pan, S. Liang, G. Cao, A review on recent developments and challenges of cathode materials for rechargeable aqueous Zn-ion batteries, J. Mater. Chem. A. 7 (2019) 18209–18236. https://doi.org/10.1039/C9TA05053A.

[74] T. Zhou, L. Zhu, L. Xie, Q. Han, X. Yang, L. Chen, G. Wang, X. Cao, Cathode materials for aqueous zinc-ion batteries: A mini review, J. Colloid Interface Sci. 605 (2022) 828–850. https://doi.org/10.1016/j.jcis.2021.07.138.

[75] N. Zhang, J.C. Wang, Y.F. Guo, P.F. Wang, Y.R. Zhu, T.F. Yi, Insights on rational design and energy storage mechanism of Mn-based cathode materials towards high performance aqueous zinc-ion batteries, Coord. Chem. Rev. 479 (2023) 215009. https://doi.org/10.1016/j.ccr.2022.215009.

[76] U. Siamionau, Y. Aniskevich, A. Mazanik, O. Kokits, G. Ragoisha, J.H. Jo, S.T. Myung,

E. Streltsov, Rechargeable zinc-ion batteries with manganese dioxide cathode: How critical is choice of manganese dioxide polymorphs in aqueous solutions?, J. Power Sources. 523 (2022) 231023. https://doi.org/10.1016/j.jpowsour.2022.231023.

[77] Y. Liao, H.-C. Chen, C. Yang, R. Liu, Z. Peng, H. Cao, K. Wang, Unveiling performance evolution mechanisms of MnO_2 polymorphs for durable aqueous zinc-ion batteries, Energy Storage Mater. 44 (2022) 508–516. https://doi.org/10.1016/j.ensm.2021.10.039.

[78] K. You, Y. Yuan, X. Liao, W. Song, X. He, H. Jin, S. Wang, Electrochemical Study of Polymorphic MnO_2 in Rechargeable Aqueous Zinc Batteries, Crystals. 12 (2022) 1600. https://doi.org/10.3390/cryst12111600.

[79] C. Yuan, Y. Zhang, Y. Pan, X. Liu, G. Wang, D. Cao, Investigation of the intercalation of polyvalent cations (Mg^{2+}, Zn^{2+}) into λ-MnO_2 for rechargeable aqueous battery, Electrochim. Acta. 116 (2014) 404–412. https://doi.org/10.1016/j.electacta.2013.11.090.

[80] C. Yang, M. Han, H. Yan, F. Li, M. Shi, L. Zhao, In-situ probing phase evolution and electrochemical mechanism of $ZnMn_2O_4$ nanoparticles anchored on porous carbon polyhedrons in high-performance aqueous Zn-ion batteries, J. Power Sources. 452 (2020) 227826. https://doi.org/10.1016/j.jpowsour.2020.227826.

[81] M. Han, J. Yao, J. Huang, Y. Tang, X. Wu, B. Lu, J. Zhou, Synergistic chemical and electrochemical strategy for high-performance Zn//MnO_2 batteries, Chinese Chem. Lett. 34 (2023) 107493. https://doi.org/10.1016/j.cclet.2022.05.007.

[82] J.C. Knight, S. Therese, A. Manthiram, Chemical extraction of Zn from $ZnMn_2O_4$-based spinels, J. Mater. Chem. A. 3 (2015) 21077–21082. https://doi.org/10.1039/c5ta06482a.

[83] Z. Liu, L. Qin, B. Lu, X. Wu, S. Liang, J. Zhou, Issues and Opportunities Facing Aqueous Mn^{2+}/MnO_2-based Batteries, ChemSusChem. 15 (2022) e202200348. https://doi.org/10.1002/cssc.202200348.

[84] D. Perez-Antolin, I. Sáez-Bernal, A. Colina, E. Ventosa, Float-charging protocol in rechargeable Zn–MnO_2 batteries: Unraveling the key role of Mn^{2+} additives in preventing spontaneous pH changes, Electrochem. Commun. 138 (2022) 107271. https://doi.org/10.1016/j.elecom.2022.107271.

[85] H. Lv, Y. Song, Z. Qin, M. Zhang, D. Yang, Q. Pan, Z. Wang, X. Mu, J. Meng, X. Sun, X.-X. Liu, Disproportionation enabling reversible MnO_2/Mn^{2+} transformation in a mild aqueous Zn-MnO_2 hybrid battery, Chem. Eng. J. 430 (2022) 133064. https://doi.org/10.1016/j.cej.2021.133064.

[86] C. Guo, Q. Zhou, H. Liu, S. Tian, B. Chen, J. Zhao, J. Li, A case study of β- and δ-MnO_2 with different crystallographic forms on ion-storage in rechargeable aqueous zinc ion battery, Electrochim. Acta. 324 (2019) 134867. https://doi.org/10.1016/j.electacta.2019.134867.

[87] M.H. Alfaruqi, J. Gim, S. Kim, J. Song, D.T. Pham, J. Jo, Z. Xiu, V. Mathew, J. Kim, A layered δ-MnO_2 nanoflake cathode with high zinc-storage capacities for eco-friendly battery applications, Electrochem. Commun. 60 (2015) 121–125. https://doi.org/10.1016/j.elecom.2015.08.019.

[88] C. Guo, H. Liu, J. Li, Z. Hou, J. Liang, J. Zhou, Y. Zhu, Y. Qian, Ultrathin δ-MnO_2 nanosheets as cathode for aqueous rechargeable zinc ion battery, Electrochim. Acta. 304 (2019) 370–377. https://doi.org/10.1016/j.electacta.2019.03.008.

[89] H. Wang, M. Liang, J. Gao, C. Ma, Z. He, Y. Zhao, Z. Miao, Robust structural stability of flower-like δ-MnO_2 as cathode for aqueous zinc ion battery, Colloids Surfaces A Physicochem. Eng. Asp. 643 (2022) 128804. https://doi.org/10.1016/j.colsurfa.2022.128804.

[90] D.-S. Liu, Y. Mai, S. Chen, S. Liu, E.H. Ang, M. Ye, Y. Yang, Y. Zhang, H. Geng, C.C. Li, A 1D–3D interconnected δ-MnO_2 nanowires network as high-performance and high energy efficiency cathode material for aqueous zinc-ion batteries, Electrochim. Acta. 370 (2021) 137740. https://doi.org/10.1016/j.electacta.2021.137740.

[91] X. Guo, J. Li, X. Jin, Y. Han, Y. Lin, Z. Lei, S. Wang, L. Qin, S. Jiao, R. Cao, A Hollow-Structured Manganese Oxide Cathode for Stable Zn-MnO_2 Batteries, Nanomaterials. 8 (2018) 301. https://doi.org/10.3390/nano8050301.

[92] C. Huang, C. Wu, Z. Zhang, Y. Xie, Y. Li, C. Yang, H. Wang, Crystalline and amorphous MnO_2 cathodes with open framework enable high-performance aqueous zinc-ion batteries, Front. Mater. Sci. 15 (2021) 202–215. https://doi.org/10.1007/s11706-021-0551-y.

[93] Y. Wu, J. Fee, Z. Tobin, A. Shirazi-Amin, P. Kerns, S. Dissanayake, A. Mirich, S.L. Suib, Amorphous Manganese Oxides: An Approach for Reversible Aqueous Zinc-Ion Batteries, ACS Appl. Energy Mater. 3 (2020) 1627–1633. https://doi.org/10.1021/acsaem.9b02119.

[94] S. Khamsanga, R. Pornprasertsuk, T. Yonezawa, A.A. Mohamad, S. Kheawhom, δ-MnO_2 nanoflower/graphite cathode for rechargeable aqueous zinc ion batteries, Sci. Rep. 9 (2019) 8441. https://doi.org/10.1038/s41598-019-44915-8.

[95] A. Huang, J. Chen, W. Zhou, A. Wang, M. Chen, Q. Tian, J. Xu, Electrodeposition of MnO_2 nanoflakes onto carbon nanotube film towards high-performance flexible quasi-solid-state Zn-MnO_2 batteries, J. Electroanal. Chem. 873 (2020) 114392. https://doi.org/10.1016/j.jelechem.2020.114392.

[96] M. Zhao, Y. Luo, L. Zhu, D. Cai, Y. Zhuang, Q. Chen, H. Zhan, Ultrathin δ-MnO_2 nanosheets branched onto N-doped carbon nanotubes as binder-free cathode electrodes for aqueous zinc-ion batteries with a high areal capacity, J. Alloys Compd. 913 (2022) 165124. https://doi.org/10.1016/j.jallcom.2022.165124.

[97] W. Zhou, A. Wang, A. Huang, M. Chen, Q. Tian, J. Chen, X. Xu, Hybridizing δ-Type MnO_2

With Lignin-Derived Porous Carbon as a Stable Cathode Material for Aqueous Zn–MnO_2 Batteries, Front. Energy Res. 8 (2020) 182. https://doi.org/10.3389/fenrg.2020.00182.

[98] H. Xu, Y. Du, A. Emin, X. Long, Y. Fu, Y. Li, J. Li, D. Liu, D. He, Interconnected Vertical δ-MnO_2 Nanoflakes Coated by a Dopamine-Derived Carbon Thin Shell as a High-Performance Self-Supporting Cathode for Aqueous Zinc Ion Batteries, J. Electrochem. Soc. 168 (2021) 030540. https://doi.org/10.1149/1945-7111/abf016.

[99] J.J.H. Kim, J. Lee, J. You, M.S. Park, M.S. Al Hossain, Y. Yamauchi, J.J.H. Kim, Conductive polymers for next-generation energy storage systems: Recent progress and new functions, Mater. Horizons. 3 (2016) 517–535. https://doi.org/10.1039/C6MH00165C.

[100] R. Balint, N.J. Cassidy, S.H. Cartmell, Conductive polymers: Towards a smart biomaterial for tissue engineering, Acta Biomater. 10 (2014) 2341–2353. https://doi.org/10.1016/j.actbio.2014.02.015.

[101] F. Zhang, C. Wang, J. Pan, F. Tian, S. Zeng, J. Yang, Y. Qian, Polypyrrole-controlled plating/stripping for advanced zinc metal anodes, Mater. Today Energy. 17 (2020) 100443. https://doi.org/10.1016/j.mtener.2020.100443.

[102] Y. Zhao, R. Zhou, Z. Song, X. Zhang, T. Zhang, A. Zhou, F. Wu, R. Chen, L. Li, Interfacial Designing of MnO_2 Half-Wrapped by Aromatic Polymers for High-Performance Aqueous Zinc-Ion Batteries, Angew. Chemie Int. Ed. 61 (2022) e202212231. https://doi.org/10.1002/anie.202212231.

[103] P. Ruan, X. Xu, J. Feng, L. Yu, X. Gao, W. Shi, F. Wu, W. Liu, X. Zang, F. Ma, X. Cao, Boosting zinc storage performance via conductive materials, Mater. Res. Bull. 133 (2021) 111077. https://doi.org/10.1016/j.materresbull.2020.111077.

[104] X. Shen, X. Wang, N. Yu, W. Yang, Y. Zhou, Y. Shi, Y. Wang, L. Dong, J. Di, Q. Li, A Polypyrrole-Coated MnO_2/Carbon Nanotube Film Cathode for Rechargeable Aqueous Zn-Ion Batteries, Acta Phys. Chim. Sin. 38 (2020) 2006059–0. https://doi.org/10.3866/PKU.WHXB202006059.

[105] X. Zhang, S. Wu, S. Deng, W. Wu, Y. Zeng, X. Xia, G. Pan, Y. Tong, X. Lu, 3D CNTs Networks Enable MnO_2 Cathodes with High Capacity and Superior Rate Capability for Flexible Rechargeable Zn–MnO_2 Batteries, Small Methods. 3 (2019) 1900525. https://doi.org/10.1002/smtd.201900525.

[106] I. Petsagkourakis, N. Kim, K. Tybrandt, I. Zozoulenko, X. Crispin, Poly(3,4-ethylenedioxythiophene): Chemical Synthesis, Transport Properties, and Thermoelectric Devices, Adv. Electron. Mater. 5 (2019) 1800918. https://doi.org/10.1002/aelm.201800918.

[107] L. Wang, X. Wang, B. Song, Z. Wang, L. Zhang, Q. Lu, Facile in situ synthesis of PEDOT conductor interface at the surface of MnO_2 cathodes for enhanced aqueous zinc-ion batteries,

Surfaces and Interfaces. 33 (2022) 102222. https://doi.org/10.1016/j.surfin.2022.102222.

[108] H. Chen, W. Ma, J. Guo, J. Xiong, F. Hou, W. Si, Z. Sang, D. Yang, PEDOT-intercalated MnO_2 layers as a high-performance cathode material for aqueous Zn-ion batteries, J. Alloys Compd. 932 (2023) 167688. https://doi.org/10.1016/j.jallcom.2022.167688.

[109] B. Zhang, J. Chen, W. Sun, Y. Shao, L. Zhang, K. Zhao, Challenges and Perspectives for Doping Strategy for Manganese-Based Zinc-ion Battery Cathode, Energies. 15 (2022) 4698. https://doi.org/10.3390/en15134698.

[110] Q. Xie, G. Cheng, T. Xue, L. Huang, S. Chen, Y. Sun, M. Sun, H. Wang, L. Yu, Alkali ions pre-intercalation of δ-MnO_2 nanosheets for high-capacity and stable Zn-ion battery, Mater. Today Energy. 24 (2022) 100934. https://doi.org/10.1016/j.mtener.2021.100934.

[111] H. Li, Z. Huang, B. Chen, Y. Jiang, C. Li, W. Xiao, X. Yan, A high-performance MnO_2 cathode doped with group VIII metal for aqueous Zn-ion batteries: In-situ X-Ray diffraction study on Zn^{2+} storage mechanism, J. Power Sources. 527 (2022) 231198. https://doi.org/10.1016/j.jpowsour.2022.231198.

[112] M.X. Lin, F. Shao, S. Weng, S. Xiong, S. Liu, S. Jiang, Y. Xu, Y. Jiao, J. Chen, Boosted charge transfer in oxygen vacancy-rich K^+ birnessite MnO_2 for water oxidation and zinc-ion batteries, Electrochim. Acta. 378 (2021) 138147. https://doi.org/10.1016/j.electacta.2021.138147.

[113] X. Li, J. Qu, J. Xu, S. Zhang, X. Wang, X. Wang, S. Dai, K-preintercalated MnO_2 nanosheets as cathode for high-performance Zn-ion batteries, J. Electroanal. Chem. 895 (2021) 115529. https://doi.org/10.1016/j.jelechem.2021.115529.

[114] W. Lv, J. Meng, Y. Li, W. Yang, Y. Tian, X. Lyu, C. Duan, X. Ma, Y. Wu, Inexpensive and eco-friendly nanostructured birnessite-type δ-MnO_2: A design strategy from oxygen defect engineering and K^+ pre-intercalation, Nano Energy. 98 (2022) 107274. https://doi.org/10.1016/j.nanoen.2022.107274.

[115] D. Wang, S. Zhang, C. Li, X. Chen, W. Wang, Y. Han, H. Lin, Z. Shi, S. Feng, Engineering the interplanar spacing of K-birnessite for ultra-long cycle Zn-ion battery through “hydrothermal potassium insertion” strategy, Chem. Eng. J. 435 (2022) 134754. https://doi.org/10.1016/j.cej.2022.134754.

[116] J. Tan, T. Feng, S. Hu, Y. Liang, S. Zhang, Z. Xu, H. Zhou, M. Wu, In situ synthesis of a self-supported MnO_2-based cathode for high-performance zinc-ion batteries by K^+ pre-intercalation, Appl. Surf. Sci. 604 (2022) 154578. https://doi.org/10.1016/j.apsusc.2022.154578.

[117] Y. Zhong, X. Xu, J.-P. Veder, Z. Shao, Self-Recovery Chemistry and Cobalt-Catalyzed Electrochemical Deposition of Cathode for Boosting Performance of Aqueous Zinc-Ion Batteries, IScience. 23 (2020) 100943. https://doi.org/10.1016/j.isci.2020.100943.

[118] F. Kataoka, T. Ishida, K. Nagita, V. Kumbhar, K. Yamabuki, M. Nakayama, Cobalt-Doped

Layered MnO_2 Thin Film Electrochemically Grown on Nitrogen-Doped Carbon Cloth for Aqueous Zinc-Ion Batteries, ACS Appl. Energy Mater. 3 (2020) 4720–4726. https://doi.org/10.1021/acsaem.0c00357.

[119] S. Yang, L. Zhang, M. Luo, Y. Cui, J. Wang, D. Zhao, C. Yang, X. Wang, B. Cao, Synergistic combination of a Co-doped σ-MnO_2 cathode with an electrolyte additive for a high-performance aqueous zinc-ion battery, ChemPhysMater. 2 (2022) 77–82. https://doi.org/10.1016/j.chphma.2022.04.007.

[120] J. Wang, J.-G. Wang, H. Liu, C. Wei, F. Kang, Zinc ion stabilized MnO_2 nanospheres for high capacity and long lifespan aqueous zinc-ion batteries, J. Mater. Chem. A. 7 (2019) 13727–13735. https://doi.org/10.1039/C9TA03541A.

[121] W.Y. Ko, A.L. Lubis, H.Y. Wang, T.C. Wu, S.T. Lin, K.J. Lin, Facile Construction of Zn-Doped Mn_3O_4–MnO_2 Vertical Nanosheets for Aqueous Zinc-Ion Battery Cathodes, ChemElectroChem. 9 (2022) e202200750. https://doi.org/10.1002/celc.202200750.

[122] Y. Zhang, X. Cui, Y. Liu, S. Cheng, P. Cui, Y. Wu, Z. Sun, Z. Shao, J. Fu, E. Xie, Aqueous Zn-MnO_2 battery: Approaching the energy storage limit with deep Zn^{2+} pre-intercalation and revealing the ions insertion/extraction mechanisms, J. Energy Chem. 67 (2022) 225–232. https://doi.org/10.1016/j.jechem.2021.09.038.

[123] M. Shi, H. Zhu, C. Chen, J. Jiang, L. Zhao, C. Yan, Synergistically coupling of graphene quantum dots with Zn-intercalated MnO_2 cathode for high-performance aqueous Zn-ion batteries, Int. J. Miner. Metall. Mater. 30 (2023) 25–32. https://doi.org/10.1007/s12613-022-2441-4.

[124] S. Zhou, X. Wu, H. Du, Z. He, X. Wu, X. Wu, Dual metal ions and water molecular pre-intercalated δ-MnO_2 spherical microflowers for aqueous zinc ion batteries, J. Colloid Interface Sci. 623 (2022) 456–466. https://doi.org/10.1016/j.jcis.2022.05.018.

[125] C. Chen, M. Shi, Y. Zhao, C. Yang, L. Zhao, C. Yan, Al-Intercalated MnO_2 cathode with reversible phase transition for aqueous Zn-Ion batteries, Chem. Eng. J. 422 (2021) 130375. https://doi.org/10.1016/j.cej.2021.130375.

[126] J. Xu, X. Hu, M.A. Alam, G. Muhammad, Y. Lv, M. Wang, C. Zhu, W. Xiong, Al-doped α-MnO_2 coated by lignin for high-performance rechargeable aqueous zinc-ion batteries, RSC Adv. 11 (2021) 35280–35286. https://doi.org/10.1039/d1ra06808c.

[127] H. Zhang, Q. Liu, J. Wang, K. Chen, D. Xue, J. Liu, X. Lu, Boosting the Zn-ion storage capability of birnessite manganese oxide nanoflorets by La^{3+} intercalation, J. Mater. Chem. A. 7 (2019) 22079–22083. https://doi.org/10.1039/C9TA08418E.

[128] F. Long, Y. Xiang, S. Yang, Y. Li, H. Du, Y. Liu, X. Wu, X. Wu, Layered manganese dioxide nanoflowers with Cu^{2+} and Bi^{3+} intercalation as high-performance cathode for aqueous zinc-ion

battery, J. Colloid Interface Sci. 616 (2022) 101–109. https://doi.org/10.1016/j.jcis.2022.02.059.

[129] J. Zeng, Z. Zhang, Y. Chen, X. Chen, H. He, J. Wang, Sodium-potassium co-doped layered manganese dioxide cathode material for high performance aqueous zinc-ion batteries, J. Electroanal. Chem. 934 (2023) 117306. https://doi.org/10.1016/j.jelechem.2023.117306.

[130] Y. Wu, M. Wang, Y. Tao, K. Zhang, M. Cai, Y. Ding, X. Liu, T. Hayat, A. Alsaedi, S. Dai, Electrochemically Derived Graphene-Like Carbon Film as a Superb Substrate for High-Performance Aqueous Zn-Ion Batteries, Adv. Funct. Mater. 30 (2020) 1907120. https://doi.org/10.1002/adfm.201907120.

[131] X.Z. Zhai, J. Qu, J. Wang, W. Chang, H.J. Liu, Y.H. Liu, H. Yuan, X. Li, Z.Z. Yu, Diffusion-driven fabrication of yolk-shell structured K-birnessite@mesoporous carbon nanospheres with rich oxygen vacancies for high-energy and high-power zinc-ion batteries, Energy Storage Mater. 42 (2021) 753–763. https://doi.org/10.1016/j.ensm.2021.08.021.

[132] X. Shi, X. Liu, E. Wang, X. Cao, Y. Yu, X. Cheng, X. Lu, Boosting the Zn ion storage ability of amorphous MnO_2 via surface engineering and valence modulation, Carbon Neutralization. 2 (2023) 28–36. https://doi.org/10.1002/cnl2.37.

[133] T. Xue, H.J. Fan, From aqueous Zn-ion battery to Zn-MnO_2 flow battery: A brief story, J. Energy Chem. 54 (2021) 194–201. https://doi.org/10.1016/j.jechem.2020.05.056.

[134] Y. Zhao, Y. Zhu, X. Zhang, Challenges and perspectives for manganese-based oxides for advanced aqueous zinc-ion batteries, InfoMat. 2 (2020) 237–260. https://doi.org/10.1002/inf2.12042.

[135] L. Godeffroy, I. Aguilar, J. Médard, D. Larcher, J. Tarascon, F. Kanoufi, Decoupling the Dynamics of Zinc Hydroxide Sulfate Precipitation/Dissolution in Aqueous Zn–MnO_2 Batteries by Operando Optical Microscopy: A Missing Piece of the Mechanistic Puzzle, Adv. Energy Mater. 12 (2022) 2200722. https://doi.org/10.1002/aenm.202200722.

[136] Y. Huang, J. Mou, W. Liu, X. Wang, L. Dong, F. Kang, C. Xu, Novel Insights into Energy Storage Mechanism of Aqueous Rechargeable Zn/MnO_2 Batteries with Participation of Mn^{2+}, Nano-Micro Lett. 11 (2019) 49. https://doi.org/10.1007/s40820-019-0278-9.

[137] M.H. Alfaruqi, S. Islam, V. Mathew, J. Song, S. Kim, D.P. Tung, J. Jo, S. Kim, J.P. Baboo, Z. Xiu, J. Kim, Ambient redox synthesis of vanadium-doped manganese dioxide nanoparticles and their enhanced zinc storage properties, Appl. Surf. Sci. 404 (2017) 435–442. https://doi.org/10.1016/j.apsusc.2017.02.009.

[138] C.F. Bischoff, O.S. Fitz, J. Burns, M. Bauer, H. Gentischer, K.P. Birke, H.-M. Henning, D. Biro, Revealing the Local pH Value Changes of Acidic Aqueous Zinc Ion Batteries with a Manganese Dioxide Electrode during Cycling, J. Electrochem. Soc. 167 (2020) 020545. https://doi.org/10.1149/1945-7111/ab6c57.

[139] L. Li, T.K.A. Hoang, J. Zhi, M. Han, S. Li, P. Chen, Functioning Mechanism of the Secondary Aqueous Zn-β-MnO_2 Battery, ACS Appl. Mater. Interfaces. 12 (2020) 12834–12846. https://doi.org/10.1021/acsami.9b22758.

[140] Y. Wu, J. Zhi, M. Han, Z. Liu, Q. Shi, Y. Liu, P. Chen, Regulating proton distribution by ion exchange resin to achieve long lifespan aqueous Zn-MnO_2 battery, Energy Storage Mater. 51 (2022) 599–609. https://doi.org/10.1016/j.ensm.2022.07.009.

[141] W. Liu, M. Chen, D. Ren, J. Tang, J. Sun, X. Zhang, B. Jiang, F. Jiang, F. Kang, pH buffer KH_2PO_4 boosts zinc ion battery performance via facilitating proton reaction of MnO_2 cathode, J. Colloid Interface Sci. 657 (2024) 931–941. https://doi.org/10.1016/j.jcis.2023.12.030.

[142] R. Zhang, P. Liang, H. Yang, H. Min, M. Niu, S. Jin, Y. Jiang, Z. Pan, J. Yan, X. Shen, J. Wang, Manipulating intercalation-extraction mechanisms in structurally modulated δ-MnO_2 nanowires for high-performance aqueous zinc-ion batteries, Chem. Eng. J. 433 (2022) 133687. https://doi.org/10.1016/j.cej.2021.133687.

[143] X. Guo, J. Zhou, C. Bai, X. Li, G. Fang, S. Liang, Zn/MnO_2 battery chemistry with dissolution-deposition mechanism, Mater. Today Energy. 16 (2020) 100396. https://doi.org/10.1016/j.mtener.2020.100396.

[144] S.J. Kim, D. Wu, N. Sadique, C.D. Quilty, L. Wu, A.C. Marschilok, K.J. Takeuchi, E.S. Takeuchi, Y. Zhu, Unraveling the Dissolution-Mediated Reaction Mechanism of α-MnO_2 Cathodes for Aqueous Zn-Ion Batteries, Small. 16 (2020) 2005406. https://doi.org/10.1002/smll.202005406.

[145] Y. Li, Y. Li, Q. Liu, Y. Liu, T. Wang, M. Cui, Y. Ding, H. Li, G. Yu, Revealing the Dominance of the Dissolution-Deposition Mechanism in Aqueous Zn−MnO_2 Batteries, Angew. Chemie Int. Ed. 63 (2024) e202318444. https://doi.org/10.1002/anie.202318444.

[146] S.-D. Han, S. Kim, D. Li, V. Petkov, H.D. Yoo, P.J. Phillips, H. Wang, J.J. Kim, K.L. More, B. Key, R.F. Klie, J. Cabana, V.R. Stamenkovic, T.T. Fister, N.M. Markovic, A.K. Burrell, S. Tepavcevic, J.T. Vaughey, Mechanism of Zn Insertion into Nanostructured δ-MnO_2: A Nonaqueous Rechargeable Zn Metal Battery, Chem. Mater. 29 (2017) 4874–4884. https://doi.org/10.1021/acs.chemmater.7b00852.

[147] H. Ao, Y. Zhao, J. Zhou, W. Cai, X. Zhang, Y. Zhu, Y. Qian, Rechargeable aqueous hybrid ion batteries: Developments and prospects, J. Mater. Chem. A. 7 (2019) 18708–18734. https://doi.org/10.1039/c9ta06433h.

[148] J. Yan, J. Wang, H. Liu, Z. Bakenov, D. Gosselink, P. Chen, Rechargeable hybrid aqueous batteries, J. Power Sources. 216 (2012) 222–226. https://doi.org/10.1016/j.jpowsour.2012.05.063.

[149] J. Han, A. Mariani, A. Varzi, S. Passerini, Green and low-cost acetate-based electrolytes for the

highly reversible zinc anode, J. Power Sources. 485 (2021) 229329. https://doi.org/10.1016/j.jpowsour.2020.229329.

[150] H. He, D. Luo, L. Zeng, J. He, X. Li, H. Yu, C. Zhang, 3D printing of fast kinetics reconciled ultra-thick cathodes for high areal energy density aqueous Li–Zn hybrid battery, Sci. Bull. 67 (2022) 1253–1263. https://doi.org/10.1016/j.scib.2022.04.015.

[151] F. Wang, Y. Liu, X. Wang, Z. Chang, Y. Wu, R. Holze, Aqueous Rechargeable Battery Based on Zinc and a Composite of $LiNi_{1/3}Co_{1/3}Mn_{1/3}O_2$, ChemElectroChem. 2 (2015) 1024–1030. https://doi.org/10.1002/celc.201500033.

[152] H.B. Zhao, C.J. Hu, H.W. Cheng, J.H. Fang, Y.P. Xie, W.Y. Fang, T.N.L. Doan, T.K.A. Hoang, J.Q. Xu, P. Chen, Novel Rechargeable $M_3V_2(PO_4)_3$//Zinc (M = Li, Na) Hybrid Aqueous Batteries with Excellent Cycling Performance, Sci. Rep. 6 (2016) 25809. https://doi.org/10.1038/srep25809.

[153] S. Cao, Y. Xiang, Q. Zou, Y. Jiang, H. Zeng, J. Li, J. Wu, X. Wu, X. Wu, L. Xiong, Preparation of $Li_3V_2(PO_4)_3$ as cathode material for aqueous zinc ion batteries by a hydrothermal assisted sol-gel method and its properties, RSC Adv. 13 (2023) 24385–24392. https://doi.org/10.1039/d3ra01816d.

[154] W. Yu, Y. Liu, L. Liu, X. Yang, Y. Han, P. Tan, Rechargeable aqueous Zn-$LiMn_2O_4$ hybrid batteries with high performance and safety for energy storage, J. Energy Storage. 45 (2022) 103744. https://doi.org/10.1016/j.est.2021.103744.

[155] A. Eftekhari, Electrochemical behavior of thin-film $LiMn_2O_4$ electrode in aqueous media, Electrochim. Acta. 47 (2001) 495–499. https://doi.org/10.1016/S0013-4686(01)00774-5.

[156] G. Yuan, J. Bai, T.N.L. Doan, P. Chen, Synthesis and electrochemical investigation of nanosized $LiMn_2O_4$ as cathode material for rechargeable hybrid aqueous batteries, Mater. Lett. 137 (2014) 311–314. https://doi.org/10.1016/j.matlet.2014.09.019.

[157] A.Z. Yazdi, J. Zhi, M. Zhou, T.K.A. Hoang, M. Han, L. Ma, T. Zheng, D. Li, P. Chen, Hierarchical Design in $LiMn_2O_4$ Particles for Advanced Hybrid Aqueous Batteries, ACS Appl. Energy Mater. 4 (2021) 7759–7766. https://doi.org/10.1021/acsaem.1c01116.

[158] X. Zhu, T.N.L. Doan, Y. Yu, Y. Tian, K.E.K. Sun, H. Zhao, P. Chen, Enhancing rate performance of $LiMn_2O_4$ cathode in rechargeable hybrid aqueous battery by hierarchical carbon nanotube/acetylene black conductive pathways, Ionics (Kiel). 22 (2016) 71–76. https://doi.org/10.1007/s11581-015-1527-7.

[159] G. Yuan, M. Geng, P. Zhang, B. Li, Hybrids of $LiMn_2O_4$ nanoparticles anchored on carbon nanotubes/graphene sheets as long-cycle-life cathode material for rechargeable hybrid aqueous batteries, J. Solid State Electrochem. 24 (2020) 601–607. https://doi.org/10.1007/s10008-020-04504-6.

[160] J. Zhi, A.Z. Yazdi, G. Valappil, J. Haime, P. Chen, Artificial solid electrolyte interphase for aqueous lithium energy storage systems, Sci. Adv. 3 (2017) e1701010. https://doi.org/10.1126/sciadv.1701010.

[161] S. Chen, R. Lan, J. Humphreys, S. Tao, Perchlorate Based "Oversaturated Gel Electrolyte" for an Aqueous Rechargeable Hybrid Zn-Li Battery, ACS Appl. Energy Mater. 3 (2020) 2526–2536. https://doi.org/10.1021/acsaem.9b02249.

[162] F. Wang, O. Borodin, T. Gao, X. Fan, W. Sun, F. Han, A. Faraone, J.A. Dura, K. Xu, C. Wang, Highly reversible zinc metal anode for aqueous batteries, Nat. Mater. 17 (2018) 543–549. https://doi.org/10.1038/s41563-018-0063-z.

[163] A. Mitha, H. Mi, W. Dong, I.S. Cho, J. Ly, S. Yoo, S. Bang, T.K.A. Hoang, P. Chen, Thixotropic gel electrolyte containing poly(ethylene glycol) with high zinc ion concentration for the secondary aqueous Zn/$LiMn_2O_4$ battery, J. Electroanal. Chem. 836 (2019) 1–6. https://doi.org/10.1016/j.jelechem.2019.01.014.

[164] H. Lu, S. Zheng, L. Wei, X. Zhang, X. Guo, Manipulating Zn^{2+} solvation environment in poly(propylene glycol)-based aqueous Li^+/Zn^{2+} electrolytes for high-voltage hybrid ion batteries, Carbon Energy. (2023) e365. https://doi.org/10.1002/cey2.365.

[165] H. Avireddy, B.W. Byles, D. Pinto, J.M. Delgado Galindo, J.J. Biendicho, X. Wang, C. Flox, O. Crosnier, T. Brousse, E. Pomerantseva, J.R. Morante, Y. Gogotsi, Stable high-voltage aqueous pseudocapacitive energy storage device with slow self-discharge, Nano Energy. 64 (2019) 103961. https://doi.org/10.1016/j.nanoen.2019.103961.

[166] A. V. Potapenko, S.A. Kirillov, Lithium manganese spinel materials for high-rate electrochemical applications, J. Energy Chem. 23 (2014) 543–558. https://doi.org/10.1016/S2095-4956(14)60184-4.

[167] A.A. Egorova, T.M. Bushkova, I. V. Kolesnik, A.D. Yapryntsev, S.Y. Kottsov, A.E. Baranchikov, Selective Synthesis of Manganese Dioxide Polymorphs by the Hydrothermal Treatment of Aqueous $KMnO_4$ Solutions, Russ. J. Inorg. Chem. 66 (2021) 146–152. https://doi.org/10.1134/S0036023621020066.

[168] A.O. Efremova, A.I. Volkov, E.G. Tolstopyatova, V.V. Kondratiev, EQCM study of intercalation processes into electrodeposited MnO_2 electrode in aqueous zinc-ion battery electrolyte, J. Alloys Compd. 892 (2022) 162142. https://doi.org/10.1016/j.jallcom.2021.162142.

[169] X. Tang, J. Zhou, M. Bai, W. Wu, S. Li, Y. Ma, Investigation of the self-discharge behaviors of the $LiMn_2O_4$ cathode at elevated temperatures: in situ X-ray diffraction analysis and a co-doping mitigation strategy, J. Mater. Chem. A. 7 (2019) 13364–13371. https://doi.org/10.1039/C9TA02718A.

[170] S. Zhang, Z. Liu, L. Li, Y. Tang, S. Li, H. Huang, H. Zhang, Electrochemical activation strategies of a novel high entropy amorphous V-based cathode material for high-performance aqueous zinc-ion batteries, J. Mater. Chem. A. 9 (2021) 18488–18497. https://doi.org/10.1039/d1ta05205e.

[171] Y. Zhang, R. Huang, X. Wang, Z. Wang, B. Song, Y. Du, Q. Lu, X. Chen, J. Sun, Facile large-scale preparation of vanadium pentoxide -polypyrrole composite for aqueous zinc-ion batteries, J. Alloys Compd. 907 (2022) 164434. https://doi.org/10.1016/j.jallcom.2022.164434.

[172] M.A. Kamenskii, S.N. Eliseeva, V. V. Kondratiev, The Electrochemical Performance of δ-MnO2 Cathode Material for Aqueous Zinc-Ion Batteries: The Role of Current Collector, ECS Trans. 105 (2021) 135–142. https://doi.org/10.1149/10501.0135ecst.

[173] Y. Tan, F. An, Y. Liu, S. Li, P. He, N. Zhang, P. Li, X. Qu, Reaction kinetics in rechargeable zinc-ion batteries, J. Power Sources. 492 (2021) 229655. https://doi.org/10.1016/j.jpowsour.2021.229655.

[174] M.F. Mathias, O. Haas, An Alternating Current Impedance Model Including Migration and Redox-Site Interactions at Polymer-Modified Electrodes, J. Phys. Chem. 96 (1992) 3174–3182.

[175] M. Li, Q. He, Z. Li, Q. Li, Y. Zhang, J. Meng, X. Liu, S. Li, B. Wu, L. Chen, Z. Liu, W. Luo, C. Han, L. Mai, A Novel Dendrite-Free Mn^{2+}/Zn^{2+} Hybrid Battery with 2.3 V Voltage Window and 11000-Cycle Lifespan, Adv. Energy Mater. 9 (2019) 1901469. https://doi.org/10.1002/aenm.201901469.

[176] G. Greczynski, T. Kugler, M. Keil, W. Osikowicz, M. Fahlman, W.. Salaneck, Photoelectron spectroscopy of thin films of PEDOT–PSS conjugated polymer blend: a mini-review and some new results, J. Electron Spectros. Relat. Phenomena. 121 (2001) 1–17. https://doi.org/10.1016/S0368-2048(01)00323-1.

[177] M.A. Kamenskii, S.N. Eliseeva, E.G. Tolstopjatova, A.I. Volkov, D. V. Zhuzhelskii, V.V. Kondratiev, The advantages of mass normalized electrochemical impedance spectra for the determination of the kinetic parameters of $LiMn_2O_4$ cathodes, Electrochim. Acta. 326 (2019) 134969. https://doi.org/10.1016/j.electacta.2019.134969.

[178] S.J. Kim, D. Wu, L.M. Housel, L. Wu, K.J. Takeuchi, A.C. Marschilok, E.S. Takeuchi, Y. Zhu, Toward the Understanding of the Reaction Mechanism of Zn/MnO_2 Batteries Using Non-alkaline Aqueous Electrolytes, Chem. Mater. 33 (2021) 7283–7289. https://doi.org/10.1021/acs.chemmater.1c01542.

[179] Z. He, Y. Lu, T. Wei, C. Hu, Complementary Operando Electrochemical Quartz Crystal Microbalance and UV/Vis Spectroscopic Studies: Acetate Effects on Zinc-Manganese Batteries, ChemSusChem. 16 (2023) e202300259. https://doi.org/10.1002/cssc.202300259.

[180] O. Zhanadilov, H.J. Kim, A. Konarov, J. Jeong, J.H. Park, K.Y. Chung, Z. Bakenov,

H. Yashiro, S.T. Myung, Layered manganese oxide cathode boosting high-capacity and long-term cyclability in aqueous Zinc-Ion batteries, Energy Storage Mater. 67 (2024) 103283. https://doi.org/10.1016/j.ensm.2024.103283.

[181] C. Li, H. Yuan, T. Liu, R. Zhang, J. Zhu, H. Cui, Y. Wang, D. Cao, D. Wang, C. Zhi, Distinguish MnO_2/Mn^{2+} Conversion/Zn^{2+} Intercalation/H^+ Conversion Chemistries at Different Potentials in Aqueous Zn||MnO_2 Batteries, Angew. Chemie. 136 (2024) e202403504. https://doi.org/10.1002/ange.202403504.

[182] X. Cui, Y. Zhang, S. Cheng, Y. Liu, Z. Shao, Z. Sun, Y. Wu, H. Guo, J. Fu, E. Xie, Achieving high-rate and durable aqueous rechargeable Zn-Ion batteries by enhancing the successive electrochemical conversion reactions, J. Colloid Interface Sci. 620 (2022) 127–134. https://doi.org/10.1016/j.jcis.2022.04.004.

[183] S. Zhao, B. Han, D. Zhang, Q. Huang, L. Xiao, L. Chen, D.G. Ivey, Y. Deng, W. Wei, Unravelling the reaction chemistry and degradation mechanism in aqueous Zn/MnO_2 rechargeable batteries, J. Mater. Chem. A. 6 (2018) 5733–5739. https://doi.org/10.1039/c8ta01031e.

[184] K. Ha, H. Moon, E.J. Joo, D.H. Jo, K.T. Lee, Role of zinc hydroxysulfates in the thermodynamics and kinetics of mild-acid Zn-MnO_2 batteries, Energy Storage Mater. 65 (2024) 103150. https://doi.org/10.1016/j.ensm.2023.103150.

[185] B. Lee, H.R. Seo, H.R. Lee, C.S. Yoon, J.H. Kim, K.Y. Chung, B.W. Cho, S.H. Oh, Critical Role of pH Evolution of Electrolyte in the Reaction Mechanism for Rechargeable Zinc Batteries, ChemSusChem. 9 (2016) 2948–2956. https://doi.org/10.1002/cssc.201600702.

[186] T.N.T. Tran, S. Jin, M. Cuisinier, B.D. Adams, D.G. Ivey, Reaction mechanisms for electrolytic manganese dioxide in rechargeable aqueous zinc-ion batteries, Sci. Rep. 11 (2021) 20777. https://doi.org/10.1038/s41598-021-00148-2.

[187] H. Chen, S. Cai, Y. Wu, W. Wang, M. Xu, S.-J. Bao, Successive electrochemical conversion reaction to understand the performance of aqueous Zn/MnO_2 batteries with Mn^{2+} additive, Mater. Today Energy. 20 (2021) 100646. https://doi.org/10.1016/j.mtener.2021.100646.

[188] S.J. Hawkes, All Positive Ions Give Acid Solutions in Water, J. Chem. Educ. 73 (1996) 516. https://doi.org/10.1021/ed073p516.

[189] K.J. Powell, P.L. Brown, R.H. Byrne, T. Gajda, G. Hefter, A.-K. Leuz, S. Sjöberg, H. Wanner, Chemical speciation of environmentally significant metals with inorganic ligands. Part 5: The Zn^{2+} + OH^-, Cl^-, CO_3^{2-}, SO_4^{2-}, and PO_4^{3-} systems (IUPAC Technical Report), Pure Appl. Chem. 85 (2013) 2249–2311. https://doi.org/10.1351/pac-rep-13-06-03.